MINISTRY OF EDUCATION AND RESEARCH

THE ANNALS OF "DUNAREA DE JOS" UNIVERSITY OF GALATI

Fascicle IX
METALLURGY AND MATERIALS SCIENCE

YEAR XXXVIII (XLIII)
September 2020, no. 3

ISSN 2668-4748; e-ISSN 2668-4756

2020
GALATI UNIVERSITY PRESS

EDITORIAL BOARD

THE ANNALS OF "DUNAREA DE JOS" UNIVERSITY OF GALATI
FASCICLE IX. METALLURGY AND MATERIALS SCIENCE
Nº. 3 - 2020, ISSN 2668-4748; e-ISSN 2668-4756
Volume DOI: https://doi.org/10.35219/mms.2020.3

Table of Contents

THE ANNALS OF "DUNAREA DE JOS" UNIVERSITY OF GALATI
FASCICLE IX. METALLURGY AND MATERIALS SCIENCE
Nº. 3 - 2020, ISSN 2668-4748; e-ISSN 2668-4756
Volume DOI: https://doi.org/10.35219/mms.2020.3

THE ANNALS OF "DUNAREA DE JOS" UNIVERSITY OF GALATI
FASCICLE IX. METALLURGY AND MATERIALS SCIENCE
Nº. 3 - 2020, ISSN 2668-4748; e-ISSN 2668-4756
Article DOI: https://doi.org/10.35219/mms.2020.3.01

UTILIZATION OF SMARTPHONE LIGHT SENSORS AS LIGHT TRANSMISSION ANALYZER DURING THE OBTAINING OF POLYMERIC PHASE INVERSION MEMBRANES

Ștefan PINTILIE, Geanina Laurenția PINTILIE, Ștefan BALTĂ
"Dunarea de Jos" University of Galati, Romania
e-mail: stefan.pintilie@ugal.ro

ABSTRACT

Smartphone sensors are gaining research interest due to continuous sensor upgrades, leading to more precise readings of these sensors. For this study, the light sensor of a smartphone was used in determining light transmittance during the phase inversion process of ultrafiltration polysulfone-membrane manufacturing. Membrane separation is one of the best available technologies when it comes to water and wastewater treatment. The purpose of this study was to correlate light transmittance, at certain demixing steps during phase inversion, with membrane porosity, pure water flux and cross-sectional SEM images. Results show close relation between light transmittance and the mentioned membrane properties.

KEYWORDS: membrane, flux, porosity, light transmittance, smartphone, light sensor

1. Introduction

Filtration using membranes have started gaining interest since the year 1907 [1]. Unfortunately, it was not until 6 decades later that membranes showed enormous potential in filtration-based applications, especially from a commercial point of view [2]. Since then, due to the efficiency of separation and lower energy consumption compared with conventional treatment methods, the membrane technology has been implemented in almost all sectors of industry that use water as a prime material and process water.

According to the International Union of Pure and Applied Chemistry, a membrane is defined as a porous or dense structure, with lateral dimensions much greater than its thickness that acts as a selective barrier between two phases, through which transfer occurs under a variety of driving forces [3].

Pressure-driven membranes are among the most used types of membrane filters [4]. Polymeric membranes cover 90% of the produced membranes sum total scale [5]. The most common method used to prepare polymeric membranes is the phase inversion process [6].

The phase inversion is a very simple process that consists in the exchange between solvent and non-solvent in the polymeric matrix, often called demixing. It is a process that covers a wide range of different techniques, the most used being immersion precipitation [7].

Different techniques are used in order to understand the membrane performance, structure and formation. Although light transmission is an acceptable method in studying membrane formation during phase inversion, little emphasis was laid emphasis was placed on using it in membrane research [6-10].

Smartphones are becoming an important tool in laboratory-related experiments, for teaching and scientific purposes [11-15], primarily due to their built-in sensors. Examples of such sensors are: the accelerometer, magnetometer, ambient light sensor, GPS, microphone, barometer, thermometer, air humidity and, in very rare situations, the Geiger counter [16].

As sensors are starting to become smaller and more performant, they are gradually transforming smartphones in devices that could replace some laboratory equipment. The most advantageous aspect in using smartphones in such means is mainly related to costs and multifunctionality.

The purpose of this study is to verify whether the smartphone sensor is a good way to measure light transmittance of a polymeric thin film during phase inversion, in order to observe the different stages of polymerization, for ultrafiltration membranes composed of 3 polymer concentrations (polysulfone).

THE ANNALS OF "DUNAREA DE JOS" UNIVERSITY OF GALATI
FASCICLE IX. METALLURGY AND MATERIALS SCIENCE
Nº. 3 - 2020, ISSN 2668-4748; e-ISSN 2668-4756
Article DOI: https://doi.org/10.35219/mms.2020.3.01

From the best of our knowledge, this technique has never been used before.

2. Materials and methods

2.1. Membrane materials and preparation

2.1.1. Membrane materials

The polymer of choice was polysulfone (PSf, Mw ~35000), and the solvent was 1-methyl-2-pyrrolidinone (NMP, C_5H_9NO, M_w ~99.13, ACS reagent grade: 99%). Both components were purchased from Sigma Aldrich.

2.1.2. Membrane preparation

The studied membranes were manufactured by phase inversion, the immersion precipitation technique. The cast solution was obtained by mixing NMP solvent with PSf polymer of different concentration.

The solutions were stirred at 1000 rpm until homogeneity was achieved. After that, the solutions were casted on a glass support, and with the help of a casting knife, the solution was casted to a fixed thickness of 250 µm. In order to produce the actual membrane, the thin film solution was immersed in a coagulation bath, composed of distilled water. Here, phase inversion takes place, leading to the demixing between the pure water and the NMP. During demixing, pores are produced in the polymeric matrix. During this procedure, light transmission analysis will be investigated. After complete demixing, phase inversion ends and the membranes are transferred in a distilled water container in order to dissolve the remaining NMP residue.

The resulted membranes were labelled according to PSf concentration, as presented in Table 1.

Table 1. *Membrane designation according to polymer concentration*

Membrane	Polymer type	Polymer conc. [wt.%]
23PSf	Polysulfone (PSf)	23
25PSf		25
27PSf		27

2.2. Methods of characterization

2.2.1. Light transmission set-up

The set-up for light transmission tests was as shown in Figure 1, which is a homebuilt device. The principle is simple, consisting in an emitting visible light beam which passes through the casted polymer solution during the whole procedure of phase inversion. This beam is recorded as light intensity [lux], being afterwards transformed in transmittance percentage.

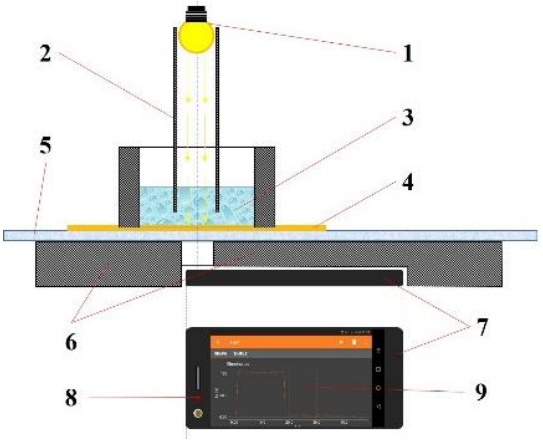

1. Light source
2. Light tunnel
3. Coagulation bath
4. Casted polymer film
5. Clear glass
6. Obscure glass support
7. Smartphone
8. Light sensor
9. Light transmittance software

Fig. 1. *Light transmittance set-up for membrane formation monitorization*

The light sensor (TCS3701) is an integrated part of a smartphone device (SM-A705FD), which is positioned under the casted polymeric film. The data received from the sensor were recorded with a special open-source software (Phyphox, RWTH Aachen University). Some technical specifications of the TCS3701 light sensor are presented in Table 2.

Table 2. *TCS3701 sensor features*

Minimum detectable illuminance: 1 mlux (100 ms
UV/IR blocking filter
14-bit data output
Maximum range (lux): 32657.0
Resolution: 1.0

THE ANNALS OF "DUNAREA DE JOS" UNIVERSITY OF GALATI
FASCICLE IX. METALLURGY AND MATERIALS SCIENCE
N°. 3 - 2020, ISSN 2668-4748; e-ISSN 2668-4756
Article DOI: https://doi.org/10.35219/mms.2020.3.01

The recorded values were exposed as light transmittance vs. time curves.

2.2.2. Porosity

The light transmission results were correlated with the membrane porosity. In order to calculate porosity, a membrane sample with a known surface (A) and thickness (h) was weighed in dry state (m_{dry}) and afterwards immersed in a liquid for at least 24h to make sure that the sample is fully wetted (m_{wet}). The liquid of choice is distilled water, which has a specific density ρ.

$$\varepsilon = \frac{m_{wet} - m_{dry}}{A \times \rho \times h} \quad (1)$$

In simple terms, porosity represents the total spaces from inside the structure of a membrane. Porosity is linked to permeation properties.

2.2.3. Pure water flux

The pure water flux, J [L m^{-2} h^{-1}], expresses the permeation performance in ideal circumstances, where the feed liquid has no impurities in its composition. In this study, pure water was used for convenience.

The flux is calculated as follows:

$$J = \frac{V}{A \times t} \quad (2)$$

Where V is the total volume [L] that passed through a known membrane area, A [m^2], within a set time, t [h].

2.2.4. Cross-section SEM microscopy

The sample cross-section morphologies were investigated using FEI Quanta 200 scanning electron microscope. All samples were sputter-coated with gold before observation to obtain conductivity during analysis.

3. Results and discussions

After the transmittance experiments of thin films during the phase inversion process, as can be seen in Figure 2, several stages can be identified. Four main stages were identified during phase inversion process. The first stage represents the instant demixing, which is the first contact between the polymeric solution film and coagulation bath. This stage is observed as a steep slope, denoting the very fast water-solvent demixing. The second stage is represented by the start in stabilization of the aforementioned demixing. Stage III will not be discussed because he fact that this step is a constant polymerization slope until full demixing is achieved. The complete solidification is reached at the last stage, where the membrane is fully polymerized.

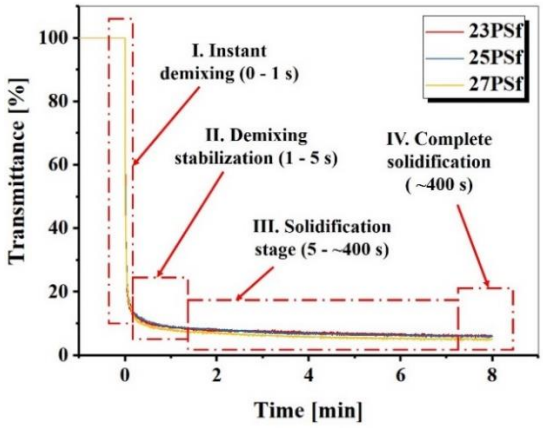

Fig. 2. *Overall light transmittances during phase inversion of the studied membranes*

It will be observed that stages I and IV are linked to the overall properties of membranes.

Although the overall graph is expressed in minutes, the other graphs will be expressed in seconds due to the fast demixing of the polymer film during phase inversion.

Every stage in light transmission is linked to special areas of the membranes cross-section, for all the studied membranes. In Figure 3 one can observe that, throughout the demixing direction, the width of the elongated pores, called macrovoids, is gradually increasing.

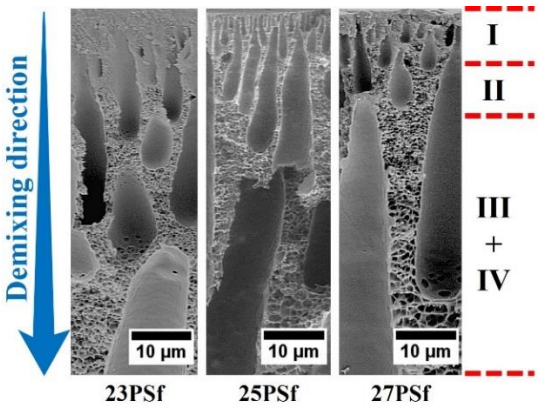

Fig. 3. *Cross-section SEM images of the studied membranes and the possible hypothesis with the regions where the four stages may occur*

THE ANNALS OF "DUNAREA DE JOS" UNIVERSITY OF GALATI
FASCICLE IX. METALLURGY AND MATERIALS SCIENCE
Nº. 3 - 2020, ISSN 2668-4748; e-ISSN 2668-4756
Article DOI: https://doi.org/10.35219/mms.2020.3.01

Based on width increase, the positioning of the four stages can be estimated. Hence, the region where the smallest macrovoids occur is at the top of the cross-section, noted by stage I of the demixing process. As the region progresses downward, it is observed that in the other stages the thickness of macrovoids gradually increases, meaning a slowing down of the demixing momentum.

In the first stage (Figure 4), the reactions between solvent and non-solvent take place at the membrane surface, which is considered as the most important stage in membrane fabrication. This happens because it establishes the permeation properties of the membrane, higher or lower flux and retention, also.

A lower transmittance during the first second of phase inversion means a fast demixing of the solvent with the water bath, which is directly proportional with the pore formation in the membrane active layer.

The sample corresponding to membrane 23PSf, the lowest polysulfone concentration, displayed the lowest light transmittance, which is indicative of fastest solvent-water demixing.

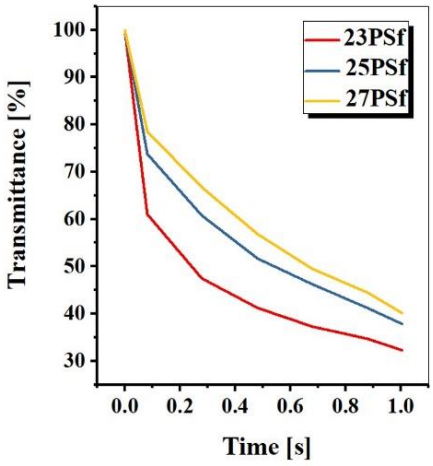

Fig. 4. *Instant demixing stage during phase inversion of the studied membranes*

Comparing transmittance with membrane structure, it is observed that with fast demixing the pore formation at membrane surface is thinner, difficult to distinguish (Figure 3 – 23PSf), while slower demixing led to observable thicker active layers (Figure 3 – 25PSf and 27PSf).

Continuing the reading to the interval of 1 to 5 seconds (Figure 5), the ability of the middle morphologies of membrane sections to stabilize is observed. Stage two shows the stabilization time of the membrane. The membrane with 27 wt% PSf show a faster demixing which result in a thinner middle layer.

Also, in stage II, the light transmittances are observed to stabilize and keep the trend up to the end of phase inversion.

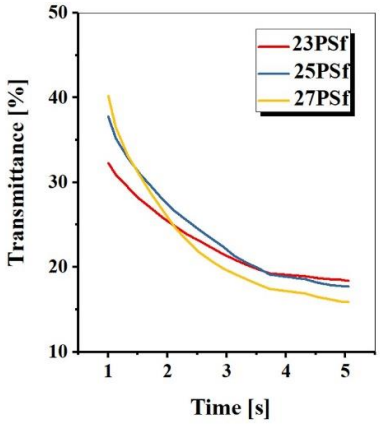

Fig. 5. *Demixing stabilization stage during phase inversion of the studied membranes*

In the final stage of the phase inversion process (Figure 6), after approx. 8 minutes, the transmittance was observed to be higher for lower polymer concentration. This phenomenon is strongly related with membrane porosity. The higher porosity leads to higher passage of light through the membrane, due to the higher frequency of macrovoids in structure.

Higher polymer concentration membranes, which is understood as the samples with lower amount of macrovoids, led to lower light transmittance.

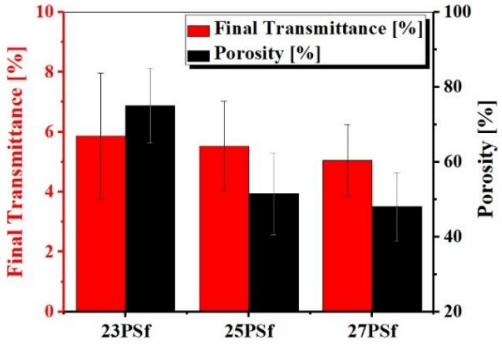

Fig. 6. *Complete stabilization stage in correlation with calculated porosities of the studied membranes*

As explained in the first stage of phase inversion, demixing is related with pore formation at membrane surface. The demixing time is directly proportional to pore formation, in which a faster demixing will lead to a higher flux due to higher number of pores.

THE ANNALS OF "DUNAREA DE JOS" UNIVERSITY OF GALATI
FASCICLE IX. METALLURGY AND MATERIALS SCIENCE
Nº. 3 - 2020, ISSN 2668-4748; e-ISSN 2668-4756
Article DOI: https://doi.org/10.35219/mms.2020.3.01

As can be observed in Figure 7, a faster demixing lead to higher water flux, represented by the 23wt% PSf membrane.

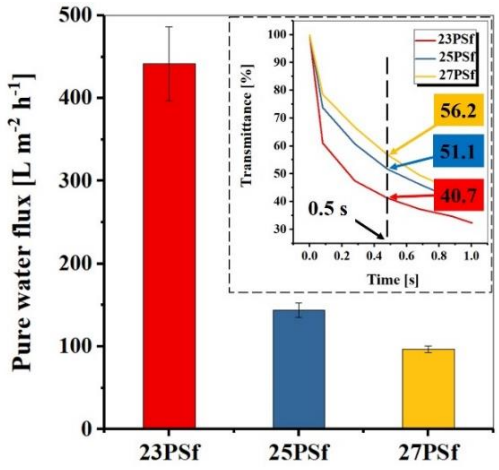

Fig. 7. *Pure water flux correlated with the transmittance occurred at 0.5 s at the stage of instant demixing (extracted from Figure 4) of the prepared membranes*

The values of the light transmittance at time of 0.5 s were extracted from Figure 4, also present in Figure 7 as an insert graph. It is obvious that the light transmittance-flux trend is inversely proportional. The highest difference, in terms of light transmittance, is between 23PSf (40.7%) and 27PSf (56.2%), respecting the pure water flux trend, also. On the other hand, the lowest difference is between the membranes with higher polymer concentration, namely 25PSf and 27PSf, with 51.1% and 56.2%, respectively.

Demixing is inversely proportional to water flux and directly proportional to polymer concentration.

4. Conclusions

Membrane characterization is very important for understanding future performances of the material. Light transmission is a good tool in determining several membrane properties and performances, before they can be used in the actual separation processes. The pure water flux and porosity were successfully correlated with the light transmittances obtained by the smartphone light sensor. The results were synchronous, showing similar trends at different polysulfone concentrations. In the near future, smartphones will become essential devices in lab research.

References

[1]. Glater J., *The early history of reverse osmosis membrane development*, Desalination, vol. 117, issue 1-3, p. 297-309, 1998.

[2]. Loeb S., The Loeb-Sourirajan, *Membrane: How it Came About*, ACS Symposium Series, vol. 53, chapter 1, p. 1-9, 1981.

[3]. Gohil J. M., Choudhury R., *Chapter 2 - Introduction to Nanostructured and Nano-enhanced Polymeric Membranes: Preparation, Function, and Application for Water Purification*, in book: Nanoscale Materials in Water Purification: Micro and Nano Technologies, Elsevier B. V., ISBN: 978-0-12-813926-4, 2019.

[4]. Zhang W., Luo J., Ding L., Jaffrin M. Y., *A Review on Flux Decline Control Strategies in Pressure-Driven Membrane Processes*, Industrial & Engineering Chemistry Research, vol. 54, issue 11, p. 2843-2861, doi: 10.1021/ie504848m, 2015.

[5]. Balta S., Tiron L.G., *Nanofiltrare*, Zigotto, Romania, ISBN 978-606-669-295-3, 2019.

[6]. Yu L. Y., Xu Z. L., Shen H. M., Yang H., *Preparation and characterization of PVDF–SiO2 composite hollow fiber UF membrane by sol-gel method*, J. of Membrane Science, vol. 337, issues 1-2, p. 257-265, DOI:10.1016/j.memsci.2009.03.054, 2009.

[7]. Li J.-F., Xu Z.-L., Yang H., *Microporous polyethersulfone membranes prepared under the combined precipitation conditions with non-solvent additives*, Polymers for Advanced Technologies, vol. 19, issue 4, doi: 10.1002/pat.982, 2007.

[8]. Fen'ko L. A., Semenkevich N. G., Bil'dyukevich A. V., *The Kinetics of Membrane Pore Structure Formation by Phase Inversion*, Membrany i membrannye tekhnologii, vol. 1, no. 1, p. 66-75, DOI: 10.1134/S0965544111070073, 2011.

[9]. Zhao S., Wang Z., Wei X., Tian X., Wang J., Yaang S., Wang S., *Comparison study of the effect of PVP and PANI nanofibers additives on membrane formation mechanism, structure and performance*, Journal of Membrane Science, vol. 385-386, p. 110-122, doi: 10.1016/j.memsci.2011.09.029, 2011, 2011.

[10]. Le X-M., Ji Y., Yin Y., Zhang Y-Y., Wang Y., He T., *Origin of delamination/adhesion in polyetherimide/polysulfone co-cast membranes*, Journal of Membrane Science, vol. 352, issues 1-2, p. 173-179, doi: 10.1016/j.memsci.2010.02.013, 2010.

[11]. Grasse E. K., Torcasio M. H., Smith A. W., *Teaching UV-Vis Spectroscopy with a 3D-Printable Smartphone Spectrophotometer*, J. of Chemical Education, vol. 93, issue 1, p. 146-151, doi: 10.1021/acs.jchemed.5b00654, 2016.

[12]. Gutierrez-Martinez J-M., Castillo-Martinez A., Medina-Merodio J-A., Aguado-Delgado J., Martinez-Herraiz J-J., *Smartphones as a Light Measurement Tool: Case of Study*, Applied Sciences, vol. 7, issue 6, 616, doi: 10.3390/app7060616, 2017.

[13]. Hussain I., Ahamad K., Nath P., *Water turbidity sensing using a smartphone*, RSC Advances, vol. 6, issue 27, p. 22374-22382, doi: 10.1039/C6RA02483A, 2016.

[14]. Koydemir H. C., Gorocs Z., Tseng D., Cortazar B., Feng S., Yan Lok Chan R., Jordi B., McLeod E., Ozcan A., *Rapid imaging, detection and quantification of Giardia lamblia cysts using mobile-phone based fluorescent microscopy and machine learning*, Lab on a Chip, vol. 15, p. 1284-1293, doi: 10.1039/C4LC01358A, 2015.

[15]. Hossain A., Canning J., Ast S., Rutledge P. J., Yen T. L., Jamalipour A., *Lab-in-a-Phone: Smartphone-Based Portable Fluorometer for pH Measurements of Environmental Water*, IEEE Sensors Journal, vol. 15, issue 9, p. 5095-5102, doi: 10.1109/JSEN.2014.2361651, 2013.

[16]. Chou T., *Precision: Principles, Practices and Solutions for the Internet of Things*, Lulu Press, Inc., U.S.A., ISBN-10: 1329843568, 2020.

THE ANNALS OF "DUNAREA DE JOS" UNIVERSITY OF GALATI
FASCICLE IX. METALLURGY AND MATERIALS SCIENCE
No. 3 - 2020, ISSN 2668-4748; e-ISSN 2668-4756
Article DOI: https://doi.org/10.35219/mms.2020.3.02

THE MECHANICAL PROPERTIES OF ORGANIC MODIFIED EPOXY RESIN

Georgel MIHU, Claudia Veronica UNGUREANU, Vasile BRIA, Marina BUNEA, Rodica CHIHAI (PEȚU)
"Dunarea de Jos" University of Galati, Cross-Border Faculty, Romania
Research and Development Centre for Thermoset Matrix Composites, Romania
e-mail: claudia.ungureanu@ugal.ro, rodica.petu@yahoo.com

ABSTRACT

Epoxy resins have been presenting a lot of scientific and technical interests and organic modified epoxy resins have recently receiving a great deal of attention. For obtaining the composite materials with good mechanical proprieties, a large variety of organic modification agents were used. For this study gluten and gelatin had been used as modifying agents thinking that their dispersion inside the polymer could increase the polymer biocompatibility. Equal amounts of the proteins were milled together and the obtained compound was used to form 1 to 5% weight ratios organic agents modified epoxy materials. To highlight the effect of these proteins in epoxy matrix mechanical tests as three-point bending and compression were performed.

KEYWORDS: mechanical properties, gluten, epoxy resin, gelatin

1. Introduction

Composites have been found to be the most promising and discerning material available in this century. The composite material has a variety of advantages, such as: excessive energy to weight ratio, convenient availability, ease and hassles free fabrication methods and improvised thermal and mechanical properties. Some unique composite materials have higher stiffness and higher-pressure rate, which is associated with metals, the strength of the composite material additionally, depends on the geometry and shape [1].

Epoxy resins are the most widely used thermosetting matrices due to their good mechanical strength, low shrinkage, excellent manufacturability, effective electrical insulation, and stable thermal properties [2]. In addition, these systems do have some environmental problems. An environmental problem of epoxy resins is that all the curing agents are toxic before the cure. Even for cured epoxy resins that seem safe, toxicity cannot be totally avoided because of the possibility of incomplete consumption of curing agents and subsequently the hazards introduced by the residue curing agents. [3]. A new approach in the development of an eco-friendly curing agent for epoxy resins in the industry is of great importance.

Among frequently used curing agents for epoxy resins, especially organic and inorganic compounds, are of prime significance in practical applications [4]. In addition, the modifying agents are small particles dispersed in the matrix material, which can be easily obtained and incorporated in the material [4-6]. Also, the organic modification agents help to improve the material by increasing the abrasion resistance and lowering the coefficient of thermal expansion [7]. Recently amino acids have been used to cure epoxy resins, which take the advantages of the reduced toxicity and environmental friendliness [8].

Protein polymers are natural macromolecules derived from plants and animals which makes them an easily obtainable, renewable resource [9]. The gelatin, a natural biopolymer, has properties like biocompatibility and water solubility, low immunogenicity, plasticity, adhesiveness, promotion of cell adhesion, growth, and cost economy, as well as the ability to form transparent gels under specific conditions. Also, gelatin has a large variety of applications, including food industry, pharmaceutical formulations and other technical products. [10-13]. Wheat gluten is an important source of proteins. Being a by-product of the starch industry, it is widely available, cheap, and fully biodegradable. Among other possible uses, wheat gluten has been extensively tested to produce renewable thermoplastic materials [14-15]. Two factors such as, use

THE ANNALS OF "DUNAREA DE JOS" UNIVERSITY OF GALATI
FASCICLE IX. METALLURGY AND MATERIALS SCIENCE
N°. 3 - 2020, ISSN 2668-4748; e-ISSN 2668-4756
Article DOI: https://doi.org/10.35219/mms.2020.3.02

plasticizers and fiber length, are usually considered for improving the mechanical properties of gluten composites [16]. Materials obtained from gluten are considered a promising source with which to produce sustainable packaging as it improves food storage. These materials have the capacity to act as a barrier against water, oxygen, and light, therefore reducing oxidation of food [17].

The objective of this study was to determine the modifications of epoxy resins properties induced by organic modification agents. Also, besides mechanical properties, chemical properties presented high potential to be investigated.

2. Materials and methods

The experiments were carried out using the Epiphen system consisting of RE4020 (resin) and DE4020 (hardener), with 100:30 ratio, due to its properties before and after polymerization [18]. Wheat gluten and gelatin were purchased from Sigma-Aldrich and were used as received.

In order to improve the mechanical response of the final polymer equal amounts of the proteins had been mixing with the resin, such as finally their weight ratios into the formed polymers to be 1%, 2%, 3%, 4% and 5%.

For organic modified polymers, two alternatives were used: firstly, disperse the powders into the resin (the main component – liquid – of an epoxy resin) and then to add the hardener (the second component of the epoxy system) and the second it was dispersing the powder inside the hardener volume and then forming the material. Taking into account the fact that, in the absence of chemical interaction, the physical interaction is probably leading to dispersion of some aggregates (powder particles surrounded by resin or hardener molecules) inside a liquid phase which for sure will differently respond after resin-hardener blending. The composite materials modified with organic agents were mixed mechanically at 300 rotation/min for 15 minutes, at 70 °C, for 24 hours. After that, the right amount of hardener was added and the new mixtures were stirred for 15 minutes to ensure the homogeneity. Then, the pre-polymers mixtures were casted into cylindrical polypropylene tubes, with 8 mm diameter and 200 mm length. The obtained materials are notated as *Eax* and *Ebx*, where *Ea* represents the material obtained by mixing the organic agents with the resin and Eb meaning the materials obtained by mixing the wheat gluten and gelatin mixture with the hardener. The *x* represents the weight ratio of the proteins (%) and takes values from 1 to 5.

After the polymerization (24 h) the samples were extracted from molds and three thermal treatments were applied (8 hours at 60 °C, 2 hours at 80 °C and 1 hour at 90 °C, to ensure a higher value of glass transition of the polymer).

The mechanical tests were performed on an *Instron* testing machine and the conditions for testing was established at a speed of 55 mm/min and the stop condition was set at a 40% drop of the loading force. The applied load was 2 kN for bending and 25 kN for compression test. Samples extraction for the mechanical analysis was performed after the thermal treatment. They have been of 160 mm length ensuring a length of 10 mm as engagement zone.

3. Results and discussion

As it has been previously reported in the literature, amino-acids, inorganic and organic compounds can be used to obtain modified epoxy materials with slightly modified properties [19-21].

The results of mechanical tests showed that the presence of wheat gluten and gelatin mixture inside the matrix had a modification in the compressive and bending response of epoxy resin. The configuration of the epoxy resin-denoted as *E0*, is illustrated in Figure 1. All the curves are the average of five tests performed for each material.

Figures 2 and 3 illustrate the compressive tests results for the polymers obtained by modifying the epoxy resin with the smallest and the highest, amounts of wheat gluten and gelatin mixture.

It can be observed that the compressive behaviour, is characteristic of thermosetting polymers with an area of elasticity below 0.1 mm, which is followed by a compaction area and the force is almost unchanged. Also, the cracking of the specimens was followed by the final tearing of materials.

The compressive modulus of unmodified epoxy (*E0*) reached the highest value while all the organic modified materials showed lower values of the parameter, possibly due to the formation of small defects of the polymer network due to high concentrations of the proteins mixture. By way of consequences, the level of loading transfer in, the compressive tests did not present any modifications regarding the maxim deformation of the material.

One usual way to get superior properties of polymers is to modify them by placing another phase, for instance a nano-sized one, into the polymer volume [22]. Amit *et al.* [23] showed that these materials should provide unique mechanical and thermal properties combined with low specific weight and high wear resistance in order to ensure the safety and economic efficiency.

The behaviour of modified materials with organic agents is almost identical to that of unmodified materials. The significant parameters obtained by the three-point bending testes were found to have similar behaviour (Fig.4 and Fig.5).

THE ANNALS OF "DUNAREA DE JOS" UNIVERSITY OF GALATI
FASCICLE IX. METALLURGY AND MATERIALS SCIENCE
No. 3 - 2020, ISSN 2668-4748; e-ISSN 2668-4756
Article DOI: https://doi.org/10.35219/mms.2020.3.02

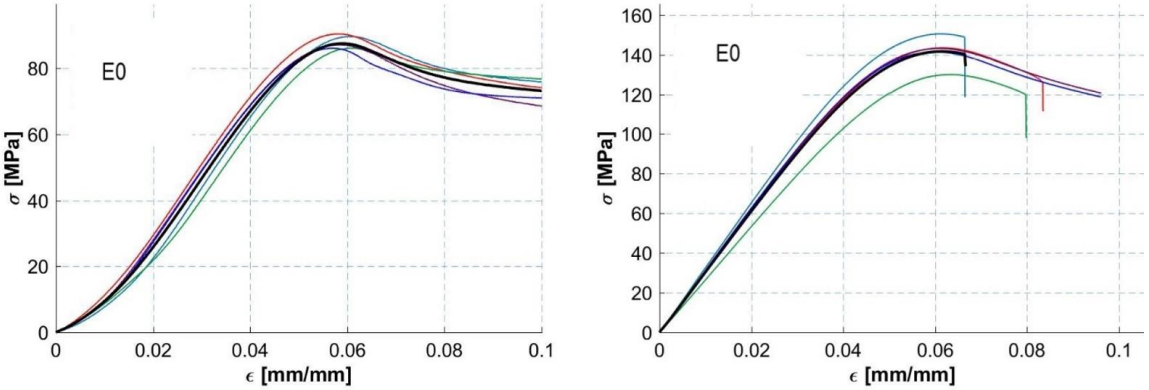

Fig. 1. *Compressive behaviour of epoxy resin (left). Bending modules of epoxy resin (right)*

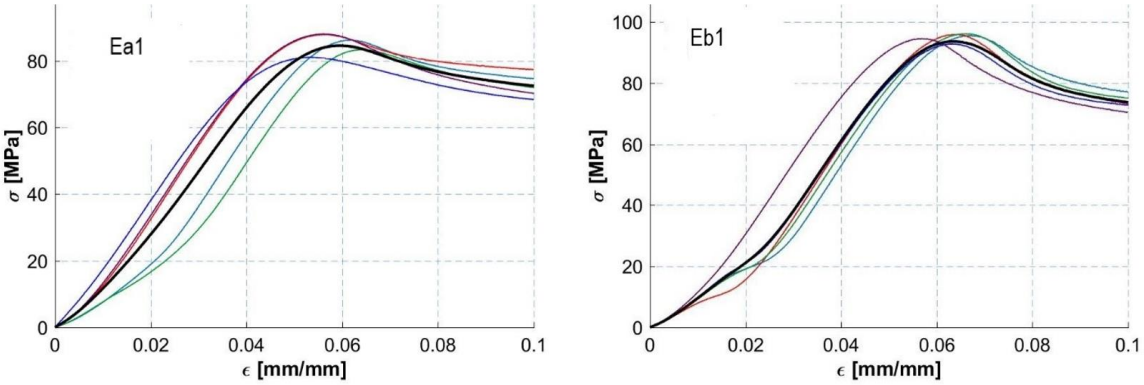

Fig. 2. *Compressive behaviour for the materials with 1% proteins mixture*

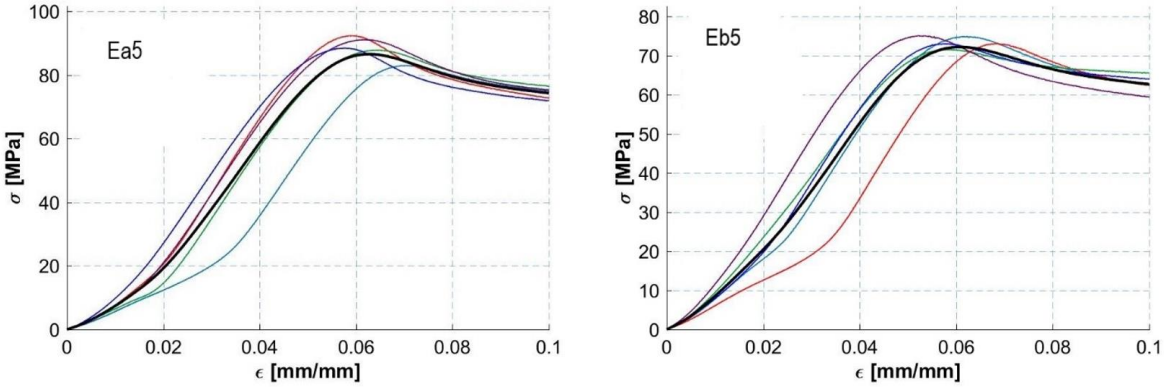

Fig. 3. *Compressive behaviour for the materials with 5% proteins mixture*

THE ANNALS OF "DUNAREA DE JOS" UNIVERSITY OF GALATI
FASCICLE IX. METALLURGY AND MATERIALS SCIENCE
Nº. 3 - 2020, ISSN 2668-4748; e-ISSN 2668-4756
Article DOI: https://doi.org/10.35219/mms.2020.3.02

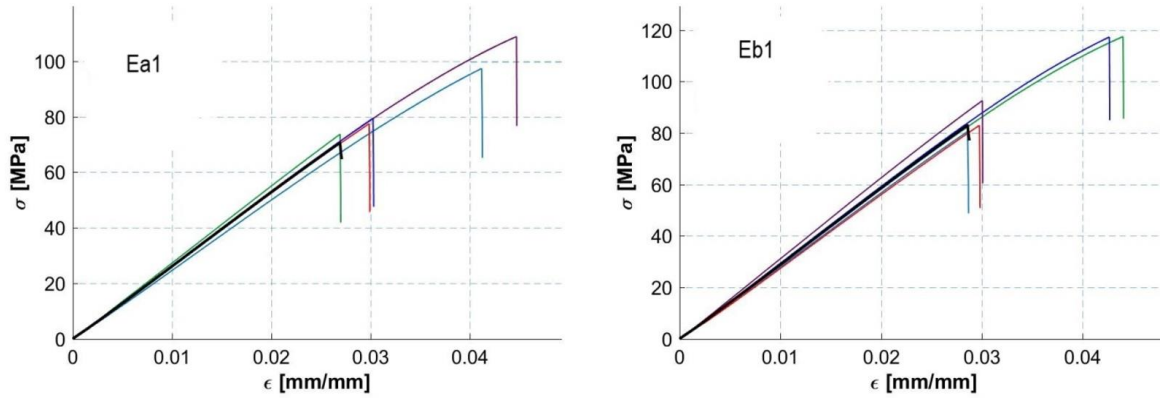

Fig. 4. *Bending modules for the materials with 1% proteins mixture*

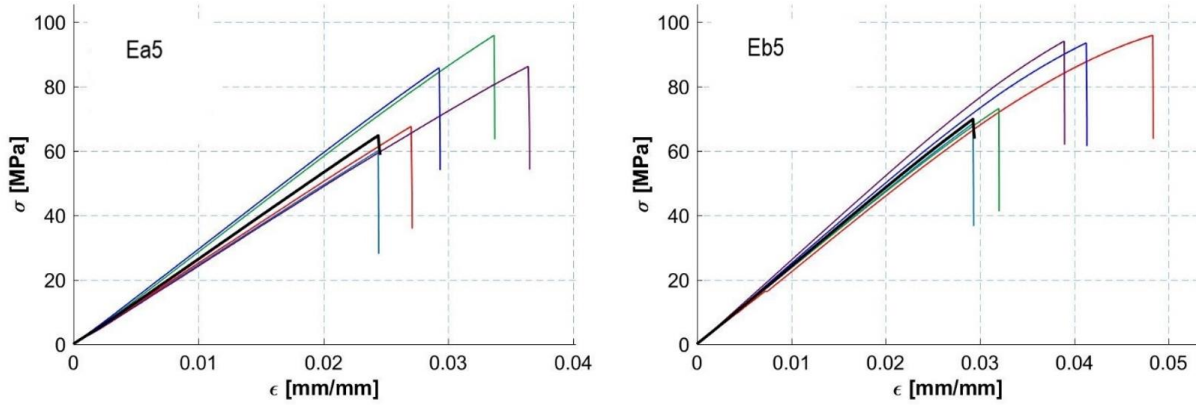

Fig. 5. *Bending modules for the materials with 5% proteins mixture*

Following these tests, the materials practically did not break during the test, demonstrating their elasticity.

For this category of materials, the others, elastic parameters analysed confirmed that the concentration of the modifying agent does not significantly influence the behaviour of the modified materials.

In addition, with the increase of solution of modifying agent concentration the elasticity limit measured during a three-point bending tests of the materials correspondingly decreased. Analysing the bending elastic modulus, it might be noticed that the proteins mixtures ratio has a considerable importance, because with increasing its ratio, the bending elastic modulus decreases.

4. Conclusions

For this study wheat gluten and gelatin had been used as modifying agents. The materials were formed by dispersing the mixture of gelatin and gluten into the resin or into the hardener and the weight ratios of organic compounds into the polymer are from 1% to 5%.

The mechanical analysis presented that the elastic modulus values are decreasing, almost proportionally, with respect to the concentration of both proteins mixtures dispersion cases.

The presence of organic mixture (wheat gluten and gelatin) inside the epoxy resin is not considerably modifying the properties of the polymer. Therefore, it is possible to continue to the next step regarding the functional analysis of the proteins in order to control the polymer sensitive properties. In addition, the modification of epoxy resin with small amounts of organic compounds could lead to an increase of their environmental acceptability.

Acknowledgements

The work of Georgel Mihu was supported by the project ANTREPRENORDOC, in the framework of Human Resources Development Operational Programme 2014-2020, financed from the European Social Fund under the contract number 36355/23.05.2019 HRD OP /380/6/13 – SMIS Code: 123847.

This work has been funded by the European Social Fund through the Sectoral Operational Programme Human Capital 2014-2020, through the Financial Agreement with the title „Burse pentru educaţia antreprenorială în rândul doctoranzilor şi

cercetătorilor postdoctorat (Be Antreprenor!)" (in English: "Scholarships for entrepreneurial education among doctoral students and postdoctoral researchers (Be Entrepreneur!)", Contract no. 51680/09.07.2019 - SMIS code: 124539.

References

[1]. Guduru R. K. R., Shaik S. H., Tuniki H. P., Domeika, A., *Development of mono leaf spring with composite material and investigating its mechanical properties*, Materials Today: Proceedings, https://doi:10.1016/j.matpr.2020.02.289, 2020.

[2]. Shen Y., Cong Y., Zhang B., Lang Q., *Influence on properties of epoxy nanocomposites with nanoparticles modified by surfactants with different molecular structures: liquid crystal, rigid and flexible segment structures*, Materials Research Express, https://doi:10.1088/2053-1591/ab38c9, 2019.

[3]. Yi L., Fei X., Kyoung-sik M., Wong C.P., *Novel Curing Agent for Lead-Free Electronics: Amino Acid*, Journal of Polymer Science: Part A: Polymer Chemistry, Vol. 44, 1020–1027, 2006.

[4]. Chihai R., Ungureanu C., Cojan A, Bîrsan I. G., Cîrciumaru A., *Organic modified epoxy resin. Tribologic aspects*, The 10th International Conference BALTTRIB'2019, https://doi.org/10.15544/balttrib.2019.03, 2019.

[5]. Xu H., Feng Z., Chen J., Zhou H., *Tribological behavior of the polyamide composite coating filled with different fillers under dry sliding*, J. of Applied Polymer Science, 104, p. 2554-2560, 2007.

[6]. Samyn P., Kalacska G., Keresztes R., Zsidai L., De Baets P., *Design of a tribotester for evaluation of polymer components under static and dynamic sliding conditions*, Proceedings of the Institution of Mechanical Engineers, Part J: Journal of Engineering Tribology 221 pp 661-674, 2007.

[7]. DeFrates K., Markiewicz T., Gallo P., Rack A., Weyhmiller A., Jarmusik B., Hu X., *Protein Polymer-Based Nanoparticles: Fabrication and Medical Applications*, International Journal of Molecular Sciences, 19(6), 1717, https://doi:10.3390/ijms19061717, 2018.

[8]. Bălan I., Bosoancă R., Căpăţină A., Graur I., Bria V., Ungureanu C., *A study regarding friction behaviour of lysine and isoleucine modified epoxy matrix*, IOP Conf. Series: Materials Science and Engineering 174.012023 doi:10.1088/1757-899X/174/1/012023, 2017.

[9]. Djagny K. B., Wang Z., Xu S., *Gelatin: a valuable protein for food and pharmaceutical industries: review*, Crit. Rev. Food Sci. Nutr. 41 (6), 481e492, 2001.

[10]. Rapisarda M., Valenti G., Carbone D. C., Rizzarelli P., Recca G., La Carta S., Fincchiaro S., *Strength, fracture and compression properties of gelatins by a new 3D printed tool*, Journal of Food Engineering, 220, p. 38-48. https://doi:10.1016/j.jfoodeng.2017.05.016, 2018.

[11]. Li X., Jiang G., Yang L., Peng S., *Study of gelatin as biodegradable shale hydration inhibitor*, Colloids and Surfaces A: Physicochemical and Engineering Aspects, 539, p. 192-200., https://doi:10.1016/j.colsurfa.2017.12.020, 2018.

[12]. Fabra M. J., Lopez-Rubio A., Lagaron J. M., *Effect of the film-processing conditions, relative humidity and ageing on wheat gluten films coated with electrospun polyhydryalkanoate*, Food Hydrocolloids, 44, p. 292-299, 2015.

[13]. Tom Keenan, Gelatin, *Polymer Science: A Comprehensive Reference Volume* 10, Pages 237-247, 2012.

[14]. Ciapponi R., Turri S., Levi M., *Mechanical Reinforcement by Microalgal Biofiller in Novel Thermoplastic Biocompounds from Plasticized Gluten*, Materials, 12(9), 1476. doi:10.3390/ma12091476, 2019.

[15]. Jin F.-L., Li X., Park S.-J., *Synthesis and application of epoxy resins: A review*, Journal of Industrial and Engineering Chemistry, 29, p. 1-11, doi:10.1016/j.jiec.2015.03.026, 2015.

[16]. Vo Hong N., Van Puyvelde P., Van Vuure A., Verpoest I., *Preparation of biocomposites based on gluten resin and unidirectional flax fibers*, Conference: ECCM15 - 15th European Conference on Composite Materials, 2012.

[17]. Gällstedt M., Mattozzi A., Johansson E., Hedenqvist M. S., *Transport and tensile properties of compression-molded wheat gluten films*, Biomacromolecules 5, p. 2020-2028, 2004.

[18]. ***, http://www.polydis.ro/wp-content/uploads/2014/08/Epiphen-4020.pdf.

[19]. Bîrsan I. G., Andrei G., Ungureanu V., Roman I., Cîrciumaru A., *Wear behavior of fabric reinforced epoxy based composites*, Proceeding of the International Conference BALTTRIB'2009, p. 158-163, 2009.

[20]. Bîrsan I. G., Andrei G., Bria V., Postolache I., Cîrciumaru A., *Tribological behavior of clay/epoxy reinforced epoxy composites*, Proceeding of the International Conference BALTTRIB'2009, p. 154-169, 2009.

[21]. Bîrsan I. G., Cîrciumaru A., Bria V., Ungureanu V., *Tribological and Electrical Properties of Filled Epoxy Reinforced Composites*, Tribology in industry, 31, 1-2, p. 33-36, 2009.

[22]. Bart J. C. J., *Additives in Polymers. Industrial Analysis and Applications*, John Wiley & Sons, 2005.

[23]. Amit C., Muhammad S. I., *Fabrication and characterization of TiO2–epoxy nanocomposite*, Materials Science and Engineering A 487, p. 574-585, 2008.

THE ANNALS OF "DUNAREA DE JOS" UNIVERSITY OF GALATI
FASCICLE IX. METALLURGY AND MATERIALS SCIENCE
N°. 3 - 2020, ISSN 2668-4748; e-ISSN 2668-4756
Article DOI: https://doi.org/10.35219/mms.2020.3.03

CuO FILMS OBTAINED BY OXIDATION OF Cu LAYERS DEPOSITED BY THE PVD PROCESS - MAGNETRON SPUTTERING

Simona BOICIUC
"Dunarea de Jos" University of Galati, Romania
e-mail: simonaboiciuc@yahoo.com

ABSTRACT

The experimental research carried out and described in this paper aimed to obtain thin films from copper oxides and their characterization from the structural point of view and the optical and electrical properties. To obtain the copper films, a PVD spray deposition system was used, consisting of a vacuum chamber with a capacity of 2 liters, a planar magnetron with ferrite magnets (ϕ40x22x9) neodymium (ϕ15x8), a vacuum pump with sliding blades, a variable source of direct current of voltage 100 - 600 volts. The atmosphere used for plasma maintenance during deposition was argon rarefied in a pressure range between $3 \cdot 10^{-2}$ - $8 \cdot 10^{-3}$ mbar. The deposits were made on glass plates. The films thus obtained were subsequently subjected to oxidation at temperatures of 200, 300 and 450 °C. It was found that the transparency of the films increases with the oxidation temperature from $1.464 * 10^{-4}$ for 200 ºC to 0.5 for 450 ºC and the surface electrical resistance also increases from 0.984 Ω for 200 ºC to 3882857,1428 Ω for 450 ºC. With increasing spray power, transparency and surface strength decrease.

KEYWORDS: CuO thin films, d.c. magnetron, electrical and optical properties

1. Introduction

Cupric oxide (CuO) is one of the most studied p-type oxide semiconductors. CuO is a semiconductor with direct transition, with the forbidden band energy in the range of 1.2-1.5 eV, with a monoclinic crystalline structure and characterized by excellent physical and chemical properties. Fig. 1 shows that in the elementary cell of CuO, a copper atom is coordinated by four oxygen atoms in a square plane configuration [1, 2].

The elementary cell contains four CuO units and is indicated by the parallelepiped. The oxygen atoms are light gray and the copper atoms are dark gray. The network parameters of the elementary cell are: a = 4.6837 (5), b = 3.4226 (5), c = 5.1288 (6), α = 90°, β = 99.54 (1) °, γ = 90° [1].

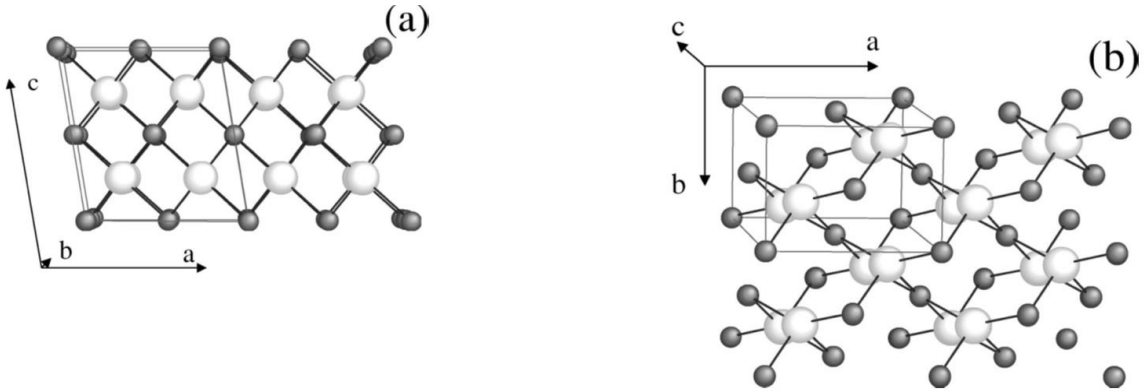

Fig. 1. *The crystalline structure of CuO* [1]

THE ANNALS OF "DUNAREA DE JOS" UNIVERSITY OF GALATI
FASCICLE IX. METALLURGY AND MATERIALS SCIENCE
Nº. 3 - 2020, ISSN 2668-4748; e-ISSN 2668-4756
Article DOI: https://doi.org/10.35219/mms.2020.3.03

The CuO nanostructured materials, especially the 1D - CuO nanowires, have enjoyed special attention, being already applied in the field of field effect transistors, photovoltaic cells, field emission Nano devices, as well as in the field of gas sensors [7].

Documentary studies have shown that different nanostructured CuO morphologies can be obtained such as: nanowires, nanowands, nanoplates, nanocureas, nanowhiskers [7].

Cu forms two types of thermodynamically stable oxides CuO and Cu_2O.

Cu_2O (copper oxide) has a cubic crystalline structure and has a forbidden band energy of 2-2.2 eV. It is a p-type semiconductor, which has a variable optical behavior due to stoichiometric deviations arising from the methods and parameters of obtaining.

Cu_2O films have a high transparency, a slightly yellowish appearance and usually absorb at wavelengths below 600 nm, while CuO (cupric oxide) absorbs strongly along the visible spectrum and is black in appearance [2].

CuO films can be obtained by different methods, such as: electrodeposition, sol-gel method, hydrothermal method, pyrolysis with sprayers, chemical vapor deposition, physical vapor deposition (thermal evaporation, sputtering), thermal oxidation.

Physical vapor deposition by magnetron sputtering is used in applications aimed at obtaining layers with multifunctional properties: hard, wear-resistant, with a low coefficient of friction, with high corrosion resistance and with specific optical and electrical properties [2-6].

The method of thermal oxidation is simple, non-polluting, has a low cost and is quite little used. It involves the deposition of a thin layer of Cu by the magnetron-assisted PVD process and its oxidation in an oven at different temperatures.

The research undertaken in this paper aimed to obtain thin copper films using magnetron sputtering process followed by thermal oxidation at different temperatures and their characterization in terms of morphology, electrical and optical properties.

2. Experimental conditions

To obtain the Cu films, a copper plate of 99.9% purity, circular with a diameter of 46.5 mm and a thickness of 1 mm was used as a target.

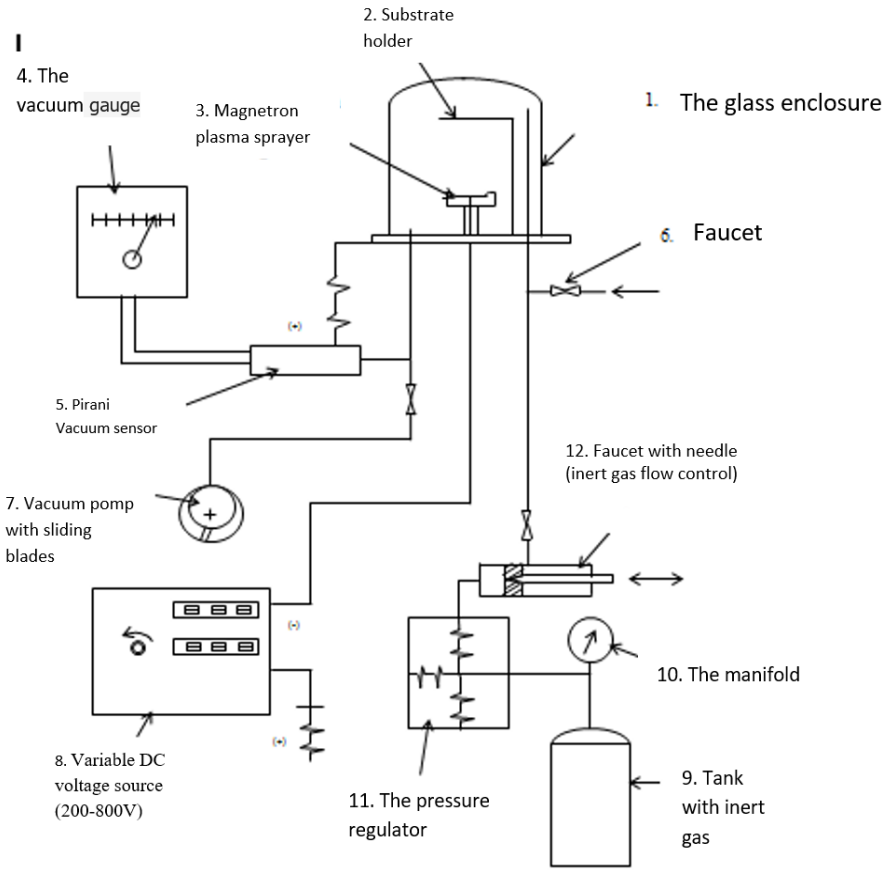

Fig. 2. *Diagram of the PVD magnetron sputtering system*

THE ANNALS OF "DUNAREA DE JOS" UNIVERSITY OF GALATI
FASCICLE IX. METALLURGY AND MATERIALS SCIENCE
Nº. 3 - 2020, ISSN 2668-4748; e-ISSN 2668-4756
Article DOI: https://doi.org/10.35219/mms.2020.3.03

We used a PVD spray deposition system, consisting of a vacuum chamber with a capacity of 2 liters, a planar magnetron with ferrite magnets (ϕ 40x22x9) neodymium (ϕ 15x8), a vacuum pump with sliding blades, a variable DC voltage source 100 - 600 volts. The scheme of the installation is shown in Fig. 2.

The deposits were made on glass plates, measuring 76x25x1 mm, which were subjected to an ultrasonic cleaning with acetone and ethanol, and finally they were rinsed with distilled water and then dried.

The installation allows the variation of the magnetron deposition substrate distance between 25 and 90 mm, and the substrate temperature can be monitored with a chromel - alumel thermocouple.

The atmosphere used for plasma maintenance during deposition was argon rarefied in a pressure range between $3 \cdot 10^{-2}$ - $8 \cdot 10^{-3}$ mbar.

A series of regimes shown in Table 1 were used to obtain the films.

Oxidation of the copper films was performed by heating them to 200 °C, 300 °C to 450 °C for 1/2 h.

Before and after oxidation, each sample was subjected to transparency and electrical resistance measurements.

The microscopic analysis of the obtained films was performed using a Neophot 2 optical microscope with computerized data acquisition.

The transparency of the films was determined using an electronic device that uses a light source and a photoreceptor. The light after passing through the deposited film is measured with the help of a photoreceptor and an amplifier and the result is displayed with an analog device.

Table 1. *Regimes for obtaining the copper films*

Sample code	Voltage [V]	Current [mA]	Pressure [mbar]	Substrate temperature [ºC]	Target distance - substrate [mm]	Deposition time [min]
1	485	100	$4x10^{-2}$	70	60	15
2	470	110	$5x10^{-3}$	68	60	10
3	470	100	$5x10^{-3}$	74	85	10
4	470	100	$5x10^{-3}$	60	85	10
5	470	100	$5x10^{-3}$	65	85	10

The electrical properties (resistivity) of the films were determined using the method of the four collinear points (probes), using a laboratory installation. As a principle it consists in injecting the current through two external points and measuring the voltage in two internal points.

In the case of thin layers, the resistivity is calculated with the relation:

$$\rho = \frac{\pi \cdot t}{\ln 2}\left(\frac{U}{I}\right)$$

where: t - layer thickness, U - measured voltage, I - applied current;

$\rho = \frac{\pi \cdot t}{\ln 2}\left(\frac{U}{I}\right)$ - represents the surface resistance of the film.

3. Results and discussions

Following the microscopic analysis, it was observed that the copper films obtained are glossy, have no cracks, are homogeneous and adherent, have a reddish colour and have a low roughness as it can be seen in Fig. 3.

The results of the transparency and electrical resistance measurements are presented in Table 2.

Corresponding to the temperature at which the oxidation took place, the structure of the samples was formed as follows [2-4, 8, 9]:

- for samples 1, 2, 3, oxidized at a temperature of 450 ºC, it is made of CuO;
- for sample 4 with the oxidation temperature of 200 ºC from Cu_2O + Cu, so there is a partial oxidation highlighted by a color different from that obtained at a temperature of 450 ºC;

THE ANNALS OF "DUNAREA DE JOS" UNIVERSITY OF GALATI
FASCICLE IX. METALLURGY AND MATERIALS SCIENCE
Nº. 3 - 2020, ISSN 2668-4748; e-ISSN 2668-4756
Article DOI: https://doi.org/10.35219/mms.2020.3.03

➢ for sample 5 where the oxidation temperature was 300 ºC the structure contains Cu_2O + CuO

Figure 4 shows the appearance of copper films for samples 1, 2, 3, oxidized at 450 °C, 1/2 h, as well as for samples 4, 5, oxidized at 200 °C, respectively 300 °C for 1/2 h.

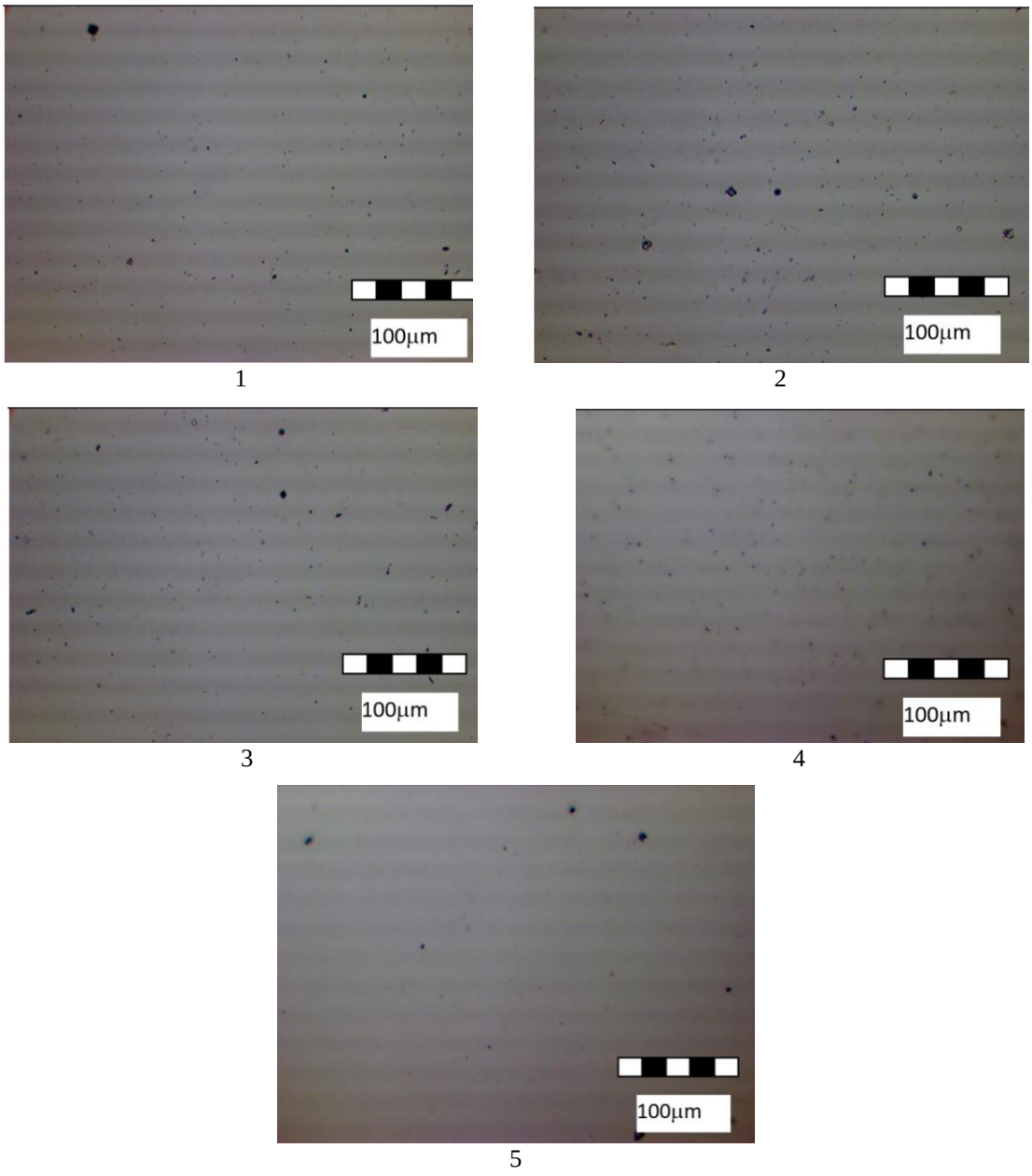

1 2 3 4 5

Fig. 3. *Micrographs of the deposited Cu films*

Analyzing Table 2 it is observable that in all films subjected to oxidation the transparency and surface resistance increase, more accentuated at a temperature of 450 ºC, and at temperatures lower than this value the increases are much smaller. This is due to the partial oxidation of the deposited copper films as well as the formation of different structures which consist of CuO in sample 3, Cu_2O+Cu in sample 4 and Cu_2O+CuO in sample 5 characterized by other properties.

The dependence of the conductive behavior of temperature CuO films leads to potential applications in the chemical industry and gas sensors.

It was found that with increasing spray power, due to improved mobility of pulverized atoms and increased energy of adsorbed atoms, there is an intensification of nucleation and growth processes

THE ANNALS OF "DUNAREA DE JOS" UNIVERSITY OF GALATI
FASCICLE IX. METALLURGY AND MATERIALS SCIENCE
No. 3 - 2020, ISSN 2668-4748; e-ISSN 2668-4756
Article DOI: https://doi.org/10.35219/mms.2020.3.03

which increases the crystallinity of the film and changes its characteristics, respectively decreasing transparency and strength (samples 2,3).

To study the kinetics of the transformation of metallic Cu into oxide, sample 5 was oxidized at 300 °C in several stages (1/2 h per stage), with a total time of 2 h. The results are shown in Tables 3 and 4.

Analysing Tables 3 and 4 it is obvious that in the case of oxidation at low temperatures a longer oxidation time is required to obtain the required electrical and transparency characteristics.

This may be due to changes in the structure and morphology of the oxidized films.

Table 2. *Determination of transparency and electrical properties of Cu films subject to oxidation*

Sample code	Initial transparency	Final transparency	Initial resistance [Ω]	Resistance after oxidation [Ω]
1	$3.906*10^{-3}$	0.437	0.7	483200
2	$2.929*10^{-4}$	0.25	0.697	198996.43
3	$3.662*10^{-4}$	0.5	0.454	3882857.1428
4	-	$1.464*10^{-4}$	0.7	0.984
5	-	0.0132	0.503	1.647

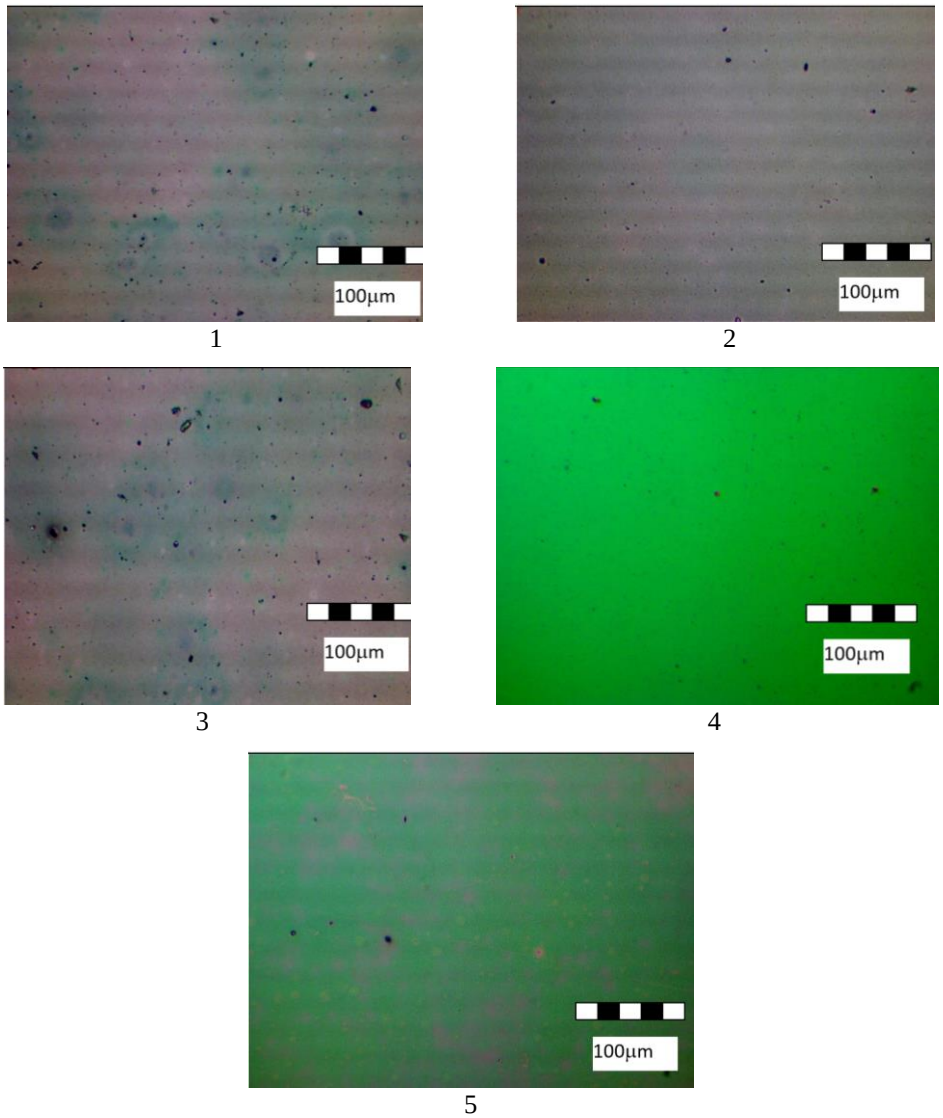

1 2 3 4 5

Fig. 4. *Micrographs of Cu films deposited and oxidized at different temperatures*

THE ANNALS OF "DUNAREA DE JOS" UNIVERSITY OF GALATI
FASCICLE IX. METALLURGY AND MATERIALS SCIENCE
Nº. 3 - 2020, ISSN 2668-4748; e-ISSN 2668-4756
Article DOI: https://doi.org/10.35219/mms.2020.3.03

Table 3. *Kinetics of Cu into oxide transformation*

Sample 5	Oxidation stages at 300 ºC				
	Initial status	I	II	III	IV
Transparency [%]	-	0.0132	1	2	2
Time [h]	0	1/2 h	1 h	1and 1/2 h	2 h

Table 4. *Kinetics of Cu into oxide transformation*

Sample 5	Oxidation stages at 300 ºC				
	Initial status	I	II	III	IV
Surface resistance [Ω]	0.503	1.647	51.46	1101041.7	2613461.5
Time [h]	0	1/2h	1h	1and 1/2h	2h

4. Conclusions

Following the experimental research, the following conclusions can be highlighted:

- The method of spraying copper in magnetron regime has a series of advantages such as: high deposition speed, obtaining films with high purity and homogeneity, high adhesion, high precision in controlling the thickness and size of grains;
- Due to the high electrical and thermal conductivity and a relatively high melting temperature, the copper deposits are intended for the realization of high-performance integrated circuits;
- The structures and properties of the obtained films depend on the sputtering power (voltage, current intensity), duration, target distance - substrate, substrate temperature;
- Following the microscopic analysis, it was observed that the obtained films showed no cracks, are homogeneous and adherent with a mirror surface;
- with the increase of the sputtering power (increase of the current and voltage) there is an increase of the film thickness;
- with the increase of the deposition time there is an increase of the film thickness and of the grain size (which can lead to the increase of the roughness); grain size is important in the case of semiconductors because it influences the size of the forbidden band and the physical properties;
- the deposition speed decreases with the increase of the distance from the target, thus determining both the decrease of the film thickness and the increase of its transparency;
- the transparency of the obtained films increased at all samples subjected to oxidation, this varying between 1,464 * 10^{-4} for oxidation at the temperature of 200 ºC and 0.5 for the oxidation temperature of 450 ºC; this is due to the change in the structure of the film following oxidation;
- the surface resistance increases after oxidation, the more accentuated the higher the oxidation temperature; it varies between 0.984 Ω for the oxidation temperature of 200 ºC and 3882857,1428 Ω for oxidation at the temperature of 450 ºC;

The modification of the conductive behavior with temperature of the obtained films is recommended in applications in the chemical industry and gas sensors.

References

[1]. Kuz'menko A. B., van der Marel D., van Bentum P. J. M., Tishchenko E. A., Presura C., Bush A. A., *Infrared spectroscopic study of CuO: Signatures of strong spin-phonon interaction and structural distortion*, The American Physical Society, Physical Review B, vol. 63, 094303-1–094303-15, 2001.

[2]. Ogwu A. A., Darma T. H., Bouquerel E., *Electrical resistivity of copper oxide thin films prepared by reactive magnetron sputtering*, Journal of Achievements in Materials and Manufacturing Engineering, vol. 24, issue 1, September 2007.

[3]. Mech K., Kowalik R., Zabinski P., *Cu thin films deposited by dc magnetron sputtering for contact surfaces on electronic components*, Archives of metallurgy and materials, issue 4, 2011.

[4]. Cheng S. L., Chen M. F., *Fabrication, characterization, and kinetic study of vertical single-crystalline CuO nanowires on Si substrates*, Nanoscale Research Letters 7:119, p. 1-7, 2012.

[5]. Ali Gelali1, Azin Ahmadpourian, Shahoo Valedbagi, Behroz, Safibonab, Bandar Astinchap, Eisa Karimzadeh, *Structure and Morphology of the Cu Films Grown by DC Magnetron Sputtering*, Journal of Basic and Applied Scientific Research, November 2013.

[6]. Minh-Tung Le, Yong-Un Sohn, Jae-Won Lim, Good-Sun Choi, *Effect of Sputtering Power on the Nucleation and Growth of Cu Films Deposited by Magnetron Sputtering*, Materials Transactions, vol. 51, no. 1, p. 116-120, 2010.

[7]. Viorica Muşat, *Filme subţiri multifuncţionale*, Editura CERMI Iaşi, 20, p. 33-59, 2005.

[8]. Papadimitropoulos G., Vourdas N., Em Vamvakas V., Davazoglou D., *Deposition and characterization of copper oxide thin films*, Journal of Physics: Conference Series 10, 2005.

[9]. Figueiredo V., Elangovan E., Goncalves G., Barquinha P., Pereira L., *Effect of post-annealing on the properties of copper oxide thin films obtained from the oxidation of evaporated metallic copper*, Applied Surface Science, vol. 254, issue 13, Publisher: Elsevier Science BV, p. 3949-3954, 2008.

THE ANNALS OF "DUNAREA DE JOS" UNIVERSITY OF GALATI
FASCICLE IX. METALLURGY AND MATERIALS SCIENCE
N°. 3 - 2020, ISSN 2668-4748; e-ISSN 2668-4756
Article DOI: https://doi.org/10.35219/mms.2020.3.04

STUDIES AND RESEARCH ON THE CORROSION BEHAVIOR OF Ni-Al_2O_3 COMPOUND COATINGS OBTAINED BY ELECTROCHEMICAL METHODS

Simona BOICIUC
"Dunarea de Jos" University of Galati, Romania
e-mail: simonaboiciuc@yahoo.com

ABSTRACT

The undertaken research which is described in this paper aims at the corrosion behaviour of composite coatings in nickel matrix using as dispersed phase technical alumina with dimensions of 5 µm and their characterization from a microstructural point of view. The corrosion resistance in the saline fog of the coatings is influenced by the microstructure, the stresses developed in the layer and the roughness.

KEYWORDS: Ni composite coatings, electrodeposition, Al_2O_3

1. Introduction

The field of composite coatings remains a top field in science and technology, currently experiencing great diversification in terms of categories of protected materials (metals, plastics, ceramics, wood or textiles) and the nature / complexity of coatings and technologies used in their application.

The electrochemical deposition of nickel is used as it improves the resistance to corrosion, oxidation and wear at high temperatures, modifies magnetic properties, ensures the reconditioning of worn or dimensionally improper parts, prepares the surface for other types of (organic or enamelled) coatings, constitutes barriers of diffusion in electronic applications.

Electrochemical deposits of nickel and nickel matrix composites are used for decorative purposes in various branches of engineering because the properties of the obtained layers can be varied by controlling the chemical composition of the bath and the deposition parameters.

They are applied in the machine building industry, the chemical industry, the nuclear industry, in telecommunications, for electronic consumables, and in the IT industry.

Over time, several mechanisms for the formation of composite coatings have been proposed. Thus, Guglielmi views the deposition process as a succession of two stages: the solid particles surrounded by the cloud of ions (cations) are transferred, adsorbed on the cathode surface due to Van der Waals forces, and the second stage involves the strong adsorption of these particles at the cathode due to the Coulomb forces developed at the interface with the support.

A frequently accepted model is the one proposed by Kurozaki which involves the transport of particles from the solution to the cathode surface by stirring. The model comprises three steps [1]:

- the uniformly dispersed particles are transported to the double electric layer by mechanical agitation;
- the charged particles are transported to the cathode surface by electrophoresis;
- the solid particles are adsorbed on the cathode surface due to the Coulomb forces developed between the particles and adsorbed anions, followed by their incorporation and growth at the interface with the support.

Another mechanism [2] assumes that a series of complex phenomena take place at the electrode - electrolyte interface. The electrodeposition processes are considered to take place in several stages: mass transport of the electroactive metallic ionic species to the cathode surface; adsorption on the cathode surface; discharge reaction at the cathode surface (charge transfer); surface diffusion of formed atoms and incorporation into the crystal lattice. The nucleation and growth of the crystal can be added to these steps.

Alumina is used as a dispersed phase to obtain composite materials due to its properties: high melting point, hardness, high thermal conductivity and electrical resistivity, high chemical resistance (it

THE ANNALS OF "DUNAREA DE JOS" UNIVERSITY OF GALATI
FASCICLE IX. METALLURGY AND MATERIALS SCIENCE
Nº. 3 - 2020, ISSN 2668-4748; e-ISSN 2668-4756
Article DOI: https://doi.org/10.35219/mms.2020.3.04

is attacked only by molten hydroxides and alkaline bisulfates and phosphoric acid) [3].

The researches undertaken in this paper aim at the corrosion behaviour of some composite coatings in nickel matrix using as dispersed phase technical alumina with dimensions of approx. 5 µm and their characterization from the microstructural point of view and of the corrosion resistance.

2. Experimental conditions

To obtain nickel coatings and nickel matrix composite coatings, a direct current source, a device provided with a magnetic stirrer and a bath temperature control system as well as an electrolyte container were used. We worked with a solution volume of 300 ml, and the experiments took place at temperatures of 50 ºC.

Watts electrolytes consisting of $NiSO_4 \cdot 6H_2O$ – 300 g/L, $NiCl_2 \cdot 6H_2O$ - 50 g/L and H_3BO_3 – 40 g/L, pH = 4.5, current density of 4 A/dm^2, a concentration of the dispersed phase of 20 g/L, stirring speed of 300 rpm, with deposition times of 60, 90, 120 minutes were used.

The electrodepositions were made by the vertical arrangement of the electrodes at a distance of 14 mm from each other. High purity nickel (99%) was used as an anode, the cathode being made of copper strip, representing the support material for deposits with dimensions of 76x20x1 mm.

The copper strip used was prepared by degreasing (organic solvents - trichlorethylene), pickling (HNO_3 + HCl at room temperature for 1-2 minutes) followed by washing with distilled water.

The metallographic analysis of the samples was performed on a Neophot 2 microscope, with the acquisition of data on the computer and highlighted the appearance of the nickel deposition surface compared to composite coatings, their adhesion, how the electrodeposited crystals grew and the presence of defects such as pores, cracks, and exfoliation.

The qualitative analysis of the surface profile was performed using the Neophot 2 microscope and Image J software.

The corrosion behavior in the salt mist of the composite layers was performed according to ISO 9227/2012 for a period of 96 hours. To perform the test, the sodium chloride solution was prepared by dissolving in distilled water, with a conductivity less than or equal to 20 µS/cm^2 at 25 ± 2 ºC, a quantity of sodium chloride, in order to obtain a concentration of 50 ± 5 g/L. The relative density of a solution with this concentration is between 1.00255 and 1.0400. The pH of the saline solution was adjusted so that the pH of the solution collected in the spray chamber was between 6.5 and 7.2. It was measured with a pH meter HI 991001, produced by "Hanna Instruments", also provided with a temperature indicator.

3. Experimental results

Following the microscopic analysis performed on the nickel coatings subject to corrosion in saline fog, it could be found that the best behavior was the P2 sample obtained at a deposition time of 90 minutes. The P3 sample obtained at a deposition time of 120 minutes showed a lower corrosion resistance due to obtaining a higher roughness, as can be seen in Fig. 2. As the deposition time increases, the thickness if the residual stresses in it can either increase, influencing the corrosion resistance or decrease.

The presence of a localized corrosion (points) can be observed, this manifesting itself first in the sections with non-uniformities or imperfections resulting from the bath or from the increase of the coating layer. It then spreads along the paths formed by these defects. A peculiarity of this form of corrosion is the fact that on the metal surface may also appear active points, besides the intact passive areas, without protective film, i.e. areas with very low anodic current densities (wide cathodic areas) and other limited areas with higher values of the current density (anodic areas).

If corrosion products accumulate in the pores or under cover, due to the fact that they have a larger volume in relation to the volume of metal from which they come as a result of the attack, the exfoliation of the coating may occur.

The microscopic analysis performed on electrochemically obtained composite coatings with nickel matrix using as dispersed phase Al_2O_3 particles subject to corrosion in salt mist showed that the best corrosion behavior was presented by the P6 sample obtained at a time of deposition of 120 minutes. This showed a higher passivation compared to the other samples and a low roughness, as can be seen in Fig. 2. The P4 sample obtained at a deposition time of 60 minutes showed a low corrosion resistance, this having a lower thickness and a higher roughness, as can be seen in Fig. 2.

The presence of dispersed phase particles led to changes in the growth mechanism of nickel crystals favoring nucleation. This results in a finer structure than pure nickel coatings with better mechanical properties and good corrosion behavior. Alumina particles act as a barrier against the movement of dislocations through the nickel matrix, and by accumulating at the grain boundary leads to increased hardness and residual stresses.

The corrosion rates resulting from the salt mist test on pure nickel coatings and nickel matrix composite coatings using Al_2O_3 particles as the dispersed phase can be seen in Fig. 3.

THE ANNALS OF "DUNAREA DE JOS" UNIVERSITY OF GALATI
FASCICLE IX. METALLURGY AND MATERIALS SCIENCE
Nº. 3 - 2020, ISSN 2668-4748; e-ISSN 2668-4756
Article DOI: https://doi.org/10.35219/mms.2020.3.04

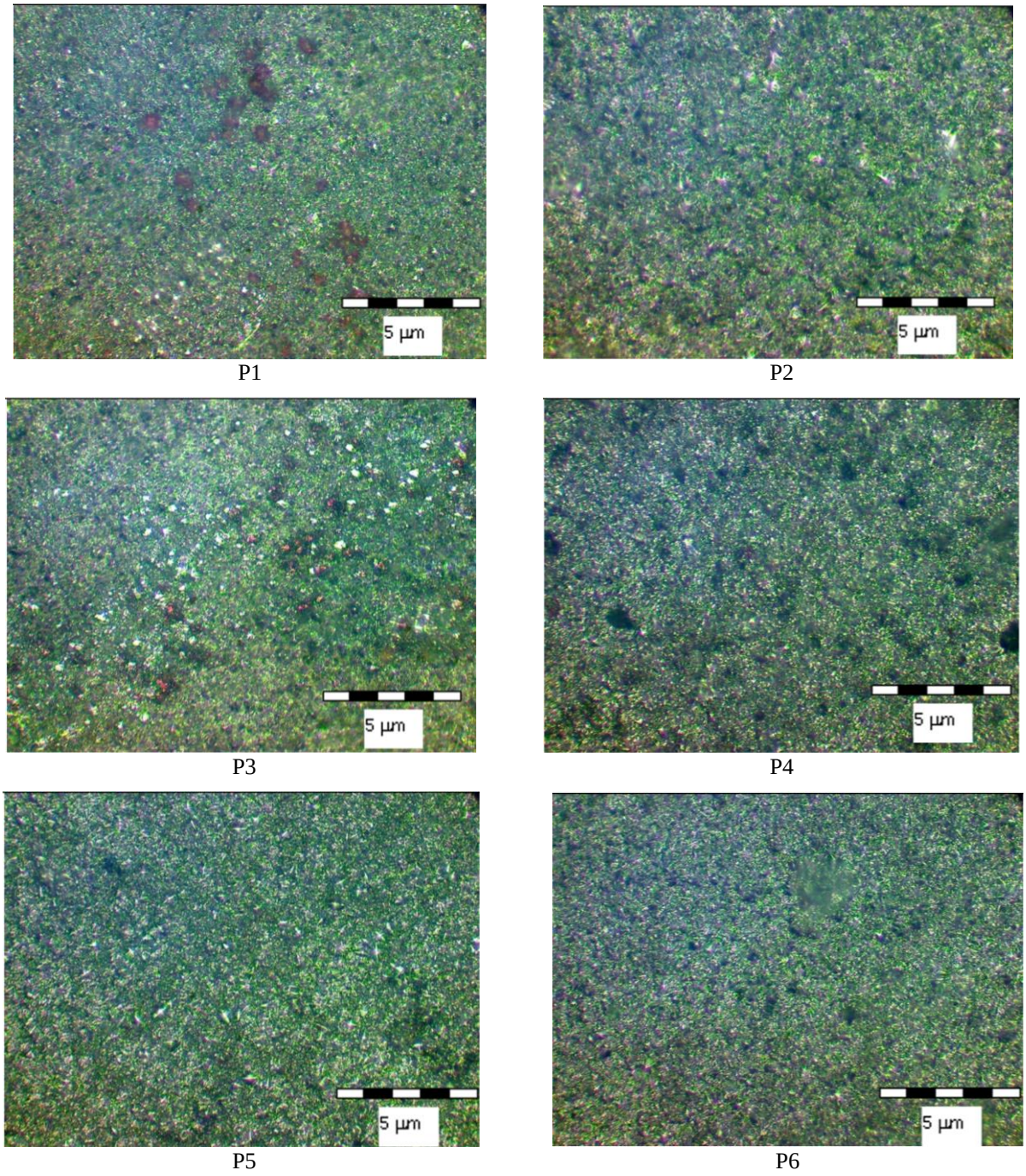

Fig. 1. *Microstructure of pure nickel coatings P1 - 60 minutes, P2 - 90 minutes, P3 - 120 minutes and of composite coatings P4 - 60 minutes, P5 - 90 minutes and P6 - 120 minutes*

Analyzing Fig. 3, it the composite coatings can be seen to have a higher passivation, and thus, a better corrosion resistance, compared to pure nickel coatings. Among the pure nickel coatings, the best corrosion compote was presented by sample P2, and in the case of composite coatings, sample P6.

THE ANNALS OF "DUNAREA DE JOS" UNIVERSITY OF GALATI
FASCICLE IX. METALLURGY AND MATERIALS SCIENCE
Nº. 3 - 2020, ISSN 2668-4748; e-ISSN 2668-4756
Article DOI: https://doi.org/10.35219/mms.2020.3.04

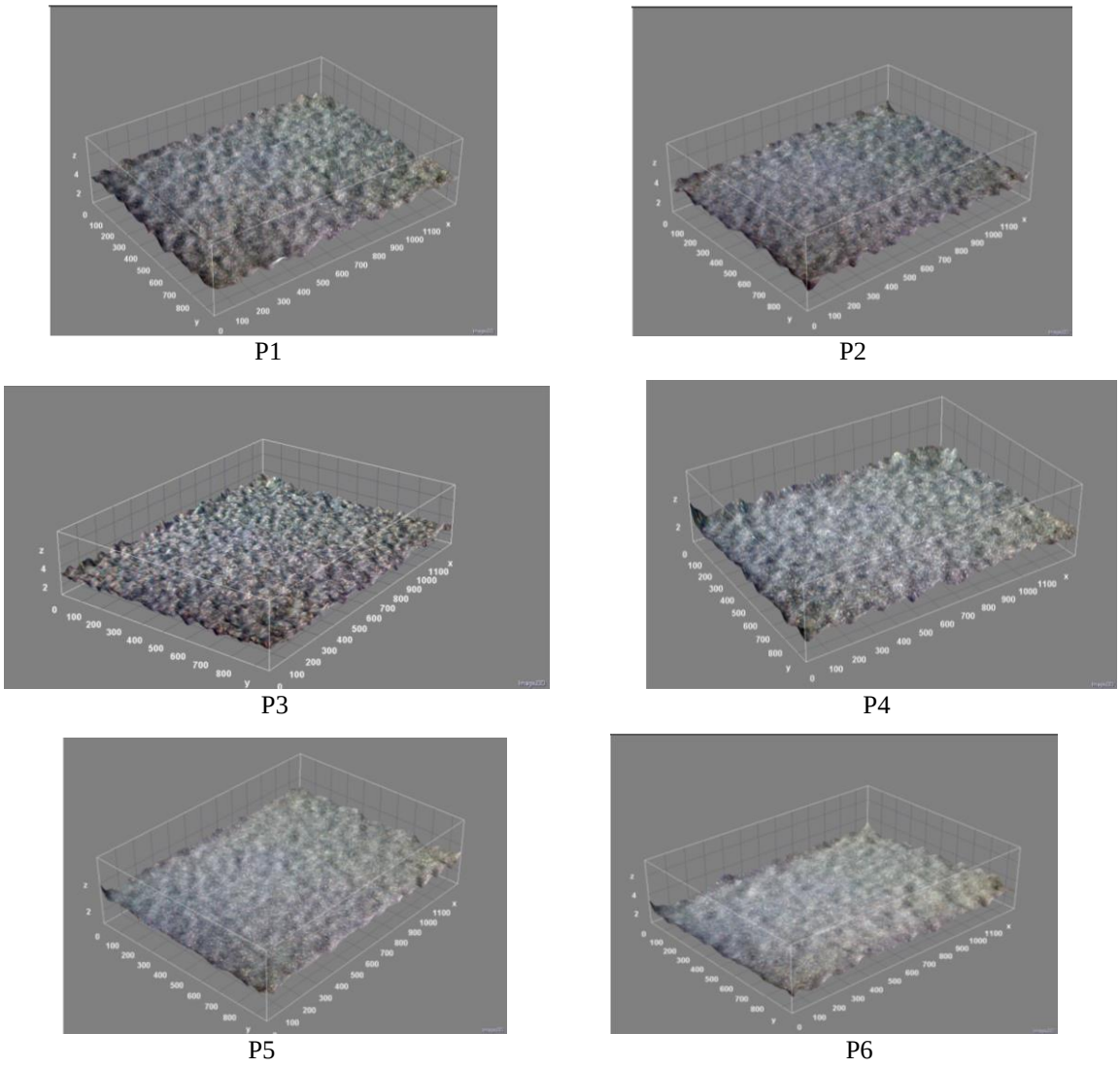

Fig. 2. *Images of the surface profile for pure nickel coatings subjected to corrosion P1 - 60 minutes, P2 - 90 minutes, P3 - 120 minutes and of composite coatings P4 - 60 minutes, P5 - 90 minutes and P6 - 120 minutes*

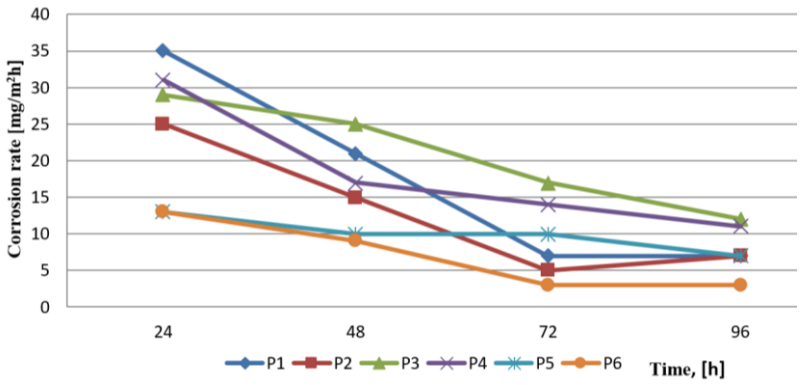

Fig. 3. *Corrosion behavior of pure nickel coatings P1 - 60 minutes, P2 - 90 minutes, P3 - 120 minutes and of nickel matrix composite coatings using Al_2O_3 particles as dispersed phase P4 - 60 minutes, P5 - 90 minutes and P6 - 120 minutes*

THE ANNALS OF "DUNAREA DE JOS" UNIVERSITY OF GALATI
FASCICLE IX. METALLURGY AND MATERIALS SCIENCE
Nº. 3 - 2020, ISSN 2668-4748; e-ISSN 2668-4756
Article DOI: https://doi.org/10.35219/mms.2020.3.04

4. Conclusions

Further to the experimental research, the following conclusions can be drawn:

- The corrosion resistance in salt mist of pure nickel coatings and nickel matrix composite coatings using Al_2O_3 particles as dispersed phase is influenced by microstructure, the stresses developed in the layer and roughness.

- As the deposition time increases, the thickness of the pure nickel coatings increases, the value of the residual stresses develops in the layer and the roughness. These aspects can have the effect of reducing corrosion resistance.

- As the roughness increases, the corrosion resistance decreases.

- Compared to pure nickel deposits, the presence of complementary phase particles led to changes in the mechanism of growth of crystals in the nickel matrix, and to a decrease in crystallites, respectively, favoring nucleation, which led to finer structures and reduced roughness. These changes resulted in the improvement of the composite coatings, which showed a higher passivation.

- The presence of Al_2O_3 particles acts as a barrier against the movement of dislocations through grains, and the accumulation at the grain limit determines the increase of residual stresses, respectively the increase of resistance to deformation. As the residual stresses in the layer increase, the susceptibility to corrosion increases.

The corrosion observed in pure nickel and electrochemically deposited composite layers is a localized one (in points), that usually is caused by chlorine ions, which manifests itself around such defects as pores, bath inclusions or micro-cracks caused by internal stresses.

References

[1]. Tushar Borkar, *Electrodeposition of nickel composite coatings*, Mumbai University India, 2007.
[2]. Cârâc G., Ştefan C. S., *Electrochimie – Principii fundamentale şi aplicaţii*, Galaţi, 2012.
[3]. Muşat V., *Ceramică aavansată*, Editura tehnică, Bucureşti, 2001.
[4]. Boiciuc S., Alexandru P., *Studies and Researches Regarding the Obtain and Characterization of Composite Nickel Coatings-Ni/Al_2O_3, Ni/Kaolin Electrochemically Produced*, The Annals of "Dunărea de Jos" University of Galati, Fascicle IX, Metalurgy and Materials Science, ISSN 1453-083X, no. 3, p. 26-35, 2016.
[5]. Boiciuc S., *Studies and researches on obtaining electrochemical composite coatings in nichel - ni / kaolin matrix*, The Annals of "Dunarea de Jos" University of Galati, Fascicle IX, Metalurgy and Materials Science, ISSN 1453-083X, September, 1/2018.

THE ANNALS OF "DUNAREA DE JOS" UNIVERSITY OF GALATI
FASCICLE IX. METALLURGY AND MATERIALS SCIENCE
No. 3 - 2020, ISSN 2668-4748; e-ISSN 2668-4756
Article DOI: https://doi.org/10.35219/mms.2020.3.05

BED FRAME FABRICATION FOR HEAVY DUTY MACHINE TOOLS OR UNIQUE OF HIGH STRENGHT MATERIALS QUEND 700

Claudiu Ioan RUSAN, Cornel CIUPAN
Technical University of Cluj-Napoca, Faculty of Machine Building, Cluj-Napoca, Romania
e-mail: rusan.claudiu@comelf.ro, cornel.ciupan@muri.utcluj.ro

ABSTRACT

The purpose of the present work is to present new manufacturing technologies process of bed frame elements, especially those with a circular or conical section, made of high strength materials, new on the market. The research based on three methods to make this bed frame elements: cold deformation method, hot deformation method and cold deformation method after soft annealing. Experimental research is focused on how the steel behaves at high temperatures, in identifying an adequate improvement treatment for parts after soft annealing, to increase the mechanical properties of this and preparation of the welding procedure specification.

KEYWORDS: high strength steel, cold and hot deformation, metal rolling, welding

1. Introduction

This theme falls into the field of engineering sciences and materials sciences, aiming to identify new technologies and solutions for the construction of specific machine tool parts, such as base of structures, bed frames, columns, etc and unique large size parts.

The purpose pursued by this work is to provide solutions to reducing the masses, reducing material consumption, lowering costs and manufacturing time by using high strength steel products on the market.

Each machine tool has a certain constructive form, dictated by the size and configuration of the workpieces, the size of the stresses produced by the cutting forces and several requirements: functional, ergonomic, and aesthetic. The most important part, which mostly ensures the shape of the machine tool is the frame, because the parts or component subassemblies of the machine tools are mounted on the frame, with their freedom to perform relative or fixed movements.

The materials used in the construction of the frames must ensure good thermal conductivity, high corrosion resistance and adequate mechanical strength. The frames can be made in various variants, such as the following materials: gray cast iron, malleable cast iron, globular cast iron, alloy cast iron and steel, but they can also be made of welded construction of sheet metal, laminated profiles, etc. Steel, in the construction of frames, is recommended for those who work with high cutting forces, shocks and vibrations [1].

The resistance conditions influence the constructive form of the bed frames by the idea that it must ensure:

- high rigidity to exclude elastic deformations that occur during machining process but also to ensure the part, a dimensional accuracy according to the requirements;
- adequate resistance to vibration to ensure higher quality surfaces [2].

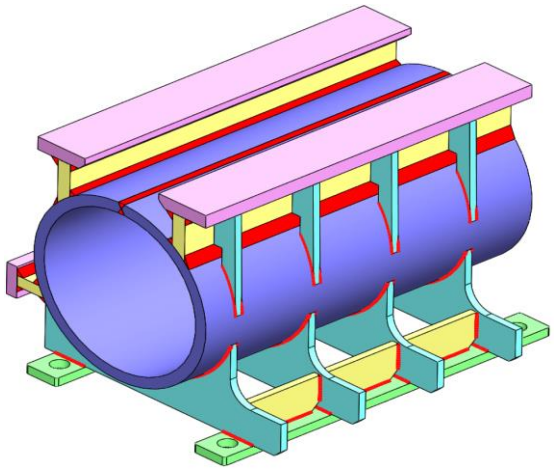

Fig. 1. *Rectangular profile bed frame with circular section*

THE ANNALS OF "DUNAREA DE JOS" UNIVERSITY OF GALATI
FASCICLE IX. METALLURGY AND MATERIALS SCIENCE
Nº. 3 - 2020, ISSN 2668-4748; e-ISSN 2668-4756
Article DOI: https://doi.org/10.35219/mms.2020.3.05

2. Bed frame elements made from fabricated steel-sheet products for welded construction

Regarding the realization of the bed frame elements by bending thick sheet metals, we can highlight several possible methods, for example: cold deformation, hot deformation, cold deformation after soft annealing.

The methods presented above have been applied experimentally, in turn to study and define an optimal technology for manufacturing the flat plates curved bed frame elements of high-strength materials such as Quend 700.

The following figure illustrates the cylindrical frame element made of sheet metal with a wall thickness of 50 mm and the quality of the material being Quend 700. Thus, during the development of the part, it is necessary to have an addition of material that will later be used making samples for mechanical tests and to study the behaviour of the material during the processes.

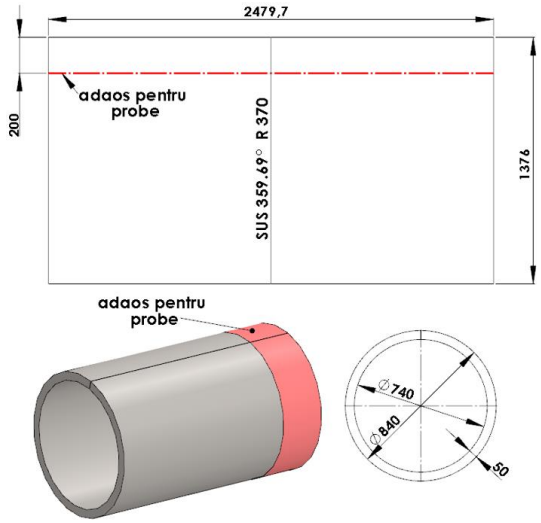

Fig. 2. *Execution drawing and development of the part*

Cylindrical and conical sheet metals rolling are obtained by bending between the rollers of rolling machines and welded along the generating line, so that the laminating fibre of the sheet obtained by rolling is in the annular direction (maximum load direction in the case of bed frames).

2.1. Cold deformation method

Cold deformation of sheet metal is done with the help of bending presses ("abkant") and rolling machines. Bending presses are used for pre-bending the ends of the sheet metal, this is mainly necessary when inserting it between the bending roller of the rolling machine.

The cold pre-bending of the Quend 700 sheet metal on bending presses requires a very high pressing force, because we need to overcome the mechanical properties of the material. If the pressing force does not overcome the mechanical properties of the material will result in the appearance of the springback phenomenon and the inability to achieve the pre-bending [3].

According to this method cold pre-bending of Quend 700 was tried on an Ermaksan Power-Bend, which develops a pressing force of 1000 tons over a length of 7100 mm. A punch with a radius of 50 mm and a lower die with an opening of 500 mm were used on the press machine, setting the properties of the material and the bending length of the part at 1376 mm, result the maximum force developed by the machine are around 300-350 tons/meter.

Fig. 3. *Press machine, Ermaksan Power-Bend 7100x1000 Ton*

Consequently, cold pre-bending of Quend 700 has failed due to the fact that this material has a very high yield strength of at least 700 MPa and tensile strength around 780-930 MPa, but mainly due to the inability of the equipment to develop a sufficiently high pressing force.

Fig. 4. *Lower die of bending press with opening of 500 mm*

THE ANNALS OF "DUNAREA DE JOS" UNIVERSITY OF GALATI
FASCICLE IX. METALLURGY AND MATERIALS SCIENCE
N°. 3 - 2020, ISSN 2668-4748; e-ISSN 2668-4756
Article DOI: https://doi.org/10.35219/mms.2020.3.05

According to the input data, the thickness and bending length of the part, bending tools, we can estimate the effective pressing force Fmax required to achieve the pre-bending with the formula below [4].

$$F_{max} = \frac{1{,}6\ R_m\ t^2\ \alpha}{10\ V}\ [\frac{tons}{m}] \quad (1)$$

Where, R_m is tensile strength in N/mm^2, t is sheet thickness in mm, α are angle coefficient in degrees (for 90° →1; 30° →1.6; 60° →1.6; 120° →1.6; 150° →0.7) and V is die opening in mm.

$$F_{max} = \frac{1{,}6\ x\ 871\ x\ 50^2\ x\ 0.7}{10\ x\ 500} = 487{,}8\ [\frac{tons}{m}] \quad (2)$$

2.2. Hot deformation method

Hot deformation method consists in pre-bending and rolling the flat plate according to the following steps:

- heating the flat plate to 750 ºC in the electric oven and performing the pre-bending operation on bending press;
- after the pre-bending on the flat plate follows the rolling on rolling machine 80x3500 up to a curvature value of R700;

Fig. 5. *Rolling machine 80x3500*

- reheating the semi-finished product to 750 °C and transported to another rolling machine, AKYAPAK Type AHS 25/35, capable of achieving the radius of curvature below R700 to close the cylindrical product with the addition of pre-bent material;
- the next operation is to cut the pre-bend addition (2x250 mm) and make the chamfers on the generators;
- then a final heating is done at 750 °C to complete the closing of the shell at a radius of R370 and spot welding on rolling machine, AKYAPAK Type AHS 25/35 before the release forces of rollers.

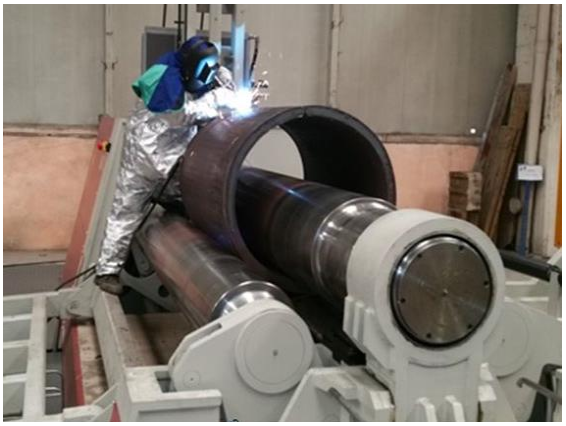

Fig. 6. *Closing of the shell at a radius of R370 and spot welding on rolling machine AKYAPAK Type AHS 25/35*

This method of manufacturing cylindrical frame elements from Quend 700 has been successfully developed but has some disadvantages that are not suitable for mass production, such as: the energy consumed by the electric oven is high for many heating and preheating, the mechanical properties of the material decrease and after the tests show, the tensile strength around 550 MPa and yield strength around 500 MPa.

Due to the results obtained from this method a third method shown below will arise.

2.3. Cold deformation method after soft annealing

Cold deformation method after soft annealing is characterized of cold pre-bending and rolling after a single heating at 750 °C and cooling in air of the flat plate product.

This method follows the phases of operations from the previous variant only this time the semi-finished product does not have to be heated during the pre-bending and rolling operations:

- performing the pre-bending operation on bending press
- after the pre-bending on the flat plate follows the rolling on rolling machine 80x3500 up to a curvature value of R700;
- transported to another rolling machine, AKYAPAK Type AHS 25/35, capable of achieving the radius of curvature below R700 to close the cylindrical product with the addition of pre-bent material;
- cutting the pre-bend addition (2x250 mm) and make the chamfers on the generators;

THE ANNALS OF "DUNAREA DE JOS" UNIVERSITY OF GALATI
FASCICLE IX. METALLURGY AND MATERIALS SCIENCE
No. 3 - 2020, ISSN 2668-4748; e-ISSN 2668-4756
Article DOI: https://doi.org/10.35219/mms.2020.3.05

- after which a last a final closing operation of the shell at a radius of R370 and spot welding on rolling machine, AKYAPAK Type AHS 25/35 before the release forces of rollers.

According to the input data, the thickness and bending length of the part, bending tools, knowing the tensile strength after soft annealing, according to the Table 7, we can estimate the effective pressing force Fmax required to achieve the pre-bending with the formula below.

$$F_{max} = \frac{1{,}6\ x\ 550\ x\ 50^2\ x\ 0.7}{10\ x\ 500} = 308\ [\frac{tons}{m}] \quad (3)$$

In conclusion, the heat treatment applied to this method aims at improving the plasticity properties of the material and is applied as a preliminary heat treatment before cold deformation, the temperature of the operation being approximately 750 °C, it being adopted depending on the chemical composition of the steel and the allotted time being between 1-2 hours, followed by a cooling in the air. At the same time, at the end of the fabrication of the cylindrical frame element, an improvement treatment must be applied according to Table 9, to raise its mechanical properties at least close to the initial state.

3. Technological stages

The technological stages follow step by step the process regarding the realization of the cylindrical and conical sheet metals rolling, from the dimensioning phase of the flat sheet metal until its complete closing, these stages are presented in more detail below.

3.1. Dimensioning the development

Calculation the length of the cylindrical sheet metal development [5]:

$$L = \pi * (D_i + s)\ [mm] \quad (4)$$

Where, D_i is inside diameter in mm, s is sheet thickness in mm, H are height of cylindrical part in mm.

To calculate the development of a conical part, it is necessary to determine several geometric parameters highlighted in the formulas below [5]:

$$D_m = D_i + \frac{s}{\cos\alpha}\ [mm] \quad (5)$$

$$d_m = d_i + \frac{s}{\cos\alpha}\ [mm] \quad (6)$$

$$G = \frac{H}{\cos\alpha}\ [mm] \quad (7)$$

$$tg\ \alpha = \frac{D_i - d_i}{2H} = \frac{D_m - d_m}{2H}\ [^0] \quad (8)$$

$$\beta = 2\pi \sin\alpha\ [rad] \quad (9)$$

$$Rp = \frac{\pi D_m - b}{\beta}\ [mm] \quad (10)$$

$$rp = \frac{\pi d_m - b}{\beta}\ [mm] \quad (11)$$

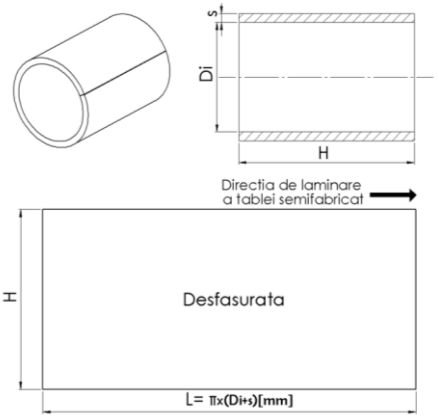

Fig. 7. *Cylindrical sheet metal development*

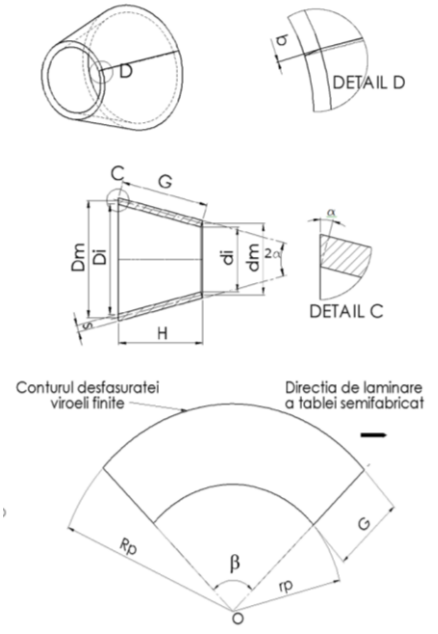

Fig. 8. *Geometric parameters of conical part and development*

THE ANNALS OF "DUNAREA DE JOS" UNIVERSITY OF GALATI
FASCICLE IX. METALLURGY AND MATERIALS SCIENCE
Nº. 3 - 2020, ISSN 2668-4748; e-ISSN 2668-4756
Article DOI: https://doi.org/10.35219/mms.2020.3.05

Where, is sheet thickness in mm, Di is maximum inside diameter in mm, di is minimum inside diameter in mm, Dm is maximum average diameter in mm, H are height of conical part in mm, G is side length of development in mm, b is the loft of conical sheet metal in mm, Rp is external radius of development in mm, rp is internal radius of development in mm.

3.2. The pre-bending process

According to figure 8 it is necessary to leave an addition at both ends to the length of the initial development since cutting, in order to be able to achieve the pre-bending on the press machine, this addition is necessary to have support on the lower die and the grip the pre-bend sheet metal on rolling machine.

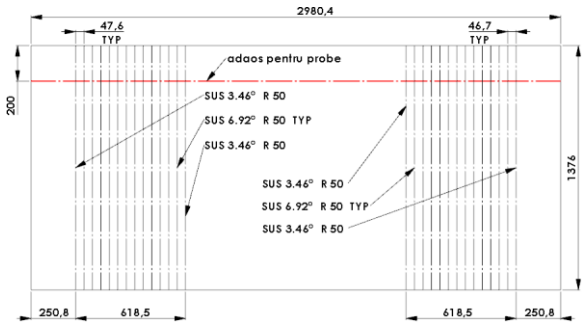

Fig. 9. *Development with pre-bending line*

The length of the development without the addition of pre-bending on the ends is 2479.7 mm, shown in Figure 2. With help of x-axis limiters of the press machine will be press on the line according to the dimensions on the development with pre-bending line drawing, and respecting the bending angles, see illustrated Figure 9. The bending starts from the length of 869.3 mm and will continue to the edge to a length 250.8 mm, with several bends equal to 14 and the size of step is equal to 47.6 mm.

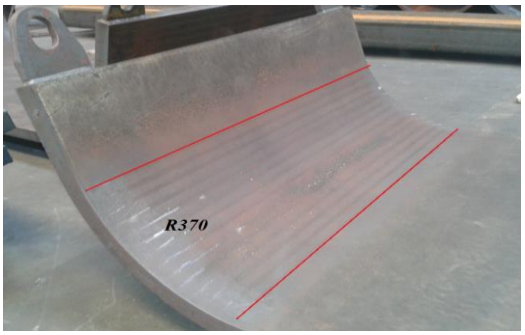

Fig. 10. *Pre-bending on press machine of the sheet metal ends at a radius R370*

At the end of the bending process, a radius check will be performed using a template with R370 mm on the entire width of the pre-bending sheet metal. The same will be done for bending the other end.

3.3. Rolling process of pre-bending plate

After pre-bending on press machine, it follows rolling on AKYAPAK Type AHS 25/35, capable of achieving the radius of curvature below R700 to close the cylindrical product with the addition of pre-bent material.

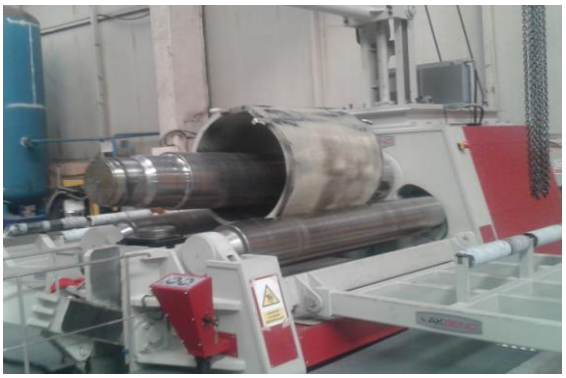

Fig. 11. *Curving the pre-bending plate on rolling machine*

3.4. Cutting excessive material process

After the pre-bending and rolling process, the addition left to the pre-bending process will be cut and then chamfers will be made for welding process. Cutting and chamfering will be performed in this case using manual plasma cutting device, followed by adjustment of the chamfer with an angle grinder acc. to the WPS (Welding Procedure Specification) documentation.

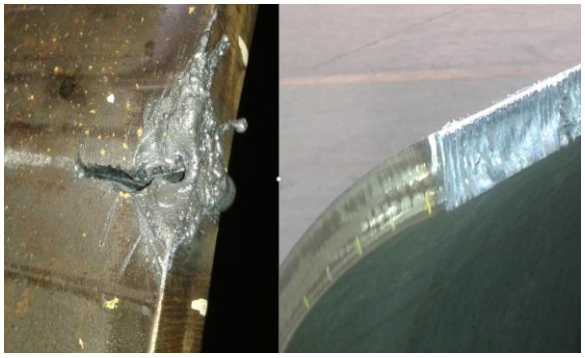

Fig. 12. *Manual plasma cutting of the pre-bend addition*

THE ANNALS OF "DUNAREA DE JOS" UNIVERSITY OF GALATI
FASCICLE IX. METALLURGY AND MATERIALS SCIENCE
Nº. 3 - 2020, ISSN 2668-4748; e-ISSN 2668-4756
Article DOI: https://doi.org/10.35219/mms.2020.3.05

Fig. 13. *Chamfering at both ends of the cut addition*

3.5. Final rolling process

After cutting the pre-bend addition and making the chamfers in the longitudinal direction, next is final closing operation of the shell at a radius of R370 and spot welding on rolling machine, AKYAPAK Type AHS 25/35 before the release forces of rollers.

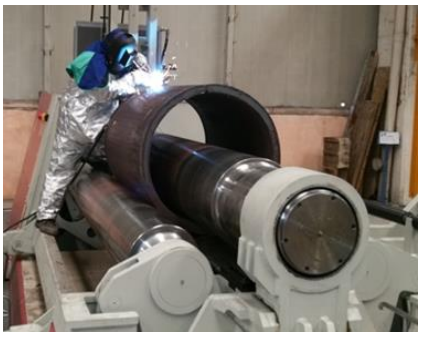

Fig. 14. *Final closing operation of the shell at a radius of R370 and spot welding on rolling machine*

3.6. Welding process and cutting addition

Welding process is a very important stage, it consists in the complete welding of the longitudinal loft according to the technology presented in chapter four, finishing it by grinding and removing of spit. The shell and the weld will be checked by the personnel responsible for performing the non-destructive and quality control.

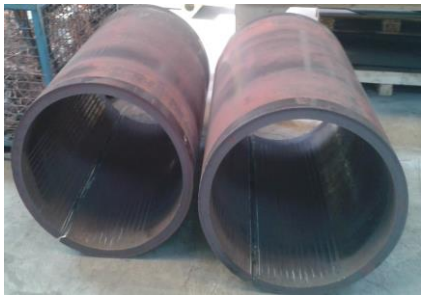

Fig. 15. *Preparation of metal shell for welding process*

Fig. 16. *Completion of the welding operation*

3.7. Calibration process

Calibration is the technological operation by which the deviations from the circularity of the sections are eliminated of cross sections in our case a cylindrical and conical sheet metals. Calibration applies only to rigid cylindrical and conical sheet metals, characterized by a ratio between the wall thickness (s) and the inside diameter (Di), which meets the criterion in the equation below.

$$\frac{s}{D_i} > 0.01 \tag{12}$$

The calibration is also performed on the rolling machines and involves the following steps:

- checking the shape deviations of the cylindrical sheet metal to be calibrated and establishing the rc calibration radius (the radius at which the rolling machine is adjusted);
- preparing the cylindrical sheet metal, usually consisting in grinding the longitudinal increased height of weld;
- tightening the cylindrical sheet metal between the upper roller of the machine and the side rollers to ensure the calibration radius;
- checking the quality (shape accuracy) of the calibrated cylindrical sheet metal.

4. Custom welding procedure specification

Welding of Quend 700 can be performed using any of the conventional welding methods available both as manual and robotic welding. In the thickness range up to 30 mm, if a heat input of 1.7 kJ/mm is used, preheating prior to welding is not needed. Welding of Quend 700 is recommended to be performed at ambient temperature not lower than +5 °C. Subsequent to welding, let the welded parts slowly cool down to room temperature. Do never accelerate the cooling process of the weld. It is always recommended to use low hydrogen electrodes when welding Quend 700 [6].

THE ANNALS OF "DUNAREA DE JOS" UNIVERSITY OF GALATI
FASCICLE IX. METALLURGY AND MATERIALS SCIENCE
N°. 3 - 2020, ISSN 2668-4748; e-ISSN 2668-4756
Article DOI: https://doi.org/10.35219/mms.2020.3.05

Table 1. *Welding Procedure Specification (EN ISO 15609)*

Transfer mode	dip + spray + globular
Welding process	135(MAG; GMAW)
Joint type	BW
Weld preparation details (sketch)	
Method of preparation and cleaning	grinding
Parental material specification	S690 QL QUEND 700
Material thickness	t_1 =50 [mm] t_2 =50 [mm]
Welding position	PA (Flat Position)
Filler metal	EN ISO 16834-A: G 69 4 M Mn3Ni1CrMo / AWS A5.28: ER100S-G
Classification and trade name	FILCORD 100
Gas (Shielding)	EN ISO 14175: M21 – Arc – 18
Gas flow rate (Shielding)	15÷18 [l/min]
Gas Nozzle (diameter)	Ø16 [mm] inside diameter
Details of back gouging/backing	bs (both sided welding; root grinding and backing run)
Preheating temperature	T_p = +150 [°C]
Interpass temperature	+150 °C ≤ T ≤ +185 °C
Post-weld heat treatment	NA
Heating and cooling rates	NA
Weaving (maximum width of run)	string beads
Stand-off distance	15 ÷ 22 [mm]
Torch angle	Lead angle = 10°- 20°

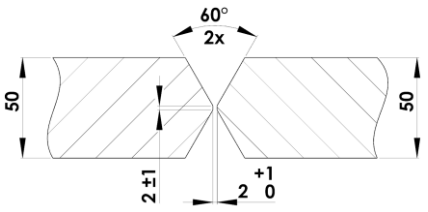

Fig. 17. *Joint design sketch*

Table 2. *Welding details*

Run	Tack+1	2÷8	9÷n
Process	135	135	135
Size of filler metal	Ø1.2 [mm]	Ø1.2 [mm]	Ø1.2 [mm]
Current	180÷190 [A]	260÷280 [A]	250÷270 [A]
Voltage	21÷23	27÷29	25÷27
Type of current/ polarity	DC^+	DC^+	DC^+
Wire feed speed	5÷6 [m/min]	9÷10 [m/min]	7÷8 [m/min]
Travel speed	13÷17 [cm/min]	26÷37 [cm/min]	22÷31 [cm/min]
Heat input Max.	10672 ÷ 16135 [J/cm]	9107 ÷ 14990 [J/cm]	9677 ÷ 15905 [J/cm]
Transfer mode	dip	spray	globular

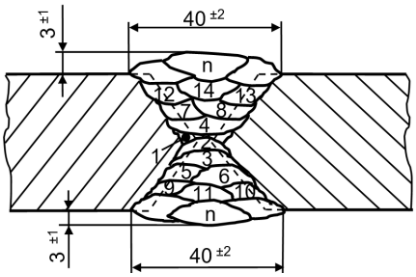

Fig. 18. *Welding sequences*

5. Properties of high strength material QUEND 700

Quend 700 is extra high yield strength structural steel obtained as a result of quenching and subsequent tempering with minimum yield strength 700 MPa [6].

5.1. Properties in initial state

Table 3. *Mechanical properties*

Yield strength $R_{p\,0.2}$ [MPa]	**Tensile strength Rm [MPa]**	**Elongation A_5**
700 min	780-930	14% min

The following material product mix is currently available of thickness 4-64 mm and width 1500-3100 mm.

THE ANNALS OF "DUNAREA DE JOS" UNIVERSITY OF GALATI
FASCICLE IX. METALLURGY AND MATERIALS SCIENCE
Nº. 3 - 2020, ISSN 2668-4748; e-ISSN 2668-4756
Article DOI: https://doi.org/10.35219/mms.2020.3.05

Ultrasonic testing (UT) is used to identify such discontinuities as inclusions, cracks, and porosity. In thickness from 8 mm and higher, all plates are UT tested and controlled against class S2, E2 in accordance with EN 10160 [6].

Table 4. *Impact toughness*

Minimum values at		
0 ºC	-20 ºC	-40 ºC
35 J	30 J	27 J

Table 5. *Carbon equivalent, typical value, %*

Plate thickness [mm]	CEV(1)	CET(2)
4 – 15	0.45	0.29
15.01 – 25	0.44	0.30
25.01 – 40	0.45	0.30
40.01 – 64	0.54	0.33

$$CEV = C+Mn/6+(Ni+Cu)/15+(Cr+Mo+V)/5 \quad (13)$$
$$CET = C+(Mn+Mo)/10+Ni/40+(Cr+Cu)/20 \quad (14)$$

5.2. Mechanical properties after soft annealing

This preliminary heat treatment is adopted for method three, the cold deformation method.

Following this heat treatment, the mechanical properties of the material will be reduced by up to 40% compared to its initial state, according to the results in Table 7. This helps to carry out the pre-bending and rolling operations of the semi-finished product with the equipment provided.

The main disadvantage is that a subsequent improvement treatment will be necessary to raise the mechanical properties, this treatment may involve water or oil quenching.

Table 7. *Mechanical properties after tempering*

Material: plate 50 [mm] **Quality: QUEND 700**			
Sample number	**1**	**2**	**3**
The heating temp. of sample [ºC]	25 (initial state)	750	750
The force [N] obtained in the test d_0= 10 [mm]	70000	44500	44000
Rm [MPa]	891	566	506
Rp [MPa]	853	501	506
A_5 [%]	15	19	20
Z [%]	62.6	71.3	70.7
Impact toughness KV (-40 ºC) [J]	162	44; 60; 82 → transversal 104; 106; 86 → longitudinal	

Table 6. *Chemical composition of Quend 700 in initial state* [6]

C	Si	Mn	P	S	Nb	Cr	V	Ti	Ni	Al	Mo	N	B
0.20	0.60	1.50	0.02	0.01	0.04	0.60	0.07	0.04	1.00	0.07	0.50	0.014	0.005

5.3. Mechanical properties when the Quend 700 are heated

In Table 8 are the results obtained from hot tensile test from Quend 700 in the initial state heated to different temperatures. As can be seen samples were heated to a certain temperature, but due to the time of handling and grip on the machine test they were cooled so in column three of the table the actual temperature at which the tensile test was performed was recorded.

With the help of a temperature gun measuring device, both the outlet temperature of the sample in the oven and the temperature before breaking the sample in the laboratory were measured.

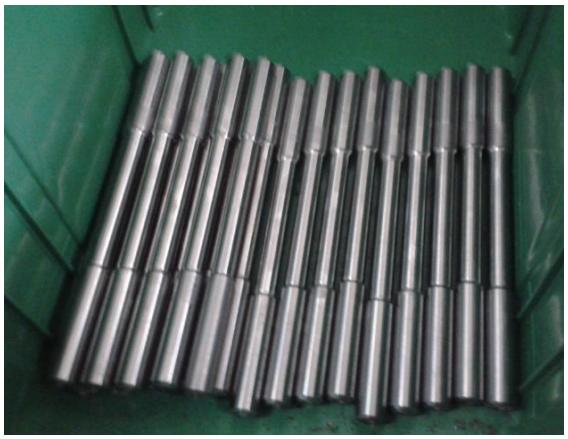

Fig. 19. *Samples test for hot tensile test*

THE ANNALS OF "DUNAREA DE JOS" UNIVERSITY OF GALATI
FASCICLE IX. METALLURGY AND MATERIALS SCIENCE
Nº. 3 - 2020, ISSN 2668-4748; e-ISSN 2668-4756
Article DOI: https://doi.org/10.35219/mms.2020.3.05

Fig. 20. *Stainless steel container*

The samples for tensile test were heated in the electric resistance furnace and transported to the physical-mechanical testing laboratory in a container made of a stainless-steel pipe lined with insulation (mineral wool) and sealed with a lid, see Figure 20.

The test report shows that the tensile strength decreases depending on the increase of temperatures according to the figures above, which led to the elaboration of the experiment from the second method of making bed frame elements. According to the results the lowest value of tensile strength is 220 MPa which was recorded at a sample temperature of 550 ºC. The yield strength could not be recorded due to the fact that the test was performed with heated samples.

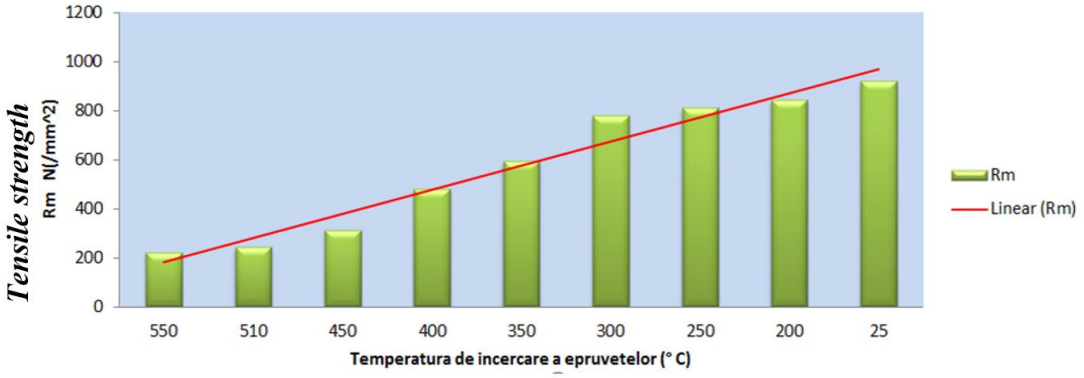

Fig. 21. *Behaviour of tensile strength depending on temperature*

Table 8. *Values of mechanical properties when the material is heated*

Material: plate 50 [mm], Quality: QUEND 700							
Sample number	**The heated temp. of sample [ºC]**	**Temperature of testing sample [ºC]**	**The force [N] obtained in the test d_0= 10 [mm]**	**Rm [MPa]**	**Rp [MPa]**	**A_5 [%]**	**Z [%]**
1	950	550	17500	220	-	40	94
2	950	510	19000	242	-	38	91
3	950	450	24500	312	-	44	87
4	780	400	37500	477	-	26.4	86.5
5	510	350	46500	592	-	15.3	84.8
6	460	300	61000	777	-	15.3	84
7	430	250	63500	808	-	15.3	68.6
8	350	200	66000	840	-	16.7	67.5

5.4. Tests to improve the material on samples

Tests to raise the mechanical properties are applied following the cold deformation and soft annealing method and its main purpose is to find an adequate heat treatment to raise the mechanical properties at least close to the initial state of the material.

The quality certificate of the Quend 700 material that accompanied its delivery indicates a tensile strength of 871 MPa and a yield strength of 830 MPa, respectively impact test KV at -40 ºC of 52 J, after soft annealing the mechanical properties of this material are as follows, the tensile strength of 566

THE ANNALS OF "DUNAREA DE JOS" UNIVERSITY OF GALATI
FASCICLE IX. METALLURGY AND MATERIALS SCIENCE
Nº. 3 - 2020, ISSN 2668-4748; e-ISSN 2668-4756
Article DOI: https://doi.org/10.35219/mms.2020.3.05

MPa and a yield strength of 501 MPa, respectively impact test KV at -40 ºC of 86 J on the longitudinal fiber.

In order to make the test samples, two pieces of material were cut from the bed frame element made in method three and an improvement treatment was applied to the two pieces.

The first piece was heated to 900 ºC and then water quenching followed by a tempering at 580 ºC with staying time of an hour and a half respectively the second piece was heated to 900 ºC and then oil quenching followed by a tempering at 580 ºC with staying time of an hour and a half. The results of this tests can be found in the table below.

Table 9. *Mechanical properties after improvement treatments in water and oil*

Material: plate 50 [mm], Quality: QUEND 700							
Sample number	**The kind of improvement treatments**	**The force [N] obtained in the test d_0= 10 [mm]**	**Rm [MPa]**	**Rp [MPa]**	**A_5 [%]**	**Z [%]**	**Impact toughness KV (-40 ºC) [J]**
1	25 (laminated state)	70000	891	853	15	62.6	162 170
2	The quenching in **water** at 900 ˚C and tempering at 580 ˚C with an hour's keeping with air cooling	63500 64750	808 824.8	745 789.8	14 14	69 68	36; 30; 18 → transversal 102; 120; 116 → longitudinal
3	The quenching in **oil** at 900 ˚C and tempering at 580 ˚C with an hour's keeping with air cooling	55000 51000	700 719	630 635	18 15	72.9 66	22; 18; 34 → transversal 94; 42; 102 → longitudinal

5.5. The improvement treatment applied to the bed frame elements

According to the results of the tests applied on the specimens from the previous subchapter in order to identify an adequate thermal improvement treatment for the cylindrical bed frame elements performed by method three.

The improvement treatment that gave the best results was water quenching and tempering, so it was decided to apply this treatment on the cylindrical bed frame elements.

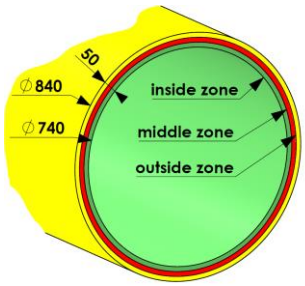

Fig. 22. *Highlighting the sampling areas after the improvement treatment*

Thus, the improvement treatment applied to the cylindrical bed frame elements consists in heating to 900 ºC and water quenching in a special basin with bubbled water. After which a tempering to 580 ºC will be applied for an hour and a half. From the additive material left on the final piece are made a series of samples for tensile and resilience tests and the results can be found in the table below.

The specimens were taken from the outside, inside and middle areas of the body of the frame element to see the effect of the improvement treatment in all areas of the material.

The most negatively affected area in a quenching and tempering is the middle one.

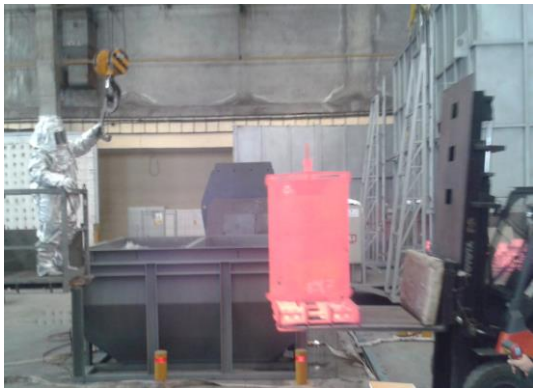

Fig. 23. *Introduction of the cylindrical bed frame elements in the basin with bubbling water*

THE ANNALS OF "DUNAREA DE JOS" UNIVERSITY OF GALATI
FASCICLE IX. METALLURGY AND MATERIALS SCIENCE
Nº. 3 - 2020, ISSN 2668-4748; e-ISSN 2668-4756
Article DOI: https://doi.org/10.35219/mms.2020.3.05

Table 10. *The final improvement treatments in water applied to the cylindrical bed frame element*

Material: plate 50 [mm], Quality: QUEND 700					
Sample number		**1**	**2** Outside of the piece	**3** Inside of the piece	**4** Middle of the piece
Improvement treatment		25 ºC (initial state)	The **water** quenching at 900 ºC and tempering at 580 ºC with an hour and a half keeping		
The force [N] obtained in the test d_0= 10 [mm]		70000 70000	62000 64000	60000 59500	56000 56500
Rm [MPa]		891 891	789 815	706 700	713.4 719.7
Rp [MPa]		828 834	739 738	677 616	649 662.4
A_5 [%]		15 15	19 17	24 24	26 26
Z [%]		62.6 71.8	71.2 67.5	68 72	70.8 69.7
Impact toughness KV [J]	**-40 [ºC]**	162 170	260 220	286 240	106 80

6. Conclusion

The manufacture of cylindrical or conical bed frame elements from Quend 700 can be achieved by several methods, most productive and economical method in our case being cold deformation after soft annealing. The cold deformation method can successfully replace the old methods of making bed frames or bed frame elements, among which we can mention the manufacturing process by casting, process that is high energy consuming.

Quend material exhibited superb mechanical properties including higher tensile strength, ductility and impact toughness and is therefore recommended in the manufacture of components for machine tools, who undergone high forces, shocks and deformations but can also be used in other applications such as: truck chassis, lifting equipment and many more.

According to the results of this study this material is not recommended be use for applications where the working and service temperature exceeds

References

[1]. Piotr B., Tadeusz N., Rafał G., *The welded CNC machine tool frame*, Czestochowa University of Technology, Institute of Mechanical Technologies, Czestochowa, Poland.
[2]. Botez E., Valda A., Velicu S., *Proiectarea maşinilor-unelte*, Editura dictatică şi pedagogică, Bucureşti, 1980.
[3]. Mori K., Akita K., Abe Y., *Springback behaviour in bending of ultra-high-strength steel sheets using CNC servo press*, International Journal of Machine Tools and Manufacture, vol. 47, p. 321-325, 2007.
[4]. ***, https://www.sm-tech.ro/files/Calculator-forta-aprox-indoire.xls, 2020.
[5]. ***, https://vdocuments.site/44241413-curs-tcmutd.html, 2020.
[6]. ***, http://www.jsoarescorreia.pt/wpcontent/uploads/1111/11/Quard-Quend-Datasheets_English.pdf, 2020.

THE ANNALS OF "DUNAREA DE JOS" UNIVERSITY OF GALATI
FASCICLE IX. METALLURGY AND MATERIALS SCIENCE
Nº. 3 - 2020, ISSN 2668-4748; e-ISSN 2668-4756
Article DOI: https://doi.org/10.35219/mms.2020.3.06

CONTROL FACTORS ON THE HEAT TREATMENT PROCESS APPLIED TO A537 STEEL FOR INCREASING HARDNESS USING HARDENING AND TEMPERING

Nelu CAZACU
"Dunarea de Jos" University of Galati, Faculty of Engineering, Dept. of Materials and Environmental Engineering, Romania
e-mail: nelu.cazacu@ugal.ro

ABSTRACT

The paper is based on laboratory experiments of heat treatments applied to samples of A537/A537M steel. The work continues other previous works aimed at modifying structures and properties of this steel, including through surface treatments. The experiments were performed using Taguchi methods from Quality Engineering. A number of four factors were selected as influencing the structure after heat treatment: heating temperature for hardening, cooling rate on hardening, time and tempering temperature. A number of nine experiments were performed using an L9 orthogonal matrix. Objective function was changed to maximum hardness after the heat treatment regime. The results show that the tempering temperature has the greatest influence on the final hardness of the A537 steel samples.

KEYWORDS: HSLA, A537/A537M, heat treatment, Taguchi methods, quality engineering

1. Introduction

The A537 steel is part of the HSLA steel group, which means that in accordance with the specifications of use, significant reductions in the mass of the finished assemblies can be obtained. The chemical composition of the steel (Table 1) leads to an equivalent carbon that allows heat treatment by hardening and tempering but also allows diffusion welding.

The A537 steel (Table 2), [1] is a *C-Mn-Si* (carbon-manganese-silicon) steel being produced in the form of thick sheet in three classes having thicknesses covering the applications: under 65 mm, between 65 mm and 100 mm and over 100 mm. In Table 2 is showing that for the same chemical composition of steel the beneficiary can choose for three classes of product depending on the heat treatment. This means that parts can be made from sheet metal that can be treated individually to obtain the most convenient complex of properties. Classes 2 and 3 can be delivered in the form of table sheets treated entirely in section by specialized installations. This form of delivery offers the most convenient price ratio per kg of product.

Table 1. *ASTM A357/357M chemical compositions* [1]

element	thickness	heat analysis	product analysis
m.u.	mm	mass %	mass %
carbon		0,24	0,24
manganese	<40	0,70... ...1,35	0,64... ...1,46
	>40	1,00... ...1,60	0,92... ...1,72
phosphorus	-	max.0,035	
sulphur	-	max.0,035	
silicon	-	0,15... ...0,50	0,13... ...0,55
copper	-	max.0,35	max.0,38
nickel	-	max.0,25	max.0,28
chromium	-	max.0,25	max.0,29
molybdenum	-	max.0,08	max.0,09

The properties are dependent on the class of manufacture, the thickness and the heat treatment applied (Table 3), respectively.

THE ANNALS OF "DUNAREA DE JOS" UNIVERSITY OF GALATI
FASCICLE IX. METALLURGY AND MATERIALS SCIENCE
No. 3 - 2020, ISSN 2668-4748; e-ISSN 2668-4756
Article DOI: https://doi.org/10.35219/mms.2020.3.06

The work continues the concerns for the optimization of the properties of A537 steel through experiments of heat treatments performed in laboratory conditions using the TM procedure from Quality Engineering. Compared to previous works, the type of objective function has changed, which has led to its own results in accordance with the literature [1].

An example is the use of this steel, which requires as much hardness as possible, when making wear parts for agricultural machines.

Table 2. *ASTM A537/537M mechanical properties in function of heat treatment* [1]

class	heat treatment	thickness	yield strength	tensile strength
u.m.	-	mm	Mpa	Mpa
1	normalized	under 65	345	485
		over 65	310	450
2	quenched and tempered	<65	415	550
		65...100	380	515
		over 100	315	485
3	quenched and tempered	under 65	380	550
		65...100	345	515
		over 100	275	485

Table 3. *Mechanical and plasticity properties in function of A537 class and thickness* [1]

properties	thickness	class 1	class 2	class 3
m.u.	mm	MPa	MPa	MPa
tensile strength	<65	485...620	550...690	550...690
	65..100	450...585	515...655	515...655
	100...150	...	485...620	485...620
yield strength	<65	345	415	380
	65..100	310	380	345
	100...150	...	315	275
Elongation in 50mm,%	50			
	<100	22	22	22
	>100	...	20	20
Elongation in 200mm,%		18	...	...

Notations:

n - target function;

i - number of experiment. i = 1…9.

Abbreviations:

HSLA - High Strength Low Alloy;
TG - Taguchi methods;
OA - Orthogonal Array;
ANOVA - Analysis of Variance;
HV - Hardness Vickers.

2 Experimental conditions

For the heat treatment experiments, samples of A537 / 537M sheet steel, with a thickness of 12.7 mm (1/2 inch), were used, for which the mentioned thickness is the characteristic dimension for heat regimes, similar to the treatment processes in factory section. The equipment used: electric heat treatment furnace with a working surface of 450 cm^2 and a maximum working temperature of 1200 °C and with thermal regimes controlled with ARE612 [2, 3]. Each of the hardening baths has 15 litres of liquid (water, stream of water, oil). The influencing factors that are considered for the given conditions of the experiment, are shown in Table 4, with the specification of some domains of variation.

The factors for the steel with hardening and tempering treatment in Table 5 were selected on the basis of the steel standard [1] and specialist literature [4, 5]. The same table shows the levels that are set for each factor (Table 5).

The L9 typed orthogonal matrix is shown in Table 6. It determines an experiment matrix with 9 lines (partially factorial experiments) and replaces a matrix with 34 with 81 lines (specific to full factorial experiments). The main mathematical properties of orthogonal matrices are related to the constant occurrence frequency of each level of each factor which ultimately leads to a mechanism for simplifying the calculation of specific errors [6-8].
The beneficial effect of reducing the number of experiments is useful only if the mathematical model of the experiment (TM, Taguchi Methods) and the mathematical model for interpretation of the results are followed. The reduction of the number of experiments and the related costs is found in the statistical approximation of the objective function of the optimal value and not in finding it as in the case of total factorial methods.

Table 7 shows the experiment matrix used to see the influence of four factors from quenching and tempering conditions on the final hardness of the samples.

Peculiar to this experiment matrix is that the lines that specify the conditions of each experiment differ greatly in their sequence. This also shows one of the difficulties of using orthogonal experiment matrices:

THE ANNALS OF "DUNAREA DE JOS" UNIVERSITY OF GALATI
FASCICLE IX. METALLURGY AND MATERIALS SCIENCE
Nº. 3 - 2020, ISSN 2668-4748; e-ISSN 2668-4756
Article DOI: https://doi.org/10.35219/mms.2020.3.06

- First: namely the variation of the experiment conditions. Achieving the required conditions is a condition for obtaining viable results.
- A second important difficulty is that if an experiment fails it must be resumed under the required conditions.

3. Results and discussions

After performing all nine complete experiments (with hardening and tempering), the samples were subjected to the Vickers surface hardness test. Three measurements (HV5, 5 kgf) were performed on each sample in central areas to eliminate the edge effect, and the result of the average hardness on each of the nine samples is shown in Table 8.

According to the initial model, it is considered a favourable dependence, when the hardness has maximum value. Taguchi recommends a "the biggest is the better" function [6, 8]. The objective function has in this case the equation:

$$n_i = 10\ log\ HV_i$$

Where: n is target function for i experiment line, and HV_i is the measured hardness for i sample [6], where $i = 1...9$.

The values of target function for all the nine experiments are shown in Table 9.

Specific TM is the construction of the average effect of each level of each factor on the whole set of experiments, by mediating the objective functions in which the level of a considered factor participates.

The calculus relations and results are centralized in Table 10 and then represented graphically in Fig. 1. These observations are found in the heat treatment regime recommended by the procedure based on the highest value of each factor level effect.

Table 4. *Factors that are considered to influence the experiment*

No.	Factors	u.m.	values domain
1	chemical compositin of steel	%	
2	temperature for quenching	°C	800..950
3	cooling speed for quenching	°C/s	0...2
4	tempering temperature	°C	620...690
5	tempering time	h	1hour/1inch thickness
6	non-uniformity of temperature in the treatment furnace	%	+/- 5%
7	chemical compozition of furnace atmosphere	%	
8	samples thickness	mm	1/2inch

Table 5. *Selected factors for A537 heat treatments experiments*

Symbol	Factors	um.	levels		
			1	2	3
A	temperature for quenching	°C	880	900	920
B	tempering temperature	°C	640	660	680
C	tempering time	h	0.5	1	1.5
D	cooling speed for quenching	°C/s	flow water	water	oil

Table 6. *L9 standardized orthogonal array* [6, 7]

experiment	factori			
	A	B	C	D
1	1	1	1	1
2	1	2	2	2
3	1	3	3	3
4	2	1	2	3
5	2	2	3	1
6	2	3	1	2
7	3	1	3	2
8	3	2	1	3
9	3	3	2	1

Table 7. *Experimental matrix with specified values of factors*

experiment	Specified factors			
	A	B	C	D
u.m.	°C	°C	h	grd.
1	880	640	0.5	flow water
2	880	660	1	water
3	880	680	1.5	oil
4	900	640	1	oil
5	900	660	1.5	flow water
6	900	680	0.5	water
7	920	640	1.5	water
8	920	660	0.5	oil
9	920	680	1	flow water

THE ANNALS OF "DUNAREA DE JOS" UNIVERSITY OF GALATI
FASCICLE IX. METALLURGY AND MATERIALS SCIENCE
No. 3 - 2020, ISSN 2668-4748; e-ISSN 2668-4756
Article DOI: https://doi.org/10.35219/mms.2020.3.06

Table 8. *Final hardness for each experiment and target function*

experiment	HVm	Target function
m.u.	daN/mm2	dB
1	317	25.01
2	303	24.81
3	289	24.61
4	315	24.98
5	286	24.56
6	305	24.84
7	330.5	25.19
8	294.5	24.69
9	309.5	24.91

Table 9. *The average effect of each level of each factor*

the average effect of each level	relation	value, dB
m_{A1}=	$1/3(n_1+n_2+n_3)$=	24.81
m_{A2}=	$1/3(n_4+n_5+n_6)$=	24.80
m_{A3}=	$1/3(n_7+n_8+n_9)$=	24.93
m_{B1}=	$1/3(n_1+n_4+n_7)$=	25.06
m_{B2}=	$1/3(n_2+n_5+n_8)$=	24.69
m_{B3}=	$1/3(n_3+n_6+n_9)$=	24.79
m_{C1}=	$1/3(n_1+n_6+n_8)$=	24.85
m_{C2}=	$1/3(n_2+n_4+n_9)$=	24.90
m_{C3}=	$1/3(n_3+n_5+n_7)$=	24.79
m_{D1}=	$1/3(n_1+n_5+n_9)$=	24.83
m_{D2}=	$1/3(n_2+n_6+n_7)$=	24.95
m_{D3}=	$1/3(n_3+n_4+n_8)$=	24.76
	media=	24.85

Table 10. *The average effect of the level of each factor*

	Factor	Levels			
		m.u.	1	2	3
A	temperature for quenching	dB	24.811	24.80	**24.93**
B	tempering temperature	dB	**25.062**	24.69	24.79
C	tempering time	dB	24.848	**24.90**	24.79
D	cooling speed for quenching	dB	24.827	**24.95**	24.76
				m	24.85

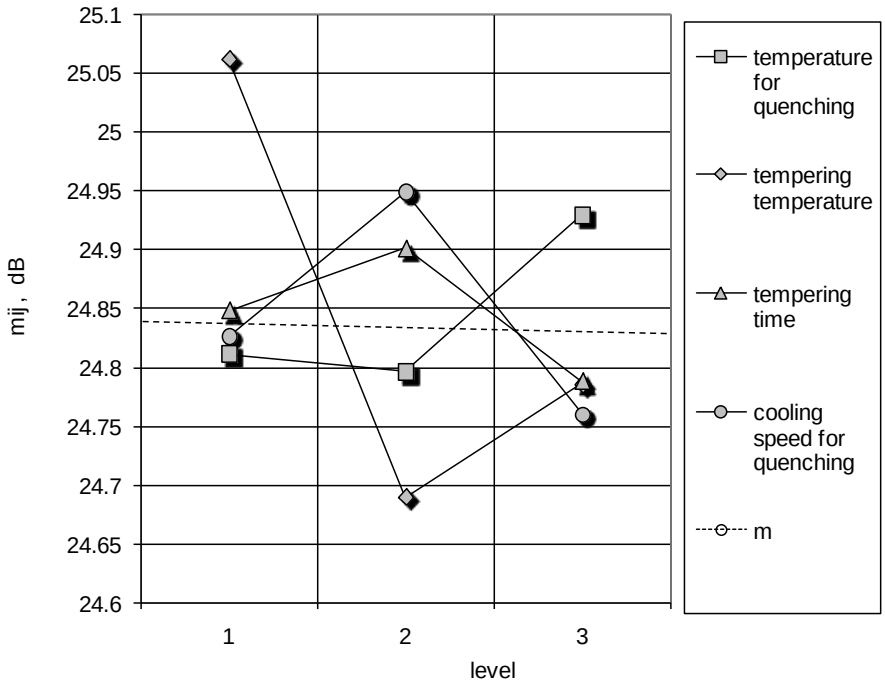

Fig. 1. *Graphical representation of the average effect of the level of each factor*

THE ANNALS OF "DUNAREA DE JOS" UNIVERSITY OF GALATI
FASCICLE IX. METALLURGY AND MATERIALS SCIENCE
Nº. 3 - 2020, ISSN 2668-4748; e-ISSN 2668-4756
Article DOI: https://doi.org/10.35219/mms.2020.3.06

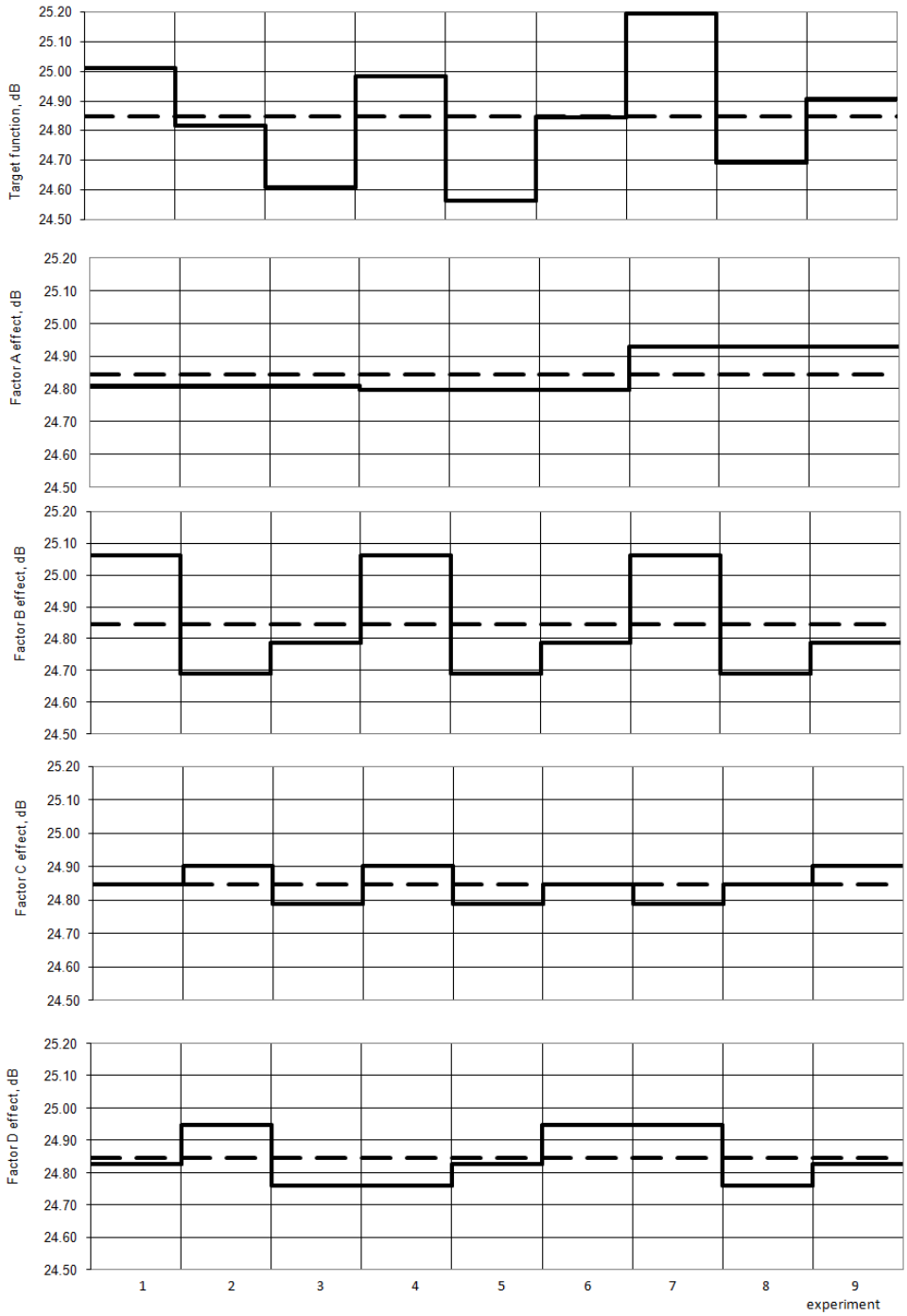

Fig. 2. *Graphical representation of the objective function with the number of the experiment and the additivity of the effect of factors A, B C and D*

4. Conclusions

Regarding the influence of the average effect of each level of the factors considered, the following can be observed:

- Heating temperature for hardening with higher value leads to increased final hardness.
- The lowest tempering temperature leads to the highest hardness.
- Cooling for hardening greatly influences the hardness, water cooling being the best solution.
- The firing time of 1h leads to a maximum hardness.

The additivity property is observed in Fig. 2. By summing the deviation from the mean of factors A, B,

THE ANNALS OF "DUNAREA DE JOS" UNIVERSITY OF GALATI
FASCICLE IX. METALLURGY AND MATERIALS SCIENCE
Nº. 3 - 2020, ISSN 2668-4748; e-ISSN 2668-4756
Article DOI: https://doi.org/10.35219/mms.2020.3.06

C and D for each experiment and leading to the objective function for that experiment. The procedure is inspired by FFT [6].

The main mathematical properties of orthogonal matrices are related to the constant occurrence frequency of each factor level which ultimately leads to a mechanism for simplifying the calculation of specific errors.

Regarding Fig. 3, which shows the influence of the factors on the experiments performed, it can be seen that the factor B (return temperature has the most important influence (almost 70%) which corresponds to the practical experience that the return temperature by thermal activation of processes determines the final mechanical properties. The second important factor is the cooling rate on hardening (drasticity of the cooling medium). Factors B and D cumulatively determine a weight of 84.5% and can be considered the control factors of the heat treatment process (hardening + tempering).

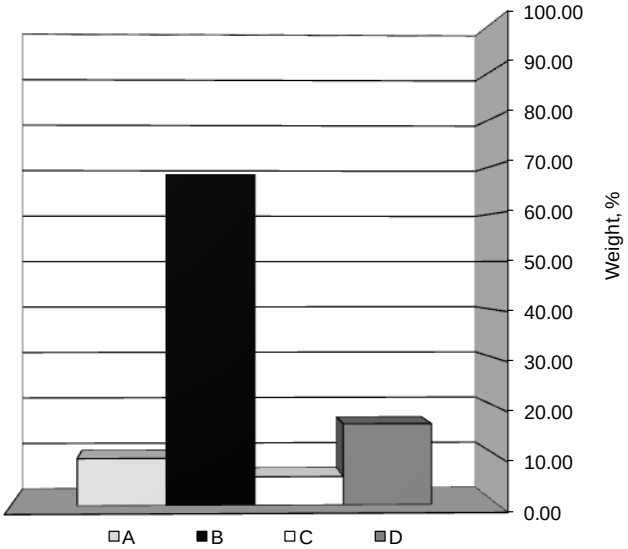

Fig. 3. *Weight factors influence on experiments*

Factors A and C accumulated an influence of approx. 15.5% and can be considered environmental factors. Technological experience shows that lower weight technological factors can be considered.

From a technological point of view, the weight of the factors practically determines the degree of precision with which the adjustments (settings) are made. If 2.5% accuracies are usually used, settings with 0.5% accuracy are made for the mentioned control factors, and max.1%. The procedure allows to reduce the variability of the finished products, the heat treatment technology applied to A537 steel being based on repeatability. The recommended optimal regime: A3B1C2D2 [6-8].

References

[1]. ***, *ASTM, International. Standard Specification for Pressure Vessel Plates, Heat-Treated, Carbon-Manganese-Silicon Steel,* ASTM A537 / A537M-13(2019) West Conshohocken, PA, 2019, www.astm.org ASTM, West Conshohocken, PA: s.n., 2020.

[2]. Cazacu Nelu, *Fluidized bed nitrocarburizing applied to astm A537 HSLA steel after pulse laser hardening*, Galați, UgalMat2016, 2016.

[3]. Dobrovici, Sorin, Cazacu Nelu, *Behavior of A537 Steel Grade in Carburizing in Fluidized Bed with Endothermic Atmosphere*, Fascicle IX, Metallurgy and Materials Science, Galați University Press, vol. no. 1, ISSN 1453-083X, 2009.

[4]. Cănănău Nicolae, Cazacu Nelu, Brenoaie Ionel, *Research Concerning the Behavior of the Thick Plates A537 to the tempering Treatments*, Fascicle IX, Metallurgy and Materials Science, Galați, s.n., p. 111-114, ISSN 1453-083X, 1996.

[5]. Cănănău Nicolae, Cazacu Nelu, Brenoaie Ionel, *Research Concerning the Quench heat Treatment of the Thick Plates by a A537 Steel*, Fascicle IX, Metallurgy and Materials Science, p. 107-110, ISSN 1453-083X, 1996.

[6]. Taguchi G., *Introduction to quality engineering into products and processes*, s.l.: Asian productivity organization, 1986.

[7]. Phadke M. S., *Quality engineering using robust design. Englewood Cliffs*, New Jersey: Prentice Hal, 1989.

[8]. Logothetis N., Wynn P. H., *Quality through design. Experimental design, Off-line Quality control and Taguchi's Contributions*, Oxford: Claderon Press, 1994.

THE ANNALS OF "DUNAREA DE JOS" UNIVERSITY OF GALATI
FASCICLE IX. METALLURGY AND MATERIALS SCIENCE
Nº. 3 - 2020, ISSN 2668-4748; e-ISSN 2668-4756
Article DOI: https://doi.org/10.35219/mms.2020.3.07

THE INFLUENCE OF THE NUMBER OF SEMI-CYCINDRICAL CUPS ON THE BEHAVIOR OF AN EXPERIMENTAL MODEL OF VERTICAL AXIS WIND TURBINE AT LOW WIND SPEED AND NO LOAD

Nelu CAZACU
"Dunarea de Jos" University of Galati, Faculty of Engineering, Dept. of Materials and Environmental Engineering, Romania
e-mail: nelu.cazacu@ugal.ro

ABSTRACT

The work is based on experiments made in the wind tunnel on experimental models of Savonius type wind turbines with blades in the shape of a semi-cylindrical cup. The number of blades changes: 2, 3, 4, 5 and 6. The experimental model allows the addition / removal of blades in the form of a semi-cylindrical cup followed by static balancing. The wind tunnel used has the measuring area 0.5m x0.5m and the length of 1.25 m and the experimental models have the interception surface at a maximum value of 10% of the cross-sectional area of the wind tunnel (diameter 158mm and height 158 mm). The experiments were performed at wind speeds between 0...9.7 m/s between peaks and no (mechanical and / or electrical) loads. The results confirm the influence of the number of semi-cylindrical cups on the rotational speed and other factors over experimental model of Savonius type turbines in no load conditions.

KEYWORDS: Savonius, S-rotor, rotation speed, semi-cylindrical cups

1. Introduction

Vertical axis wind turbines (VAWT) have some features attractive enough for use in hybrid lighting. Although the efficiency is low (maximum 14.81%) [1] the constructive simplicity, the independence of the wind direction, the high torque are the basic characteristics that today are corroborated with the increase of the luminous efficiency of the LED lighting systems from 100lm/W to recent 200 lm/W (Haitz's law) [2].

That is why the design of the vertical axis wind system must be maximized by finding the most accurate aerodynamic structure, shape and dimensions [3-5].

From the start, the main disadvantage of the proposed wind turbine model is the variability of the output speed and the useful torque with the wind speed (Fig. 1). The aim is about the intrinsic variability of the wind converter [6, 7]. Variability is given by the wind. For the proposed location (Galați, Romania) the values medium a maximum of average wind is showing in Fig. 2. It has values: maximum 61 Km/h (16.9 m/s) and average 20 km/h (5.55 m/s).

Therefore, the use of VAWTs is indicated because there is an average value of the wind speed in their working range and the behavior at a maximum speed of over 15 m/s must be solved mechanically.

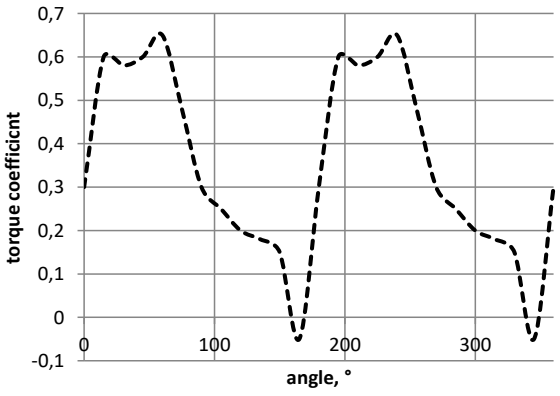

Fig. 1. *Axis torque variation for SWT* [6]

The work is based on experiments made in the wind tunnel on experimental models of Savonius type wind turbines with blades in the shape of a semi-cylindrical cup. The number of blades changes: 2, 3,

THE ANNALS OF "DUNAREA DE JOS" UNIVERSITY OF GALATI
FASCICLE IX. METALLURGY AND MATERIALS SCIENCE
No. 3 - 2020, ISSN 2668-4748; e-ISSN 2668-4756
Article DOI: https://doi.org/10.35219/mms.2020.3.07

4, 5 and 6. An EMs of maximum dimensions is made for the wind tunnel (158 x158 mm), removable and to which the blades can be added or removed. EM consists of 2 base plates of 0.4 mm Al sheet. 2, 3 4, 5 or 6 blades can be attached (Al sheet with a thickness of 0.4 mm). This is possible by designing the experimental model with removable semi-cylindrical cups. EM is fixed on a frame with two sleepers: the lower crossbar has a tip bearing in the middle and the speed-reading system with 60-slot disc and IR window optocoupler with window.

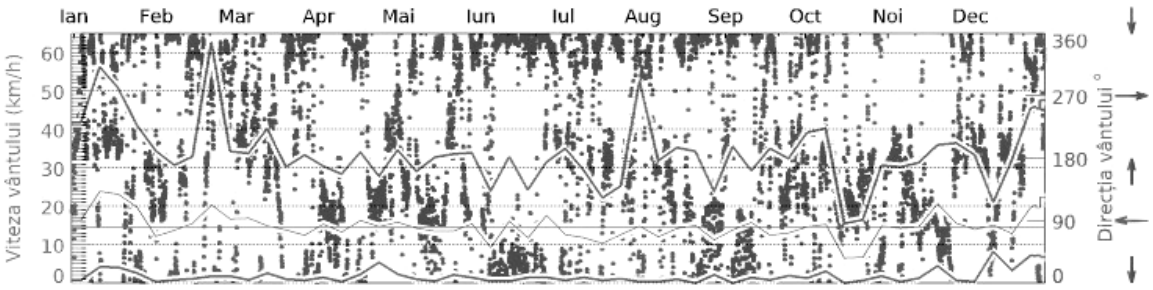

Fig. 2. *History of maximum, minimum and average values for the city of Galati for 2019* [8]

Notations:

u - tip blade speed, m/s;
$\dot{V}$ - volumic debit m^3/h;
$\dot{m}$ - mass debit, kg/m^3;
A - swept aria, m^2;
p - wind power, W;
ρ - air density, kg/m^3;
n - rotation speed, rpm;
C_D - drag coefficient;
λ - specific speed.

Abbreviations

VAWT - Vertical Axis Wind Turbine;
HAWT - Horizontal Axis Wind Turbine;
EM - Experimental Model;
LED - Light Emitting Diode;
Pb - Lead (lead Battery);
Cd-Ni - Cadmium-Nickel (Cadmium-Nickel battery;
NiMh - Nickel metal hydride battery;
LiPo - Lithium Polymer Battery;
S2CNL - Savonius 2 Cups No Load;
S3CNL - Savonius 3 Cups No Load;
S4CNL - Savonius 4 Cups No Load;
S5CNL - Savonius 5 Cups No Load;
S6CNL - Savonius 6 Cups No Load.

The upper cross member has two working possibilities. A bearing similar to the one at the bottom, when practically the system works between the tips with a minimum mechanical friction load. The second variant is with the connection of a three-phase generator 3V...24V, a case in which the system has a mechanical load and to which a variable electric (resistive) load can be connected, in order to observe the influence of the electric load on the wind turbine performance. The electrical efficiency of the EM for the considered electric load can be calculated.

The system is equipped with a data acquisition system which is purchased with an anemometer speed, model speed, load current and voltage at the generator (rectified and filtered). The system calculates the wind speed, wind power on the interception area, power on the electric load and the electrical efficiency of the wind turbine (which also includes the mechanical efficiency).

It represents graphically the quantities purchased for wind speeds between 0...9.5 m/s, with fixed steps of 0.5 m/s. The adjustment of the wind speed is done manually and therefore a time is maintained on each gear to stabilize the operation of the wind tunnel and the EM of the wind turbine.

Wind energy is pure kinetic energy and can be partially transformed into mechanical work [1, 2].

$$E = 0{,}5mv^2 \quad (1)$$

The volume flow over the swept area is:

$$\dot{V} = Av \quad (2)$$

And the mass flow is:

$$\dot{m} = \rho Av \quad (3)$$

The power of wind is depending by wind speed (v), air density (ρ) and swept area (A):

$$P = 0{,}5\rho Av^3 \quad (4)$$

For the VAWT, the Betz limit is (14.81%) [1].
The influence of air density over wind power is:

THE ANNALS OF "DUNAREA DE JOS" UNIVERSITY OF GALATI
FASCICLE IX. METALLURGY AND MATERIALS SCIENCE
No. 3 - 2020, ISSN 2668-4748; e-ISSN 2668-4756
Article DOI: https://doi.org/10.35219/mms.2020.3.07

$$\rho_a = \frac{353.049}{T} e^{-0,034\frac{z}{T}} \quad (5)$$

Pushing force is for an object fixed on the surface a placed in the path of an air flow:

$$\frac{F}{A} = \frac{1}{2} p v^2 C_D \quad (6)$$

C_D is defined as an important parameter when it comes to wind resistance.

The power extracted from a wind power by a VAWT Savonius type is depending by Drag force is:

$$P = \frac{1}{2} p v^3 C_D A \quad (7)$$

In case of wind turbines, the relative speed is:

$$v_r = v - u \quad (8)$$

The specific power is:

$$\frac{P}{A} = \frac{1}{2}(v-u)^2 C_D u \quad (9)$$

The VAWT extract power at axis by the relation:

$$P = C_p \rho_a H v_i^3 \quad (10)$$

The axis torque is as follows:

$$P = C_m \rho_a R^2 H v_i^2 \quad (11)$$

The power conversion efficiency is defined by the extracted power related to wind power.

$$\eta = \frac{P}{P_v} = \frac{\frac{1}{2}\rho(v-u)^2 C_D u A}{\frac{1}{2}\rho A v^3} \quad (12)$$

$$\eta = \frac{(v-u)^2 C_D u}{v^3} \quad (13)$$

Experimental Models (EMs) were made of 0.4 mm thick aluminum sheet with dimensions of H = 158 mm and D = 158 mm.

The interception surface (swept area) is variable with the angular position of the cups shown in Fig. 1.

With the increase of the number of cups swept area approaches the maximum value which is 10% of the area of the measuring section of the wind tunnel

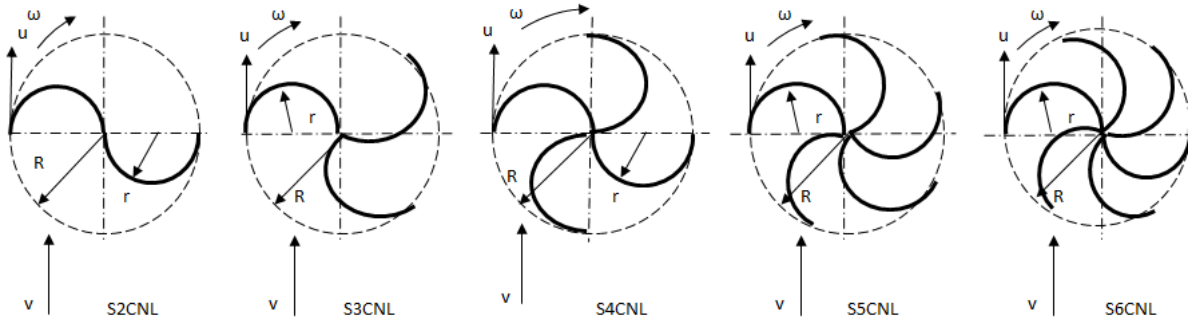

Fig. 1. *cross sections through the experimental models used*

Table 1

no.	experimental model	n	m	A_s min	A_s max
m.u.		-	kg	m^2	m^2
1	S2C	2	0.092	0.008	0.025
2	S3C	3	0.117	0.02	0.025
3	S4C	4	0.141	0.02	0.025
4	S5C	5	0.166	0.023	0.025
5	S6C	6	0.191	0.023	0.025

THE ANNALS OF "DUNAREA DE JOS" UNIVERSITY OF GALATI
FASCICLE IX. METALLURGY AND MATERIALS SCIENCE
Nº. 3 - 2020, ISSN 2668-4748; e-ISSN 2668-4756
Article DOI: https://doi.org/10.35219/mms.2020.3.07

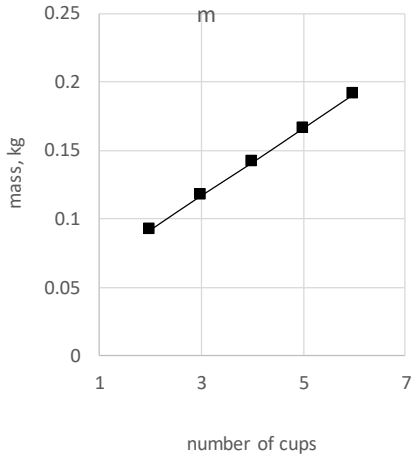

Fig. 3. *The variation of the mass of the experimental models with the number of cups*

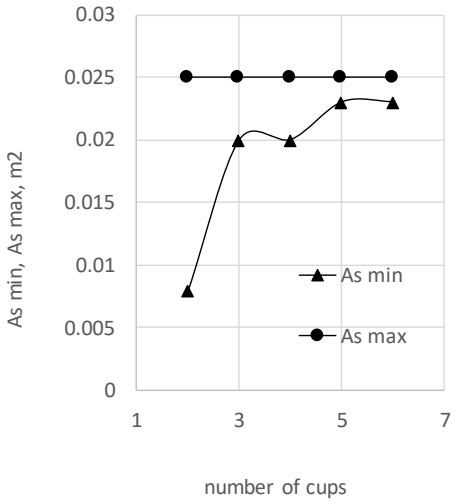

Fig. 4. *The minimum and maximum swept area variation with the number of EM cups*

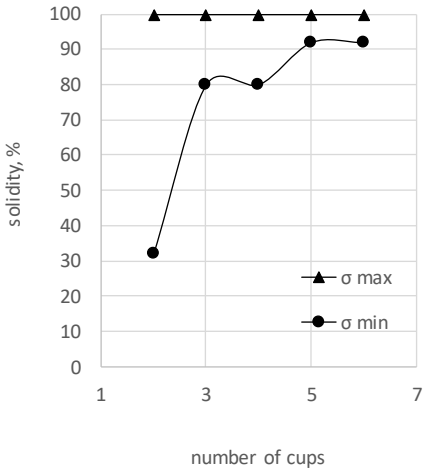

Fig. 5. *The variation of the solidity of the experimental models with the number of cups*

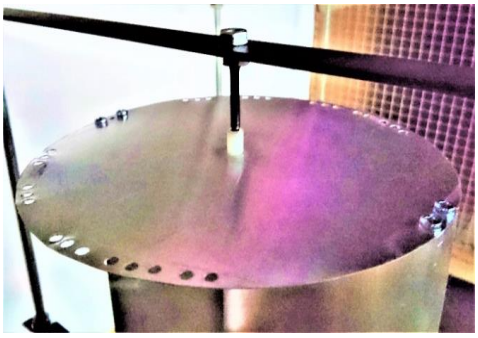

Fig. 6. *Detail regarding the upper bearing*

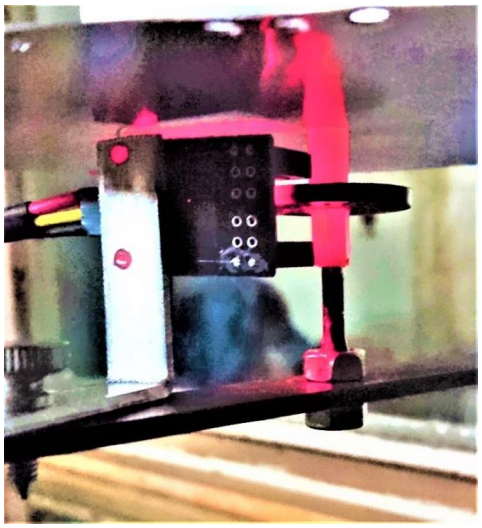

Fig. 7. *Detail of lower bearing and rotary speed transducer*

Fig. 8. *Experimental model with 2 semi-cylindrical cups (S2CNL) fixed on the test frame*

THE ANNALS OF "DUNAREA DE JOS" UNIVERSITY OF GALATI
FASCICLE IX. METALLURGY AND MATERIALS SCIENCE
Nº. 3 - 2020, ISSN 2668-4748; e-ISSN 2668-4756
Article DOI: https://doi.org/10.35219/mms.2020.3.07

Fig. 9. *Experimental model with 3 semi-cylindrical cups (S3CNL) fixed on the test frame*

Fig. 10. *Experimental model with 4 semi-cylindrical cups (S4CNL) fixed on the test frame*

Fig. 12. *Experimental model with 6 semi-cylindrical cups (S6CNL) fixed on the test frame*

2. Experiments

The experiments were performed from the maximum wind speed to the minimum, so that the stopping speed of the experimental model is mentioned. A further study will also address the starting speed of experimental models and the differences between the stopping speed and the starting speed.

The experiments were performed in the conditions of the lowest mechanical friction in the bearings, using a tribological system steel tip and plastic bearing and adequate lubrication.

The experiments were developed on a full-factorial matrix. 5 experimental models of vertical axis wind turbines with 2, 3, 4, 5 and 6 semi-cylindrical buckets (Fig. 6....10) and coded S2CNL, S3CNL, S4NL, S5CNL and S6CNL were used. For each, 14 speed measurements were made at 50 s intervals to stabilize the air flow regime.

The experiments for determining the influence of the number of blades on the rotational speed when operating without load (idling) are shown in the diagrams in Fig. 11 to Fig. 15.

The wind speed changes by progressively decreasing from the maximum value to zero time in which both the wind speed and the rotational speed of the experimental EM model are recorded. The experiment is repeated for all five experimental models and the results are shown in the diagrams mentioned.

The diagrams recorded with the variation of the rotational speed of the EM with the progressive decrease of the wind speed show that the EMs behave differently in the range of wind speeds achieved in the wind tunnel. Thus, the maximum rotation speed is approximately between 6.7 m/s and 7.7 m/s. the rotation of the models is done at values of wind speed between 1.9 m/s and 4 m/s.

The experimental 2-bucket model (S2CNL) reaches the highest rotational speed at almost 800 rpm, has a continuous decrease in rotational speed with wind speed and stops rotation at just over 4 m/s.

S2CNL has the lowest mass, has a large variation of the torque with the angle of rotation and wind speed (ref CN) and the rotation stops abruptly at bm values per 4 m/s of wind speed.

The experimental 3-bucket model (S3CNL) has a proportional variation of the rotational speed at high wind speeds. At wind speeds of approx. 6 m/s has a local maximum rotational speed and stops from rated at 3.5 m/s.

The experimental model with 4 semi-cylindrical buckets (S4CNL) has a linear range of decreasing rotational speed as follows: at the maximum wind speed used approx. 670 rpm and slowly decreases to approx. 625 rpm when the wind speed drops to 7 m/s.

THE ANNALS OF "DUNAREA DE JOS" UNIVERSITY OF GALATI
FASCICLE IX. METALLURGY AND MATERIALS SCIENCE
Nº. 3 - 2020, ISSN 2668-4748; e-ISSN 2668-4756
Article DOI: https://doi.org/10.35219/mms.2020.3.07

below this speed the experimental model has a rapid decrease in speed and stops at 3.75 m/s.

The experimental model with 5 buckets (S5CNL) tested without loading, has two operating areas: one with constant rotation speed and approx. 670 rpm, for wind speeds from 9.7 m/s to 7 m/s and then a sudden drop and stop at 3.75 m/s wind speed.

The experimental 6-bucket model (S6CNL) also tested without loading has a behavior similar to that of the S5CNL has two operating areas: one with constant rotational speed and approx. 670 rpm, for wind speeds from 9.7 m/s to 7 m/s and then a sudden drop and stopping at 1.25 m/s wind speed.

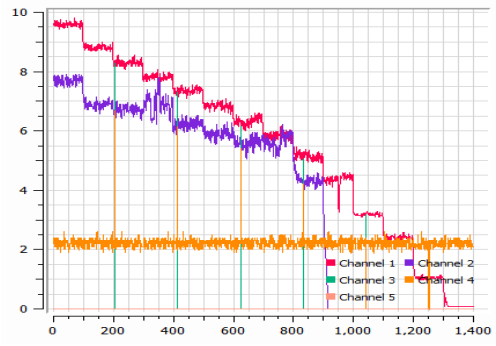

Fig. 13. *Variation of the rotational speed of the experimental model S2CNL with wind speed*

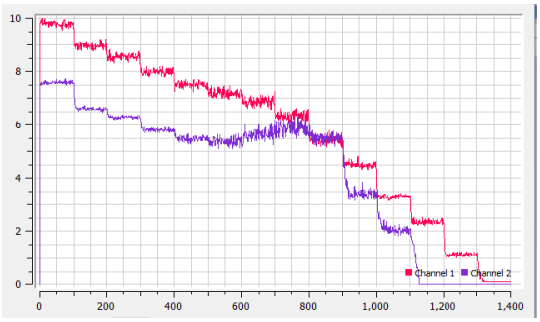

Fig. 14. *Variation of the rotational speed of the experimental model S3CNL with wind speed*

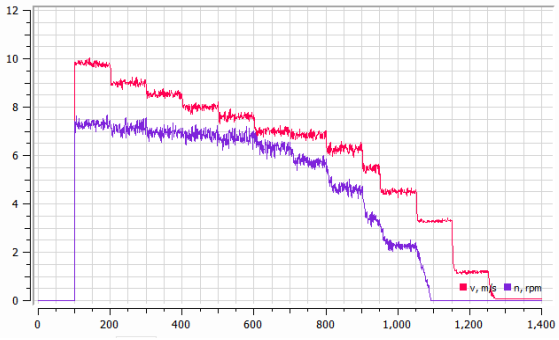

Fig. 15. *Variation of the rotational speed of the experimental model S4CNL with wind speed*

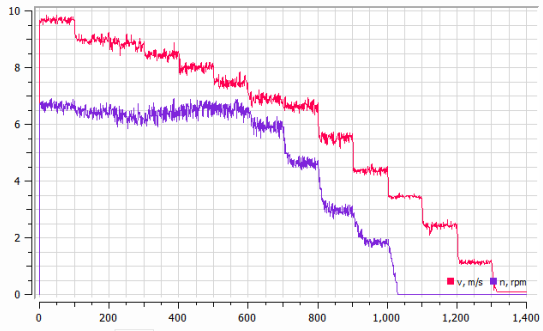

Fig. 16. *Variation of the rotational speed of the experimental model S5CNL with wind speed*

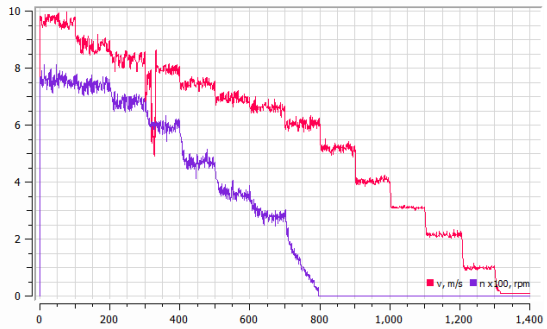

Fig. 17. *Variation of the rotational speed of the experimental model S6CNL with wind speed*

3. Results

Based on the measurements are shown in Fig. 17 the variation of the rotation speed of the experimental models with the wind speed. The stopping speed of the six EMs is between 2 and 4 m/s and the maximum rotation speed in the range of 650-750 rpm. The variation curves have an approximately linear area after which they tend towards a maximum value.

The analysis of the influence of wind speed on the specific speed is shown in Fig. 17 and in this case the curves are grouped in the form of a band in the diagram. EMs has the best behavior with 3 semi-cylindrical cups (S3CNL) which has the best sensitivity to wind speed and the largest λ of about 0.8 at about 5.5 m/s Compared to other models has the largest λ (with small exceptions).

From the point of view of the aerodynamics of the components of the mentioned EM, it is important to reach the highest possible values of the Reynolds number. The length of the semi-cylindrical blade in the section is considered the flow length. The variation of the Re number with the wind speed is shown in Fig. 18. The different composition of the three-bucket model (S3CNL) is observed which does not reach more than 30000. The other experimental models behave similarly and the results form a band

THE ANNALS OF "DUNAREA DE JOS" UNIVERSITY OF GALATI
FASCICLE IX. METALLURGY AND MATERIALS SCIENCE
No. 3 - 2020, ISSN 2668-4748; e-ISSN 2668-4756
Article DOI: https://doi.org/10.35219/mms.2020.3.07

that at 10 m/s speed of the wind reaches the Re number over 100000. The wind power has a variation with the third power of the wind speed which is seen in Fig. 19.

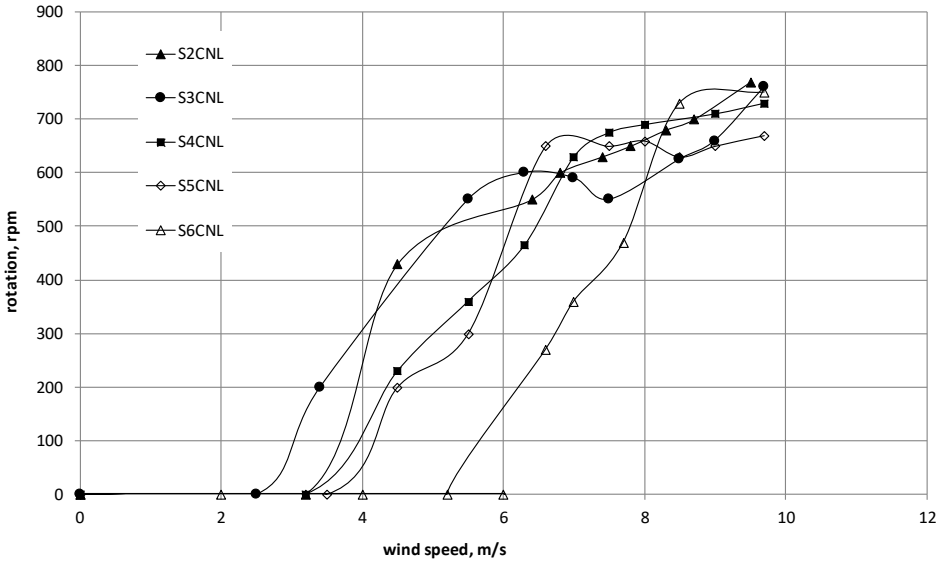

Fig. 18. *Variation of the rotation speed of the experimental models (EM) with the wind speed*

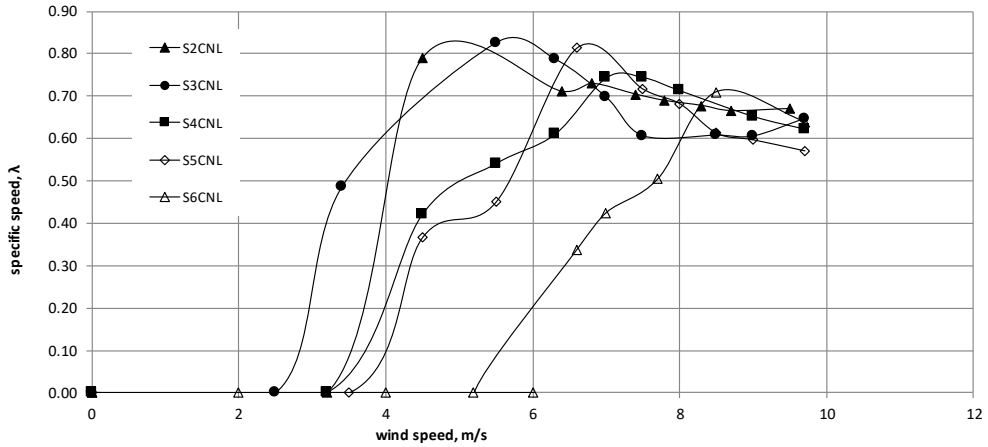

Fig. 19. *Influence of wind speed on specific speed (λ)*

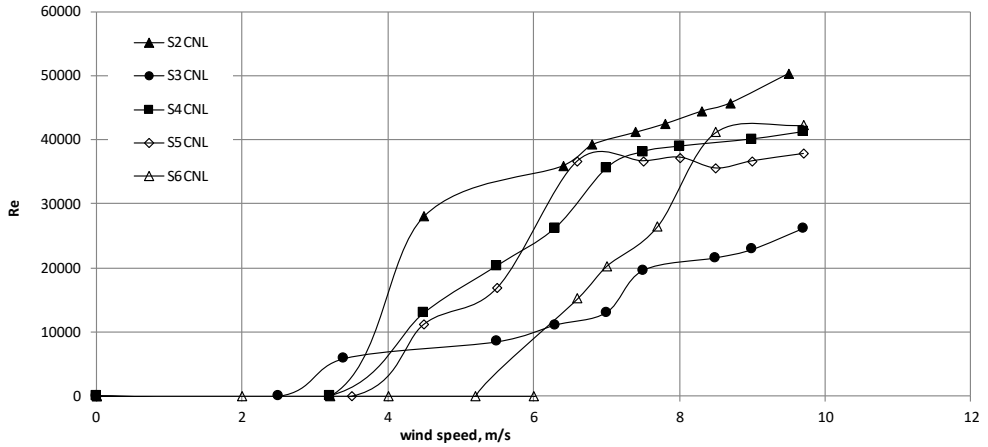

Fig. 20. *The influence of wind speed on the Re number*

THE ANNALS OF "DUNAREA DE JOS" UNIVERSITY OF GALATI
FASCICLE IX. METALLURGY AND MATERIALS SCIENCE
N°. 3 - 2020, ISSN 2668-4748; e-ISSN 2668-4756
Article DOI: https://doi.org/10.35219/mms.2020.3.07

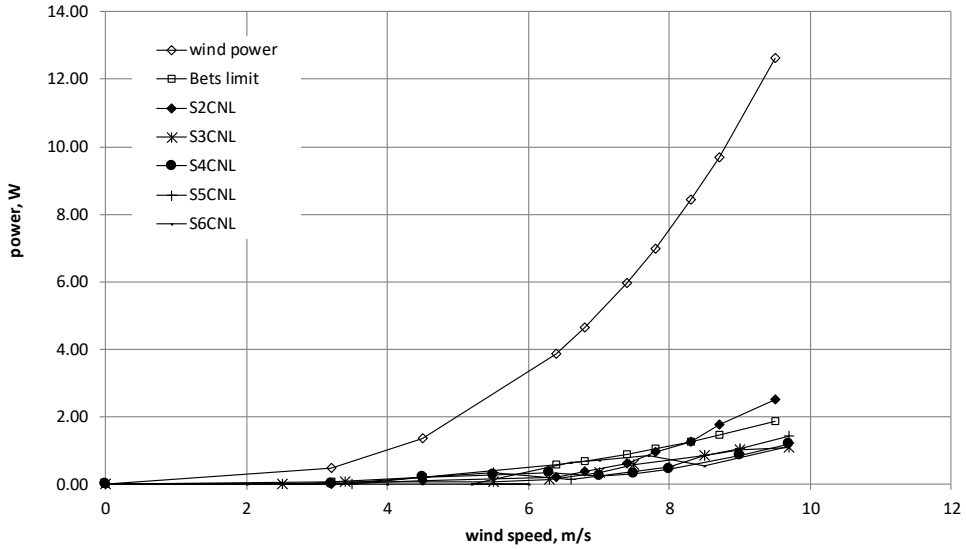

Fig. 21. *The influence of wind speed on power*

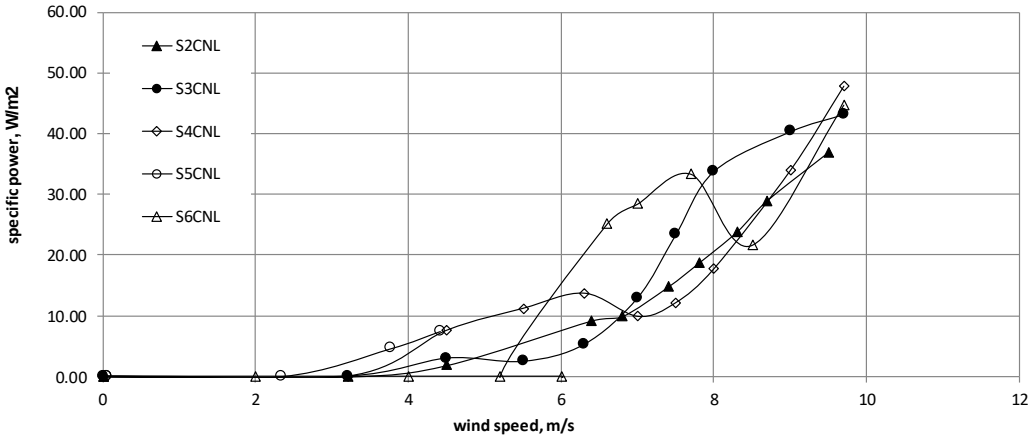

Fig. 22. *The influence of wind speed on specific power*

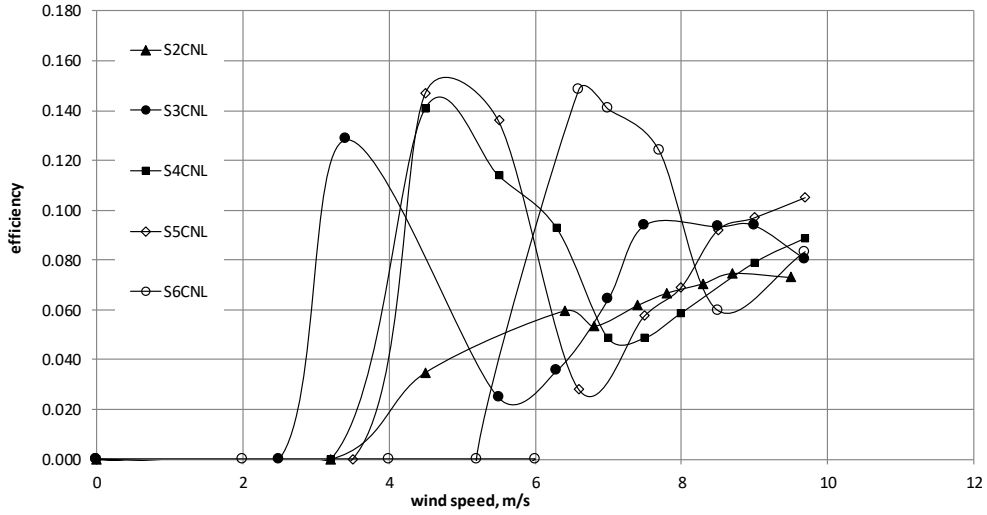

Fig. 23. *The influence of wind speed on the efficiency of converting wind energy into mechanical work*

THE ANNALS OF "DUNAREA DE JOS" UNIVERSITY OF GALATI
FASCICLE IX. METALLURGY AND MATERIALS SCIENCE
Nº. 3 - 2020, ISSN 2668-4748; e-ISSN 2668-4756
Article DOI: https://doi.org/10.35219/mms.2020.3.07

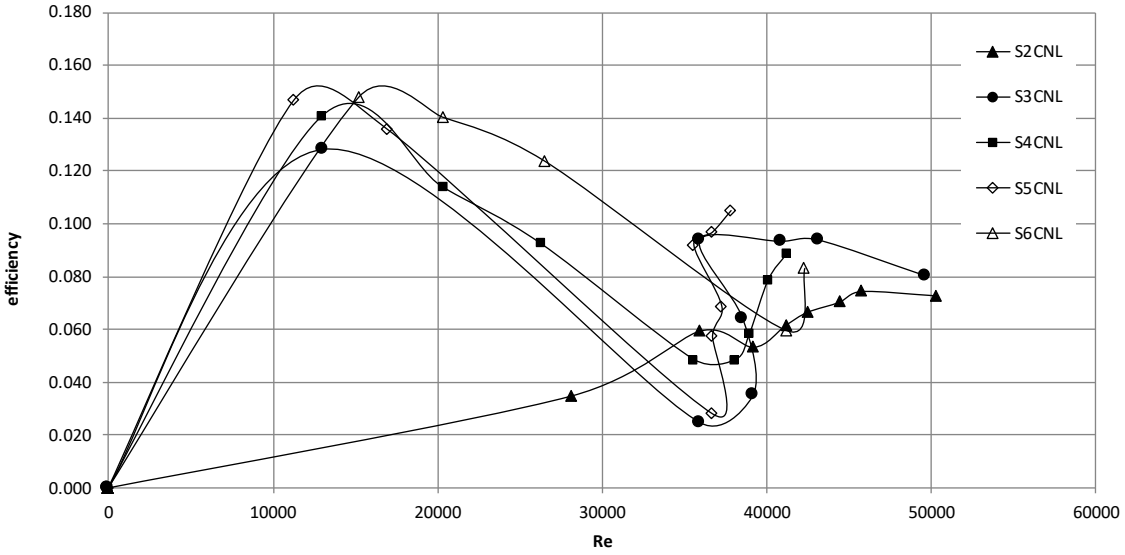

Fig. 24. *Variation of conversion efficiency with the Re number*

The Betz limit (14.81%) also varies with the same allure, which represents the maximum limit for the conversion of wind energy into other forms of energy. All the shaft powers for the researched experimental models are above this value.

In Fig. 20 it is observed that the allure of the specific power variation curves at the axis have a local maximum that is positioned depending on the number of blades of the experimental model.

The efficiency of the conversion of wind energy into mechanical work is shown in Fig. 21. It is observed that the efficiency depends on the number of cups of the model. For all experimental models the efficiency has an area where a local maximum is present, followed by a minimum and then an increase in efficiency up to the test speeds used given below the value of the local maximum. The peripheral speed of the experimental model u cannot be greater than the wind speed v unless forces other than D (drag force) appear. For all experimental models subjected to experiments in the wind tunnel we have a maximum influence of the Re number on the conversion efficiency (Fig. 22). Thus, S2CNL has 6% at Re about 35000.

The variation curves have the same allure of variation and the Re number increases approximately linearly to lambda 0.7 to 0.8 (Fig. 23). The linear areas depend on the number of cups and there is an increase in the Re number with the number of cups. After a value the Re number increases with decreasing peripheral speed of EM (lambda decreases).

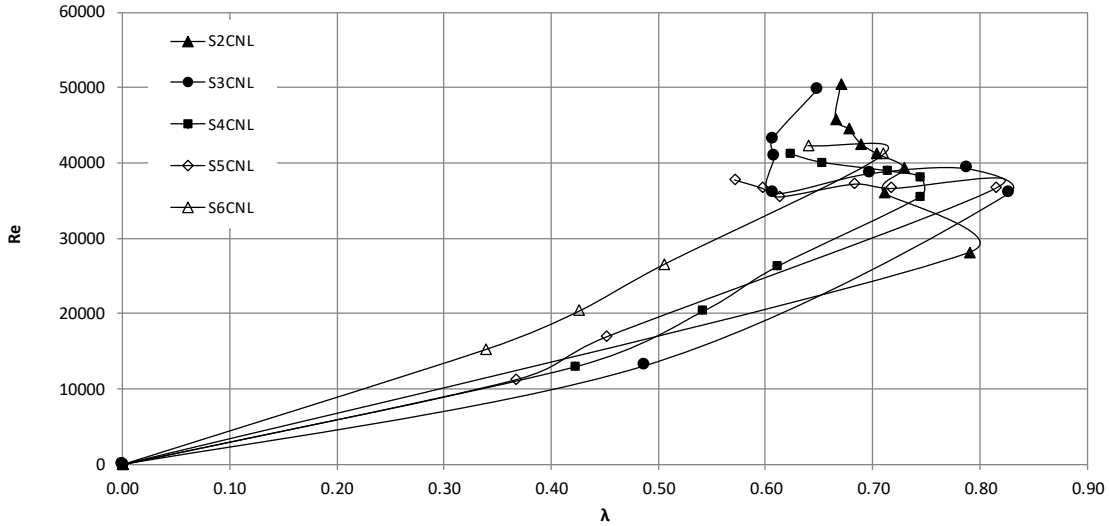

Fig. 25. *The influence of Lambda specific speed on the Re number*

THE ANNALS OF "DUNAREA DE JOS" UNIVERSITY OF GALATI
FASCICLE IX. METALLURGY AND MATERIALS SCIENCE
N°. 3 - 2020, ISSN 2668-4748; e-ISSN 2668-4756
Article DOI: https://doi.org/10.35219/mms.2020.3.07

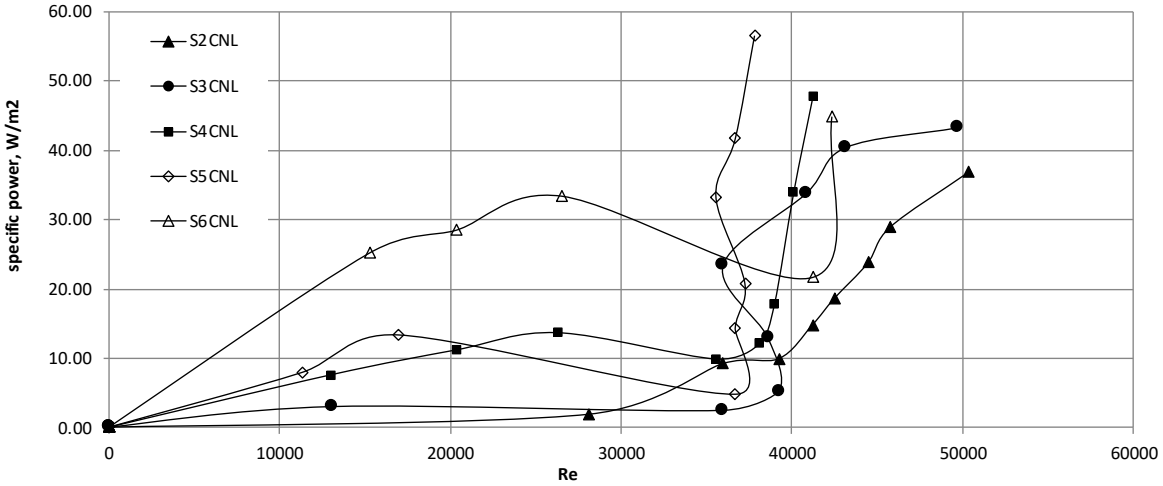

Fig. 26. *Influence of the Re number (flow quality) on axis specific power*

Axis-specific power variation curves have a local maximum at a value of the Re number that depends on the number of cups of EM. Thus, the EM with six S6CNL blades reaches 34 W/m^2 at 25000 Re and the one with 5 cups (S5CNL) 14W / m2 at Re 15000. This EM has after Re 35000 an increase of the specific power up to over 55 W/m^2. The experimental models with two cups (S2CNL) and three cups (S3CNL) reach 25 W/m^2 at Re 50000 and 45 W/m^2 at Re 50000, respectively.

4. Conclusions

Wind energy is a form of energy that can be partially converted into mechanical work and then into electrical energy through the Betz limit. Energy conversion is supported by a mathematical model of conversion and by various structures of the wind system.

The paper focused on the Savonius VAWT model for which the experimental VAWT models were developed. The number of semi-cylindrical cups of some Savonius experimental models with 2, 3, 4, 5 and 6 semi-cylindrical cups have been modified (SC2CNL, SC3CNL, SC4CNL, SC5CNL and SC6CNL).

The results show that under the wind test conditions between 0…9.7 m/s, we have a major influence of the number of semi-cylindrical cups on the rotation speed of the experimental models.

All experimental models have a stop threshold which also depends on the number of semi-cylindrical cups of the experimental model.

It is found that the 3-cup EM co (S3CNL) has the best sensitivity to low wind speeds (Fig. 16).

The lowest sensitivity and the highest stopping threshold are at EM with 5 and 6 semi-cylindrical cups (S5CNL and S6CNL).

The model with two semi-cylindrical cups (S2CNL) reaches the maximum speed as over 60000. The high values of the Re number also contribute to the fineness of the surface of the material used to make semi-cylindrical cups (0.4mm thick laminated aluminum sheet). The most uniform increase of the Re number 0 has EM with 2 cups (S2CNL) which after a rapid increase at the Re number 30000 at about 5.5 m/s has an approximately linear increase up to over 60,000.

For S4CNL, S5CNL and S6CNL (Fig. 20) the values of the local maximum specific power increase and the highest value corresponds to the model with 6 cups, being almost 35 W/m^2.

Regarding the efficiency of conversion (Fig. 21), the S2CNL has the lowest efficiency of 6%; S3CNL reaches 13% and S4SNL at over 14%. The experimental models with 5 and 6 cups (S% CNL and S6CNL) is close to the maximum efficiency limit for this VAWT model, which has as driving force D (drag force). The efficiency of the conversion depends on the wind speed with a maximum curve for each experimental model (Fig. 21). A similar dependence is on the Re number. The efficiency of the conversion depends on the wind speed with a maximum curve for each experimental model. A similar dependence is on the Re number (Fig. 22).

With the increase of the number of semi-cylindrical cups to five and six respectively, the efficiency of the conversion of wind energy into mechanical work reaches almost the Betz line (14.81%) specific for this type of VAWT, at 4.5 m/s and 6.5 m/s, respectively.

References

[1]. Hau Erich, *Wind Turbines, Fundamentals, Technologies, Applications, Economics*, s.l.: Springler, 2006.

[2]. Manwell J. F., McGowan J. G., Rogers A. L., *Wind Energy Explained. Theory, Design and Application*, s.l. John Wiley & Sons Ltd., p. 590, 2002.
[3]. The European Wind energy association, *Wind in power*, 2010 European statistics, 2011.
[4]. Piggot Hugh, *Small Wind Turbine Design Notes*, 1998.
[5]. Menet J. L., Bourabaa N., *Increase in a savonius rotor efficiency*.
[6]. Archer Cristina L., Jacobson Mark Z., *Evaluation of global wind power*, Journal of Geophysical Research, vol. 11, D12110, 2005.
[7]. Cazacu Nelu, *Load Behavior of a Vertical Axle Wind Turbine Model with Four Blades Periodically Couple Aerodynamically*, The Annals of "Dunarea de Jos" University of Galati, Fascicle IX, Metallurgy and Materials Science, Galati University Press, vol. 3, p. 5-11, ISSN 2668-4748; e-ISSN 2668 4756, 2018.
[8]. Cazacu Nelu, *Improving the Powerful Behavior of an ExperimentaL model of Savonius Turbine (S-rotor) with Couple Aerodynamic Additional Blades*, The Annals of "Dunarea de Jos" University of Galati, Fascicle IX, Metallurgy and Materials Science, Galati University Press, vol. 2, p. 49-53, ISSN 1453-083X, 2018.
[9]. Cazacu Nelu, *The Influence of Number of Blades and the Number of Levels on Behaviorof the "S-rotor" Experimental Model*, The Annals of "Dunarea de Jos" University of Galati, Fascicle IX, Metallurgy and Materials Science, Galati University Press, vol. 4, p. 58-63, ISSN 1453-083X, 2017.
[10]. Cazacu Nelu, *The Behavior of an Experimental Model of Wind Turbine with Vertical Axle with Overlapped Cups at Low Wind Speeds*, The Annals of "Dunarea de Jos" University of Galati, Fascicle IX, Metallurgy and Materials Science, Galati University Press, vol. 4, p. 51-57, ISSN 1453-083X, 2017.
[11]. Cazacu Nelu, Lucaci Bogdan Cătălin, *Functional Model of Savoniuus Type Verrtical Axis Wind Turbine with Periodoc Coupling of Adjacent Vertical Blades*, The Annals of "Dunarea de Jos" University of Galati, Fascicle IX, Metallurgy and Materials Science, vol. 4, p. 69-76, 2014.

THE ANNALS OF "DUNAREA DE JOS" UNIVERSITY OF GALATI
FASCICLE IX. METALLURGY AND MATERIALS SCIENCE
Nº. 3 - 2020, ISSN 2668-4748; e-ISSN 2668-4756
Article DOI: https://doi.org/10.35219/mms.2020.3.08

RESEARCHES CONCERNING THE CONFIGURATION OF GEOTEXTILES IN THE EXECUTION OF REGULATORY WORKS IN THE RIVERBEDS

Paul Vivian SION, Mihail LUCA, Mihaela AVRAM
Technical University "Gheorghe Asachi" of Iasi, Romania
e-mail: mluca2004@yahoo.com

ABSTRACT

The paper deals with the behaviour at hydrodynamic action of the geotextiles used in carrying out the regularization and shore defence works located in riverbed. The geotextiles have lately presented applications for the execution of bottom thresholds, of the management dams in riverbed. Also, geotextiles have become an important component in the structure of river defence works on riverbeds. The research was carried out on the lower course of the Moldova River in the area of Pildesti, Neamț County. The dynamic action of the floods, through the liquid and solid flows, influences the stability and the resistance over time of the constructions made from geotextiles. The researchers analysed the behaviour of the geo-bags made of polyester bags filled with local materials (sand and gravel stabilized with cement), used in the structure of the bottom thresholds, steering dams and in the shore defence works. The research results indicate a differentiated behaviour of the geo-bags depending on the location (in the water, or on the shore) and the mode of action of the water (dynamic or static). The action of the water, through the liquid and solid flow, degraded the structure of the geo-bags by breaking and emptying the filling material. The geo-bags showed a reduced resistance to the action of the alluvial material, especially when the dosage of cement indicated by the design was not achieved. The research highlighted the good behaviour of the geo-bags in the erosion phenomenon of the riverbed, when they were mulched on the erosion zones and ensured the continuity of the constructions in the riverbed (bottom thresholds and shore defences).

KEYWORDS: bottom threshold, degradation, erosion, geo-bag, steering dam

1. Introduction

The river regularization works are part of the watercourses to ensure the stability of the hydrological and hydraulic parameters on a well-determined sector. The design of the works of regularization and defence of the bank in the riverbed is realized with hydrological parameters (flows, levels, levels of defence, protected surfaces, etc.) obtained by the statistical processing of the data collected over large intervals [1, 4, 7].

The hydrological changes of the last time period influence the behaviour of the regularization and shore defence works located in the erodible riverbeds [12]. The morphological change in time of the riverbed determines new actions on the stability of the hydrotechnical constructions with the role of shore defence [5, 10, 9].

The shore defences are made of natural materials (wood, stone), artificial materials (plain and reinforced concrete, plastics) and composites. The shore defence works can be rigid (reinforced concrete slabs, stone) and elastic (stone gabions, geo-bags). The rigid-type defence does not behave effectively in erodible beds [10].

Geotextiles are used in the execution of bottom thresholds, steering dams and river bed crossings. Geotextiles have become an important component in the structure of shore defence works on riverbeds formed in weakly cohesive rocks [3, 10].

The paper deals with the behaviour of water geotextiles used in the regularization and shore defence works located in the riverbeds.

THE ANNALS OF "DUNAREA DE JOS" UNIVERSITY OF GALATI
FASCICLE IX. METALLURGY AND MATERIALS SCIENCE
N°. 3 - 2020, ISSN 2668-4748; e-ISSN 2668-4756
Article DOI: https://doi.org/10.35219/mms.2020.3.08

2. Material and research method

The research was carried out in two areas located on the lower course of the Moldova River (Figure 1). The riverbed in the two areas consists of alternating layers of ballast, dusty sand and clay sand from the alluvial transport. The river foundation is weakly cohesive, which favours erosion of the riverbed and the banks [4, 9, 14].

The research areas are located on the lower course of the river Moldova, as follows (Figure 2):

- zone I is located near the town of Soci, Mirosloveşti commune, Iaşi county;
- the second zone is located downstream of the town of Pildesti, Neamţ county.

A condition for selecting the research areas was given by their endowment with works to regulate the riverbed executed from geo-bags. Also, the shore defence works should be made of concrete slabs and geo-bags. This situation is present on the lower course of the river Moldova.

The Moldova River presents in the research area a characteristic route of the lower course located in a low slope field area (Figure 3). The direction of flow of the river is NW - SE. The river Moldova presents the following characteristics up to the hydrometric station (SH) Tupilati: length - 176.60 km, surface of the river basin - 3951 km^2, slope - 1.30‰, average altitude - 236 m, average multiannual flow - 32.9 m^3/s, solid flow in suspension - 43.2 Kg/s [11, 13].

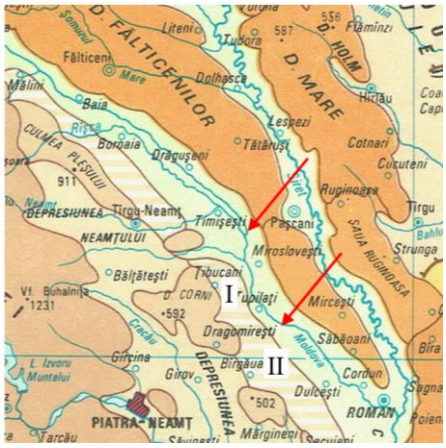

Fig. 1. *Location of the research areas on the physical map of the Moldova River: I - Soci area; II - Pildesti area* [14]

The research used hydrological data taken from the Tupilaţi Hydrometric Station, Neamţ County (average and maximum flows) [10].

Theoretical and experimental research was carried out in the following directions:

1. Researche regarding the modification of the constructive parameters of the regularization and shore defence works existing in the study areas.
2. Research on the behavior of the regularization works in time on the erosive action of water.
3. Research on the behavior of geotextiles in natural and anthropic actions in the site.
4. Analysis of solutions to improve the regularization solutions made with geotextiles in riverbeds.

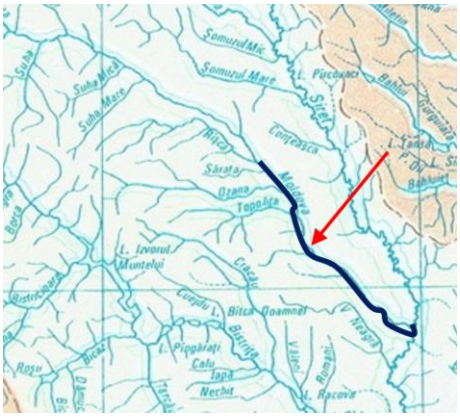

Fig. 2. *Localization in the hydrographic network of the lower course of the Moldova River* [13]

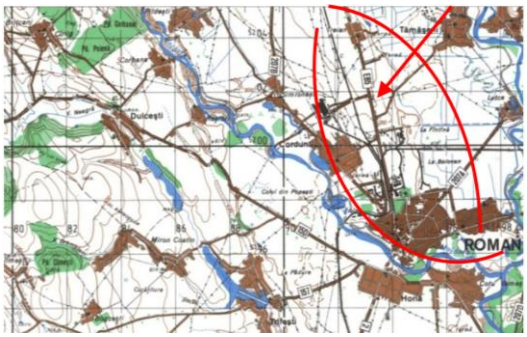

Fig. 3. *Location of the research area 2, Pildesti area, on the lower course of the Moldova River*

3. Results and discussions

3.1. Geotextiles used in the work of river regularization

Plastics are used in the construction of river defence works due to the high mechanical resistance to stretching. Some plastics are impermeable to very small thicknesses and have great flexibility. The realization of materials with large lengths and surfaces, with reduced weight, contributes to the increase of the execution efficiency [3, 10].

The introduction of the plastics materials in the structure of the hydrotechnical works is made with an

THE ANNALS OF "DUNAREA DE JOS" UNIVERSITY OF GALATI
FASCICLE IX. METALLURGY AND MATERIALS SCIENCE
N°. 3 - 2020, ISSN 2668-4748; e-ISSN 2668-4756
Article DOI: https://doi.org/10.35219/mms.2020.3.08

easy technology and at relatively low costs. From the plastics used in river defence works, the geotextiles are detached. They are made in a wide range of types and have applicability under various geotechnical conditions. However, plastics are difficult to degrade over time or can hardly degrade [3]. Lately, biodegradable materials such as geotextiles, which replace part of plastics, have been used.

Geo-synthetic materials are flat structures of polymeric materials. The most commonly used types of geo-synthetics are geotextiles, geomembranes and geogrids. The functions performed by these are the following: separation, filtration, reinforcement, drainage, sealing and erosion protection [3].

Fig. 4. *Shore protection from non-woven geotextile mounted on the profiled slope of the river* [10]

Fig. 5. *Protection from geogrid + geotextile mounted on the profiled river bank* [9]

Geotextiles are materials made of polyester or polypropylene, woven or non-woven, being presented in a variety of thicknesses and strengths, depending on the scope. Geotextiles are classified according to their fabrication / non-woven, thermofixed and special type. Geotextiles are combined with geogrids for making ballast layers or reinforced earth walls. Geotextiles are flexible, which allows them a very good moulding on the mounting surface [3, 10].

A variety of geotextiles are used in the execution of the river bank consolidation works, at the embankment of dams and dams, at land masses, at drainage works and at support walls.

Biodegradable geotextiles are made in the form of textile fabrics, they are flat structures of plant (e.g. jute, coconut fibres) or animal (e.g. wool) materials. The most widely used biodegradable geotextiles are in the form of fabrics, seams and pressed bands [10].

Fig. 6. *Geotextile wool fabric mounted on the bank of a river as a support for the defence of the river* [9]

The woollen fabric is geotextile made from natural, non-reinforced wool fibres, which are biologically degraded in about 2-3 years. Grass seeds are placed over the woollen fabric placed on the river bank, and above these a filling with vegetable soil is performed. By using this composite, the sliding planes on the slope are avoided and the conditions for the protection with vegetal layer are ensured.

Over the last 25 years, work has begun to regulate rivers in geo-bags filled with ballast or ballast mixed with cement. Geo-bags are bags or mattresses made of polyester fabric stuffed with local materials [10]. Geo-bags are used for the protection of the river or lake shore, at the embankment dam etc.

Geo-bags have limited mobility on the three directions. Also, the commissioning technology is accessible and at a reduced price. The main disadvantage of the geo-bags is given by the mechanical resistance reduced to the action of the alluviums carried by the water.

The geo-bags are made for riverbed, steering dams, bottom thresholds, closing sleepers and mainly shore protection [10].

THE ANNALS OF "DUNAREA DE JOS" UNIVERSITY OF GALATI
FASCICLE IX. METALLURGY AND MATERIALS SCIENCE
Nº. 3 - 2020, ISSN 2668-4748; e-ISSN 2668-4756
Article DOI: https://doi.org/10.35219/mms.2020.3.08

a

b

Fig. 7. *Protection from geo-bags mounted on the river bank: a - bag/mattress-type geo-bag; b - shore defence from geo-bags* [9]

3.2. The result of the researches regarding the geo-bags behaviour in the works of river regularization

The studies and researches were carried out on sectors of the Moldova River located on the lower course, where regularization of the riverbed and shore defence works were performed using geo-bags. The river of Moldova in the two research areas presents a foundation formed by weakly cohesive rocks [4, 6].

Table 1. *Maximum flow rates (Qmax) with calculation probability (p (%)) for the study sector on the Moldova River* [3]

p (%)	2	5	10	20	50	95
Q_{max} (m^3/s)	1650	1275	1.000	558	31.0	2.13

The analysis of the structural and functional status of the geo-bags type works was carried out by in situ inspection, topographic measurements, visualization of the degradation forms, measurement of the geometrical parameters of the degradations, realization of photo and video surveys, etc. The data taken from the field were compared with those existing in the technical design documentation, or in similar works performed internally and externally.

The hydrological data analysis has revealed a high frequency of floods in the last 20 years in the study area. The hydrological studies carried out in the study area indicated the calculation and verification rates considered when designing the regularization and shore defence works (Table 1) [4].

A. Analysis of the behaviour of the shore defence works in the 1st research area, Soci area

In the Soci research area there is the hydrotechnical construction of the Moldova River sub-crossing by the Timisesti-Iasi adduction pipes (three steel pipes, of which two with a diameter of 1000 mm and a third with a diameter of 800 mm). The riverbed was calibrated, and the bank was protected with concrete slabs on the river's sub-crossing sector. The hydrotechnical work was executed between 1969 and 1971.

Between 2004 and 2012 there were a series of major floods on the river Moldova [4, 6], which partially and totally degraded the defences on some sections (Fig. 8.a).

a

b

Fig. 8. *Shore protection in the Sochi area: degraded concrete slabs (year 2008)* [4]*; b - defence from geo-bags (photo Sion, 2019)*

The technical expertise carried out in 2012 highlighted the state of degradation of the shore protection as a result of the action of water at floods, but also of the absence of maintenance works [4]. In 2015 the pipelines located in the subversion of the Moldova River were rehabilitated. Also, the shore

THE ANNALS OF "DUNAREA DE JOS" UNIVERSITY OF GALATI
FASCICLE IX. METALLURGY AND MATERIALS SCIENCE
Nº. 3 - 2020, ISSN 2668-4748; e-ISSN 2668-4756
Article DOI: https://doi.org/10.35219/mms.2020.3.08

defence was rehabilitated by using geo-bags as a solution to the instability of the foundation ground (Figure 8.b).

The shore defence is made of a structure of rectangular-shaped geotextile mattresses with a length of 1.50 m, width 0.80 m, height 30-40 cm and filled with ballast (Figure 8.b). The geotextile mattresses are placed with the long side parallel to the shore. Laying the mattresses horizontally was done in chess. Geo-bags in contact with water were filled with ballast mixed with cement [4].

The research was carried out between 2017-2019 and analyzed the behaviour of the shore protection executed from geo-bags. Field analysis and data processing indicated the following results:

- the shore defence behaved well in the action of the floods of 2016 and 2018, without showing significant degradation (Figure 8.b);
- a small number of geo-bags placed in the water contact layer were degraded by breaking down by the alluviums; the ruptures are in the direction of the water and have lengths of 3.0 - 8.0 cm;
- there was no movement of geo-bags vertically and horizontally.

B. Analysis of the behaviour of the regularization and shore defence works in the II research area, Pildesti area

The works of regularization and defence of the shore on the Moldova River in this area have the role of ensuring the optimal functioning of the underground water catchment in Pildesti. The riverbed was moved to the left bank. And through the bottom thresholds, the water level was raised to ensure the conditions of water capture.

The works of regularization and defence of the shore were executed from 1996. They were executed of reinforced concrete and stone. The floods on the river Moldova in 1994-2006 progressively degraded the works from the riverbed and from the shore. In order to remedy the works, consecutive renovations were carried out until 2006. The 2006 flood partially destroyed these works. The rehabilitation works of 2006 used in parallel geo-bags for the execution of the works of the river and the protection of the shore [10].

The shore protection and regularization works initially performed were made up of the following [8]:

- regularization works: moving the minor riverbed near the left bank through steering dams and closing sleepers; calibration of the flow section to a width of 90 m;
- shore defence works: reinforced concrete slabs supported on a simple concrete beam.

After 2006, works were carried out on the bank and on the shore, defence using geo-bags (geotextile bags filled with ballast) (Figure 9). Subsequent works carried out in 2017 (steering dock, closing dock, shore defence) were performed only with geo-bags [10].

The research was carried out between 2015 and 2019 and analyzed the behaviour of the shore protection executed from geo-bags. The analyzes performed in the field were realized at intervals of 3-5 months, or after passing a flood. The data processing and interpretation indicated the following results:

- the works made from geo-bags behaved differently depending on their location (in the riverbed and on the shore) and the complex of natural and anthropic actions;

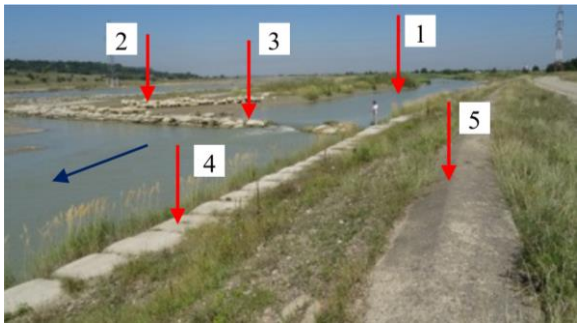

Fig. 9. *Works with geo-bags in the riverbed: 1 - diverted riverbed; 2 - steering dam; 3- bottom threshold; 4 - shore defence; 5 - old shore defence (photo, Sion, 2019)*

- the floods of 2006, 2008, 2016 and 2018 broke the submersible water steering dam to the river bank on the left bank; the phenomenon was determined by the maximum flow and the action of the alluviums (Figure 10);

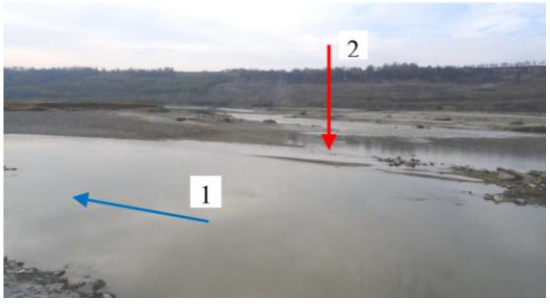

Fig. 10. *View of the branching area of the riverbed: 1 - deviated riverbed; 2 - steering dam (photo, Sion, 2015)*

- the destructive influence of the alluviums is relatively intensified by the presence of a ballast

THE ANNALS OF "DUNAREA DE JOS" UNIVERSITY OF GALATI
FASCICLE IX. METALLURGY AND MATERIALS SCIENCE
N°. 3 - 2020, ISSN 2668-4748; e-ISSN 2668-4756
Article DOI: https://doi.org/10.35219/mms.2020.3.08

located at a distance of about 200-300 m from the area of technological change of the riverbed;

Fig. 11. *Structural degradation of a bottom threshold made from geo-bags (photo, Sion, 2018)*

- the closure cross executed from geo-bags was broken at the 2016 flood, which caused the main river to be moved to the right bank: the geo-bags were displaced by the action of the water from the site;
- the bottom thresholds made on the deflected bed and executed from geo-bags have the role of raising the water level; the bottom threshold is made of 2–4 rows of vertical geo-bags; the height of the bottom thresholds is 0.60-1.60 m;
- the degradation of the bottom thresholds by the hydrodynamic action is differentiated along the riverbed; degradation is manifested by moving geo-bags horizontally and vertically (Figure 11);
- some of the bottom thresholds analyzed were degraded by partially destroying a variable number of geo-bags and moving some downstream, or at the base of the threshold (Figure 12);

Fig. 12. *General view of the structural degradation of a bottom threshold made from geo-bags under hydrodynamic action (photo, Sion, 2019)*

- the analysis carried out in the field showed the total degradation of the geo-bags by breaking and evacuating the filling material; geo-bags partially emptied of material were moved from the downstream position, which changed the water discharge positions;

Fig. 13. *Degradation of works from geo-bags on water action on the Moldova River: 1 - bottom threshold; 2 - shore defence (photo, Sion, 2019)*

- the shore defence made from geo-bags is located at a variable distance from the old shore defence executed from concrete slabs (Figure 13 and 14);
- shore protection from geo-bags is located at a variable distance from the old shore protection work carried out from concrete slabs (Figure 9, 13 and 14);
- a limited number of shore protection geo-bags are degraded by rupture as a result of flooding carried by floods (Figure 15);

Fig. 14. *General view of the left bank defence works: 1 - old concrete slab work; 2 - new work from geo-bags (photo, Sion, 2018)*

- the analysis in the field showed that some of the geo-bags are degraded by local rupture and tearing by the flocks of sheep and goats passing through the shore area;

Research conducted on the lower course of the river Moldova has shown that the presence of weakly cohesive rocks in the bedrock foundation in time determines the loss of the stability of the regularization and defence works of the rigid type. A great influence on the degradation of the works is the action of the high frequency floods and important alluvial transport.

The results of the researches carried out in the two areas showed a satisfactory and differentiated behaviour of geo-bags at the action of the water

THE ANNALS OF "DUNAREA DE JOS" UNIVERSITY OF GALATI
FASCICLE IX. METALLURGY AND MATERIALS SCIENCE
N°. 3 - 2020, ISSN 2668-4748; e-ISSN 2668-4756
Article DOI: https://doi.org/10.35219/mms.2020.3.08

depending on the location of the site (on the bank or on the shore), the way of completion and the quality of the filling.

Fig. 15. *Details on forms of degradation of geo-bags under natural and anthropic actions (photo, Sion, 2019)*

The works of regularization and defence of the elastic type bank work efficiently with the erodible riverbeds, they behave well in the settlements and movements in vertical and horizontal plane. Works in geo-bags do not affect the environment through the contribution of concrete and metal.

The morphological changes of the riverbed imply the modification of the calculation parameters when designing the regularization works regarding the hydrological data and the mechanical characteristics [4, 8].

An important conclusion is represented by the ecological behaviour of the geo-bags. Shore defence in geo-bags allows fine alluvium to be deposited on mattresses, thus forming areas for aquatic flora and fauna growth [2].

4. Conclusions

The studies and researches carried out on the lower course of the Moldova river revealed the different degradation of the old shore defence works following the hydrodynamic erosion of the foundation and the concrete slabs.

Studies and research carried out in recent years have highlighted the possibility of using geo-bags when carrying out regularization works subject to frequent action of floods with important solid transport.

The research carried out in two study areas revealed a variable behaviour of the geo-bags in the action of the water depending on the location (river / riverbed), their mode of accomplishment and the filling quality.

Elastic-type shore defence works, geo-bags type, work effectively with erodible riverbeds, behave well in vertical / horizontal settlements and displacements and do not affect the environment.

Ensuring optimal environmental protection conditions in the watercourses area requires the use of biodegradable geotextiles when carrying out regularization works.

References

[1]. Avram M., *Researches regarding the impact of the hydroclimatic risk factors on the design, the technologies of development and the exploitation of the works of regularization of the rivers*, Research Report 2, Technical University "Gheorghe Asachi" of Iasi, 2016.

[2]. Bica I., *Elements of environmental impact*, Matrixrom Publishing House, Bucharest, 2000.

[3]. Găzdaru A., Manea S., Feodorov V., Batali L., *Geosynthetics in construction*, Edit. Romanian Academy, 1999.

[4]. Luca M., *Update on rehabilitation technical expertise in the area of under-crossing the river Moldova, Timişeşti water adduction pipes, Soci area, Iasi county*, Polias-Instal Iasi Company, 2012.

[5]. Luca M., Tamaşanu F., Luca Al., L., Ilie G., *Research on the stability of the defence works to eroded river beds*, Ovidius University Annals, Series: Civil Engineering, Issue18, Ovidius University Press, p. 33-41, 2016.

[6]. Luca M., Avram Mihaela, Luca Al. L., Chirica Ştefania, *Studies and researches on natural and antropic risk the Moldova's lower course*, PESD, vol. 12, no. 2, "Al. I. Cuza University of Iasi", p. 183-193, 2018.

[7]. Manoliu I. A., *Regulations of rivers and waterways*, Ed. Did. and Pedag., Bucharest, 1973.

[8]. Neuhold C., Stanzel P., Nachtnebel H. P., *Incorporating river morphological changes to flood risk assessment: uncertainties, methodology and application*, Natural Hazards and Earth System Sciences, no. 9, p. 789-799, 2009.

[9]. Romanescu G., Stoleriu C., *Causes and Effects of the Catastrophic Flooding on the Siret River (Romania) in July-August 2008*, Natural Hazards, 69, p. 1351-1367, 2013.

[10]. Sion P. V., *Documentary study on the design, execution and exploitation of the works of river regularization in the concept of "green regularization"*, Research Report 1, Doctoral School of the Technical University "Gheorghe Asachi" in Iaşi, 2019.

[11]. Ujvari I., *The geography of Romania's waters*, Edit. Scientific, Bucharest, 1972.

[12]. Vamanu E., Olariu P., *Hydroclimatic hazards in the Siret hydrographic area in the context of geographic changes*, Collection of papers, Annual Scientific Session INMH Bucharest, 2002.

[13]. ***, *Atlas of Water Cadastre in Romania*, Ministry of Environment, Bucharest, 1992.

[14]. ***, *The geographical Atlas of Romania*, Didactic and Pedagogical Publishing House, Bucharest, 1985.

MANUSCRISELE, CĂRŢILE ŞI REVISTELE PENTRU SCHIMB, PRECUM ŞI ORICE CORESPONDENŢE SE VOR TRIMITE PE ADRESA:

MANUSCRIPTS, REVIEWS AND BOOKS FOR EXCHANGE COOPERATION, AS WELL AS ANY CORRESPONDANCE WILL BE MAILED TO:

LES MANUSCRIPTS, LES REVUES ET LES LIVRES POUR L'ECHANGE, TOUT AUSSI QUE LA CORRESPONDANCE SERONT ENVOYES A L'ADRESSE:

MANUSCKRIPTEN, ZIETSCHRITFTEN UND BUCHER FUR AUSTAUCH SOWIE DIE KORRESPONDENZ SID AN FOLGENDE ANSCHRIFT ZU SEDEN:

After the latest evaluation of the journals by the National Center for Science Policy and Scientometrics (**CENAPOSS**), in recognition of its quality and impact at national level, the journal will be included in the B^+ category, 215 code (http://cncsis.gov.ro/userfiles/file/CENAPOSS/Bplus_2011.pdf).

The journal is already indexed in:

DOAJ: https://doaj.org/

SCIPIO-RO: http://www.scipio.ro/web/182206

EBSCO: http://www.ebscohost.com/titleLists/a9h-journals.pdf

Google Academic: https://scholar.google.ro

Index Copernicus: https://journals.indexcopernicus.com

Crossref: https://search.crossref.org/

The papers published in this journal can be viewed on the website: http://www.gup.ugal.ro/ugaljournals/index.php/mms

Name and Address of Publisher:
Contact person: Elena MEREUȚĂ
Galati University Press - GUP
47 Domneasca St., 800008 - Galati, Romania
Phone: +40 336 130139
Fax: +40 236 461353
Email: gup@ugal.ro

Name and Address of Editor:
Prof. Dr. Eng. Marian BORDEI
"Dunarea de Jos" University of Galati, Faculty of Engineering
111 Domneasca St., 800201 - Galati, Romania
Phone: +40 336 130208
Phone/Fax: +40 336 130283
Email: mbordei@ugal.ro

AFFILIATED WITH:

- THE ROMANIAN SOCIETY FOR METALLURGY
- THE ROMANIAN SOCIETY FOR CHEMISTRY
- THE ROMANIAN SOCIETY FOR BIOMATERIALS
- THE ROMANIAN TECHNICAL FOUNDRY SOCIETY
- THE MATERIALS INFORMATION SOCIETY (ASM INTERNATIONAL)

Edited under the care of the FACULTY OF ENGINEERING

Annual subscription (4 issues per year)

Fascicle DOI: https://doi.org/10.35219/mms

Volume DOI: https://doi.org/10.35219/mms.2020.3

Editing date: 15.09.2020
Number of issues: 200
Printed by Galati University Press (accredited by CNCSIS)
47 Domneasca Street, 800008, Galati, Romania